AD-A191 136 IDA GAMMA-RAY LASER ANNUAL SUMMARY REPORT (1985) 1/2
INVESTIGATION OF THE FEA..(U) INSTITUTE FOR DEFENSE
ANALYSES ALEXANDRIA VA B BALKO ET AL. JUN 86
UNCLASSIFIED IDA-P-2021 IDA/HQ-86-33654 MDA903-84-C-0031 F/G 9/3 NL

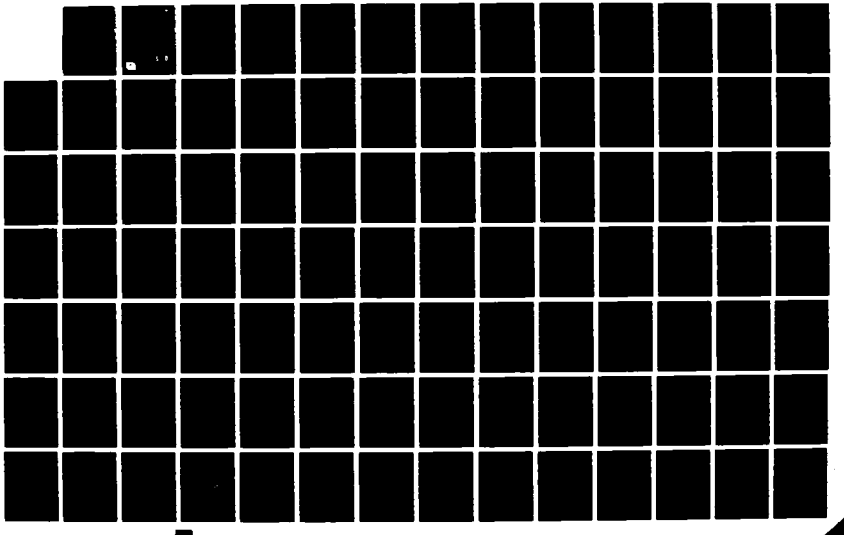

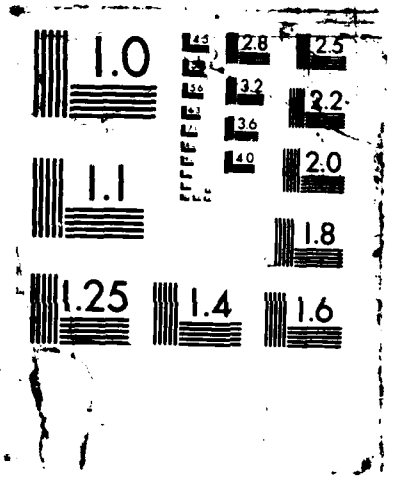
1.0
1.1
1.25
1.4
1.6
1.8
2.0
2.2
2.5
2.8
3.2
3.6
4.0

IDA PAPER P-2021 (REV.)

IDA GAMMA-RAY LASER ANNUAL SUMMARY REPORT (1985)

INVESTIGATION OF THE FEASIBILITY OF DEVELOPING A LASER USING NUCLEAR TRANSITIONS

(REVISED EDITION)

Bohdan Balko
Leslie Cohen
Francis X. Hartmann
Editors

June 1986

Prepared for

Innovative Science and Technology Office
Strategic Defense Initiative Organization
James Ionson, *Director*

INSTITUTE FOR DEFENSE ANALYSES
1801 N. Beauregard Street, Alexandria, VA 22311

IDA Log No. HQ 88-33034

REPORT DOCUMENTATION PAGE

1a. REPORT SECURITY CLASSIFICATION UNCLASSIFIED	1b. RESTRICTIVE MARKINGS
2a. SECURITY CLASSIFICATION AUTHORITY NA	3. DISTRIBUTION/AVAILABILITY OF REPORT Approved for public release; distribution unlimited.
2b. DECLASSIFICATION/DOWNGRADING SCHEDULE NA	
4. PERFORMING ORGANIZATION REPORT NUMBER(S) IDA Paper P-2021 (Rev.)	5. MONITORING ORGANIZATION REPORT NUMBER(S)
6a. NAME OF PERFORMING ORGANIZATION Institute for Defense Analyses 6b. OFFICE SYMBOL (If applicable)	7a. NAME OF MONITORING ORGANIZATION DoD-IDA Management Office, OUSDRE
6c. ADDRESS (City, State, and Zip Code) 1801 N. Beauregard Street Alexandria, VA 22311	7b. ADDRESS (CITY, STATE, AND ZIP CODE) 1801 N. Beauregard Street Alexandria, VA 22311
8a. NAME OF FUNDING/SPONSORING ORGANIZATION Strategic Defense Initiative Organization 8b. OFFICE SYMBOL (If applicable)	9. PROCUREMENT INSTRUMENT IDENTIFICATION NUMBER MDA 903 84 C 0031
8c. ADDRESS (City, State, and Zip Code) Washington, DC 20301-7100	10. SOURCE OF FUNDING NUMBERS PROGRAM ELEMENT: / PROJECT NO.: / TASK NO.: T-R2-316 / WORK UNIT ACCESSION NO.:

11. TITLE (Include Security Classification) IDA Gamma-Ray Laser Annual Summary Report (1985): Investigation of the Feasibility of Developing a Laser Using Nuclear Transitions (Revised Edition)

12. PERSONAL AUTHOR(S).
Bohdan Balko, Leslie Cohen, Francis X. Hartmann, Editors

13. TYPE OF REPORT	13b. TIME COVERED	14. DATE OF REPORT (Year, Month, Day)	15. PAGE COUNT
Final	FROM 8-85 TO 6-86	June 1986	170

16. SUPPLEMENTARY NOTATION

17. COSATI CODES			18. SUBJECT TERMS (Continue on reverse if necessary and identify by block number)
FIELD	GROUP	SUB-GROUP	Nuclear Laser, Gamma-ray laser, Graser, Superradiance, Mössbauer effect, Borrmann effect, Dressed nuclear states, Nuclear isomers, Nuclear magnetic resonance, fine-narrowing, Nuclear data, Nuclear structure.

19. ABSTRACT (Continue on reverse if necessary and identify by block number)

This report summarizes the IDA research effort in FY 1985 in investigating the feasibility of developing a γ-ray laser.

20. DISTRIBUTION/AVAILABILITY OF ABSTRACT ☐ UNCLASSIFIED/UNLIMITED ☒ SAME AS RPT. ☐ DTIC USERS	21. ABSTRACT SECURITY CLASSIFICATION UNCLASSIFIED
22a. NAME OF RESPONSIBLE INDIVIDUAL Bohdan Balko	22b. TELEPHONE (Include Area Code) (703) 578-2991 22c. OFFICE SYMBOL

DD FORM 1473, 84 MAR 83 APR edition may be used until exhausted. All other editions are obsolete

IDA PAPER P-2021 (REV.)

IDA GAMMA-RAY LASER ANNUAL SUMMARY REPORT (1985)

INVESTIGATION OF THE FEASIBILITY OF DEVELOPING A LASER USING NUCLEAR TRANSITIONS

(REVISED EDITION)

Bohdan Balko
Leslie Cohen
Francis X. Hartmann
Editors

June 1986

IDA

INSTITUTE FOR DEFENSE ANALYSES

Contract MDA 903 84 C 0031
Task T-R2-316

ABSTRACT

This report summarizes the IDA research effort in FY 1985 in investigating the feasibility of developing a γ-ray laser.

CONTRIBUTORS

A. Artna-Cohen

B. Balko

L. Cohen

F.X. Hartmann

C. Hayes

E.C. Zimmermann

PREFACE

In January 1985, Dr. James A. Ionson, the Director of the Science and Technology Directorate of SDIO asked the research staff at IDA to investigate the feasibility of developing a gamma-ray laser. The staff responded with a two-part investigation. The first part consisted of determining the extent of work that had been done, who was currently working in the field, and what work should be encouraged or supported. The second part involved the study of specific aspects to clarify important critical issues concerning the various pumping schemes that surfaced at the workshop as well as the gamma-ray laser system as a working device.

The first part of the program was addressed by convening an assembly consisting of research workers directly involved in gamma-ray laser work and others involved in ancillary fields such as nuclear structure, radiation propagation in crystals, Mössbauer Effect, and optical lasers. The proceedings of the workshop are being released as a separate document. The attendees at that workshop included most of the people who later submitted detailed proposals to the Innovative Science and Technology Office in areas of research related to the development of a gamma-ray laser.

The second part of the program resulted in this report, which comprises ten papers. Each is an independent study related to a specific pumping scheme, such as the search for a candidate nucleus for that scheme; or is related to a specific effect common to all schemes, such as superradiance. In this report our goal is to address those problems on which all current schemes are pegged, and the search for new innovative schemes. The work is continuing.

CONTENTS

SUMMARY

A. INTRODUCTION

Because of its potential impact upon the SDI, the IST Gamma-Ray Laser Program was designated an IST Special Project by Dr. James A. Ionson. In January, 1985, as an important aspect of this project, Dr. Ionson asked the IDA research staff to undertake an overall investigation to determine the current status of gamma-ray laser technology and to initiate an effort to investigate the feasibility of developing a gamma-ray laser. IDA responded with a two-pronged effort. First, the research staff hosted a Gamma-Ray Laser Workshop on 21-22 May, 1985 and then published the proceedings of that workshop. Collaterally, the IDA staff undertook a series of studies that either highlighted and delved more deeply into critical issues emerging from the workshop, or involved independent examinations of gamma-ray laser research that others were not addressing. This report constitutes a major part of that work for FY 85.

B. THE WORKSHOP

1. Background

Since the invention of the ammonia laser in 1954, there has been an ongoing search for new and novel sources of coherent radiation. The drive has been motivated by both basic research and the anticipated potential applications. A concomitant has been a move in the direction of ever-shorter wavelength or ever-higher photon energy. This means either using the interaction of charged particles with man-made periodic structures as in the Free-Electron Laser, or using transitions between electronic

quantum states in heavy atoms deprived of their inner electrons or between nuclear quantum states of the atom. The latter could, in principle, make available photon energies ranging from a fraction of a keV to several MeV. These photons could, in principle, lead to very intense beams of coherent radiation whose short wavelengths would permit greater penetration of matter than is possible with current laser sources. With that penetration would come the ability to deposit energy deeper into a target. Also, the shorter wavelength would produce diffraction phenomena that could enable the scanning of objects with resolutions heretofore unachievable. However, there was a problem -- the emission of these energetic photons produced a nuclear recoil that Doppler-shifted the photon energies outside the narrow bandwidths of the well-defined nuclear levels. The discovery of the Mössbauer Effect in 1958 resolved this problem and led to speculation here and abroad about the prospects of a nuclear-based laser.

2. Results of the Workshop

The IST/IDA Gamma-Ray Laser Workshop, held in May 1985, was attended by about 30 people, including leading U.S. workers in the field, experts in ancillary fields having an impact on the graser (gamma-ray laser), and SDI and IDA personnel. The outcome of the workshop is discussed in Refs. 1 and 2. In brief, the discussions and findings of the workshop fall into two categories. The first covers general requirements for and probable characteristics of a graser. The second includes five general pumping schemes described by the speakers.

The following general conclusions are in the first category:

1. The graser will probably be a crystalline rod containing nuclei whose energy levels include the lasing pair. The dimensions will probably be of the order of a few centimeters long, by a few microns in diameter.

2. The Mössbauer* Effect will be essential.
3. The Campbell-Borrmann Effect** will probably be essential for reducing nonresonant absorption.
4. The graser emission will, most likely, have to be superradiant.
5. A good nuclear data base, compatible with the needs of the various pumping schemes will be essential.

Among the five schemes presented at the workshop, four relied on the Mössbauer Effect; one did not use it. The latter is referred to as the Recoil Laser. All the schemes required the nuclei to be in a long-lived excited state (i.e., an isomeric state). The four schemes were named: (1) Coherent Upconversion, (2) Incoherent Upconversion or Two-Step Pumping, (3) Long-Lifetime Gamma-Ray Laser, and (4) Nuclear Interlevel Transfer Driven by Electronic Transitions. Coherent Upconversion immerses the laser rod containing the isomeric nuclei in an RF (or other coherent) electromagnetic field, which induces a nuclear transition to another nuclear state "dressed" by the electromagnetic field. The latter is a short-lived state that decays through a photon cascade to the upper level of the lasing pair. With Incoherent Upconversion, a flash x-ray source or a laser is used to excite the isomer by resonant, single-photon

---

*When a nucleus emits a photon, the energy of that photon is generally downshifted from the transition energy by an amount that is several orders of magnitude larger than the width of the level. However, a fraction, f, of the nuclei will transmit the recoil momentum to the entire crystal in which the nuclei are imbedded. In this case, emission occurs with essentially the full transition energy. The fraction, f, increases as the transition energy and temperature decrease and as the Debye temperature of the crystal increases. This phenomenon of recoilless emission (and absorption) is called the Mössbauer Effect.

**The Campbell-Borrmann Effect involves the transmission of radiation through a crystal when the radiation direction with respect to certain planes in the lattice coincides with a Bragg diffraction angle. In such cases the absorption of that radiation by the atomic electrons can be strongly diminished.

absorption to the short-lived state. The rest of the scheme is the same as the first. The difficulty in having the isomer itself as the upper level is that its long lifetime corresponds to a very narrow width, and the natural inhomogeneities of the crystalline environment cause broadening effects which greatly exceed this width, thereby destroying the stimulation resonance. The Long-Lifetime Laser scheme used nuclear magnetic resonance (NMR) techniques to reduce the width-broadening effects by several orders of magnitude and permit the isomer to release its stored energy as laser radiation. In the Interlevel Transfer Scheme, an optical laser is used for single or multi-photon excitation of an atom. Then one or more virtual photons transfer this excitation energy from the electrons to the nucleus and enable a transition from the isomeric state to a short-lived state. The latter state is either the upper state of a lasing pair or is a state which allows a cascade to the upper state. Finally, the Recoil Laser resembles the Two-Step (or Incoherent) Pumping Scheme. The isomeric nuclei are in atoms of a gas. Their thermal motion is reduced to zero velocity by laser cooling techniques. They are then optically pumped to a lasing or cascading level and lase at a frequency equal to the resonant frequency downshifted by the Doppler recoil.

C. TOPICS AND RESULTS

Each chapter that follows is an independent study affecting either one of the five pumping schemes of Category 2 or expanding on one of the topics included under Category 1.

Chapter 1 compares the Long-Lifetime and the Coherent and Incoherent Upconversion Schemes and discusses the issues that are critical to achievement of lasing in each case.

Chapter 2 contains an introduction to the type of nuclear information available in compilations at national centers. In addition, a laser grade nuclear data base is established specifically for the Long-Lifetime Laser Scheme. Over 200 isomers are identified.

Chapter 3 is a study of the parameters involved in selecting candidates to achieve lasing in the Long-Lifetime Laser Scheme. These parameters include the effects of nuclear structure, the host lattice and population inversion. Approximately 200 isomers are studied. Of these, ^{60}Co, ^{94}Nb, ^{165}Dy, and ^{113}Sn are nuclei that are candidates with a sufficiently high gain not to require a Campbell-Borrmann Effect. However, inhomogeneous broadening still presents a problem.

Chapter 4 discusses the sources of inhomogeneous broadening of resonances, experimental procedures for narrowing these resonances, and the times required to do so. This study shows that the narrowing of the inhomogenously broadened resonance may be achieved in a time shorter than the nuclear lifetime.

Chapter 5 analyzes anti-Stokes Raman cross sections in a generic ^{186}Re-like system. The context is the achieving of lasing in the Incoherent Upconversion Scheme, in which ^{186}Re is frequently given as the prime candidate. Given the most likely nuclear parameters, it is shown that unrealistically high photon fluxes are required to achieve gain.

Chapter 6 deals with a theoretical study of the nuclear structure of ^{186}Re which is a prominent candidate in the Incoherent Upconversion Scheme. The approximate positions

of the nuclear levels are determined from a systematic study of well known related nuclei. The spacing between the isomeric and upper cascading levels is shown to be an order of magnitude greater than previously assumed.

Chapter 7 proposes an innovative Mössbauer scattering experiment that would unambiguously resolve disagreements in interpreting the results of an experiment that is cited as evidence in support of the Coherent Upconversion Scheme.

Chapter 8 proposes an experimental procedure based on baking a sample to populate any nuclear states that may exist within a few electronvolts of any known isomer. Such information is important for both the Coherent Upconversion and the Two-Step Schemes.

Chapter 9 examines the differences in the semi-classical and the Dicke theories of superradiance and discusses recent experimental results in light of these differences.

Chapter 10 examines the possibility of lasing from a relativistic beam of nuclei in an excited state where deexcitation with recoil is permitted. This study is an extension of the Recoil Scheme, and shows that the current status of accelerator technology is not at a point where a recoil graser is feasible.

D. CONCLUSIONS AND RECOMMENDATIONS

The development of a γ-ray laser requires a close collaboration of workers in nuclear structure solid-state physics, Mössbauer spectroscopy, γ-ray optics, and materials science. This report describes the research performed at IDA in support of some of the concepts for developing an γ-ray laser. The

work initiated in this report shows that extensive research has yet to be done for each proposed scheme to establish its feasibility. In general:

1. The data base established and specialized to serve the needs of the long lifetime scheme must be extended to include portions devoted to the specific needs of the other major schemes.
2. Theoretical techniques, such as the systematics study of the structure of ^{186}Re, and experimental techniques, such as the thermodynamic one of Chapter VIII, must be used to supplement the nuclear data base where potentially promising candidates are characterized by critical gaps in knowledge.
3. Where possible, experiments must be performed to resolve issues that are critical to establishing the feasibility of a major scheme such as the experiment proposed in Chapter VII to establish whether or not certain nuclear states are being "dressed" by the electromagnetic field.
4. Unusual schemes, such as the Recoil Laser, which are not ruled out by physics (but which, due to the present state of technology, are currently not feasible) should continue to be pursued.

Specifically:

1. For the upconversion concepts we found that unrealistic fluxes (10^{30} photons/cm^2, even without consideration of the shielding by atomic electrons) were required to invert ^{186}Re, the only candidate so far proposed. Better candidates have to be identified if this concept is to be seriously considered. Multiphoton upconversion, the "dressed state concept" or coherent upconversion ideas have to be checked with calculations based on the properties of real isomers.

2. The idea of promoting nuclear transitions through the excitation of the atomic electron cloud is innovative and intriguing. The coupling mechanism between the electrons and nuclei has to be investigated to determine whether the electrons can initiate and mediate energy transfer.* This concept is presented in Chapter I, but not evaluated in detail. The transfer mechanism has to be examined in future work to determine its viability.
3. For the line-narrowing concept, we found four candidate isomers (^{60}Co, ^{94}Nb, ^{165}Dy, ^{113}Sn) which could lase if neutron fluxes of $10^{17} cm^{-2} sec^{-1}$ were available for inversion and the expected inhomogeneous broadening of the lines in these isomers could be reduced to about ten times the natural line widths. With Borrmann Effect reduction of the electronic absorption or enhanced coupling of electromagnetic radiation to the nuclei, these requirements on the line narrowing could be reduced. This is the only concept for which real candidates have been identified and all the lasing requirements examined.
4. In this report, we have also discussed the concept of Dicke superradiance because a superradiant pulse is the most likely mechanism for the emission process in all the lasing schemes. Further work in superradiance has to be directed to the effects of nuclear characteristics, of recoilless transitions (Mössbauer Effect), wavelengths shorter than interatomic spacings, inhomogeneous broadening of lines, and long lifetimes (isomers).

*Transfer between an isomeric level and a lasing level.

I. ON THE DEVELOPMENT OF GAMMA-RAY LASERS USING LONG-LIVED NUCLEAR ISOMERS

Gamma rays have many important applications because of their short wavelengths, high penetrating power, and ability to ionize atoms and molecules. Grasers, or γ-ray lasers, which would provide intense, controllable, and directable coherent sources of such radiation, in which phase as well as intensity have significance, would have a revolutionary impact on most fields where both γ-rays and x-rays are used already or where extensions into this range are desirable.

The extension of lasers or coherent sources of radiation into the nuclear regime is important because nuclei and nuclear resonance transitions have unique properties not characteristic of atomic or molecular transitions.

The characteristics include:

- High transition energies (short wavelengths)
- High energy definition (narrow linewidths)
- Existence of long-lived isomeric levels

These three characteristics are summarized as follows:

(1) Nuclear resonant transitions range in energy from tens to millions of eV. These energies are generally orders of magnitude higher than energies of atomic transitions even though there is some overlap. Conventional x-ray lasers are being developed that operate in the high ultraviolet region of the spectrum; there are no proposed systems to extend the range of x-ray lasers into the 10 keV or higher energy region. The latter region is expected to be at the lower end of the operating range of γ-ray lasers. In general, higher energy radiation penetrates deeper into materials.

(2) The high-energy resolution of nuclear resonant transitions showing the Mössbauer Effect (10^{-8} eV and narrower linewidth) coupled with the high intensities expected from gamma-ray lasers would be revolutionary in the field of nuclear spectroscopy.

(3) The existence of long-lived nuclear isomeric levels with lifetimes on the order of seconds to years would permit the manufacture of isomeric crystals with weaker beams or fluxes than are required for short wavelength x-ray lasers. Also, energy could be stored for a time on the order of the isomeric lifetime, thereby making the concept of a "nuclear battery" realizable. With the gamma-ray laser there would be a capability of storing energy in the amount of 10^9 J/cm^3, which exceeds energy storage in liquid fuels or conventional batteries by several orders of magnitude (10^4 to 10^5).

Although the γ-ray laser has not been developed yet, some technical problems have been identified and solutions are being sought in various ways. (See for example, Refs. 2 and 3.)

In particular, the possible use of long-lived Mössbauer isotopes (lifetimes > 1 sec) for γ-ray laser development has attracted considerable attention because of:

- The reduced requirement on pumping power for the inversion (a function of the long pumping time),
- The possibility of storing energy for a long time (on the order of the lifetime) in the inverted state, and
- The possibility of delayed externally controlled energy release.

The major problem with using long-lived isomeric transitions in γ-ray laser development is inhomogeneous broadening resulting from slightly different environments at different nuclei sites. This broadening has been observed with all Mössbauer isotopes but is particularly devastating to the

resonance phenomena with the ultra-narrow natural linewidths associated with the long-lived isomeric transitions.

Inhomogenous broadening destroys resonance between nuclei in a crystal and prevents the observation of the Mössbauer Effect in long-lived isomeric transitions. In what follows we discuss four approaches to the solution of this problem.

The first approach uses line narrowing by external fields to restore resonance and promote stimulated emission. Two other approaches use additional high flux radiation to promote the system through a direct nuclear - electromagnetic field interaction either to a nearby short-lived nuclear level or to a "dressed state" of the system which could then be stimulated to make a transition to the ground state. The fourth approach would use high flux laser radiation (or other means) to excite the atomic electrons, which in the process of deexcitation would excite nuclear transitions from the isomeric to the nearby lasing level.

The four procedures are compared in Fig. 1. In all cases, the first step is to prepare a long-lived nuclear state, which is on the order of 10 to 100 keV above the ground state, through neutron capture or some other mechanism. In the line-narrowing scheme, Fig. 1(a) suppression of inhomogeneous broadening by pulsed RF techniques is used to restore resonance between nuclei and induce emission of laser radiation. Such RF techniques are being used routinely in high resolution nuclear magnetic resonance (NMR) work but have not been applied to Mössbauer isotopes yet.

The two direct-transfer techniques use a second, short wavelength, intense pulse to promote the nucleus from the initial long-lived inhomogenously broadened level with energy E_e to another near-lying but short-lived state. This new state could be either naturally occurring and accessible by optical or x-ray lasers as shown in Fig. 1(b), or a "dressed state" resulting from intense coherent excitation by an EM field as

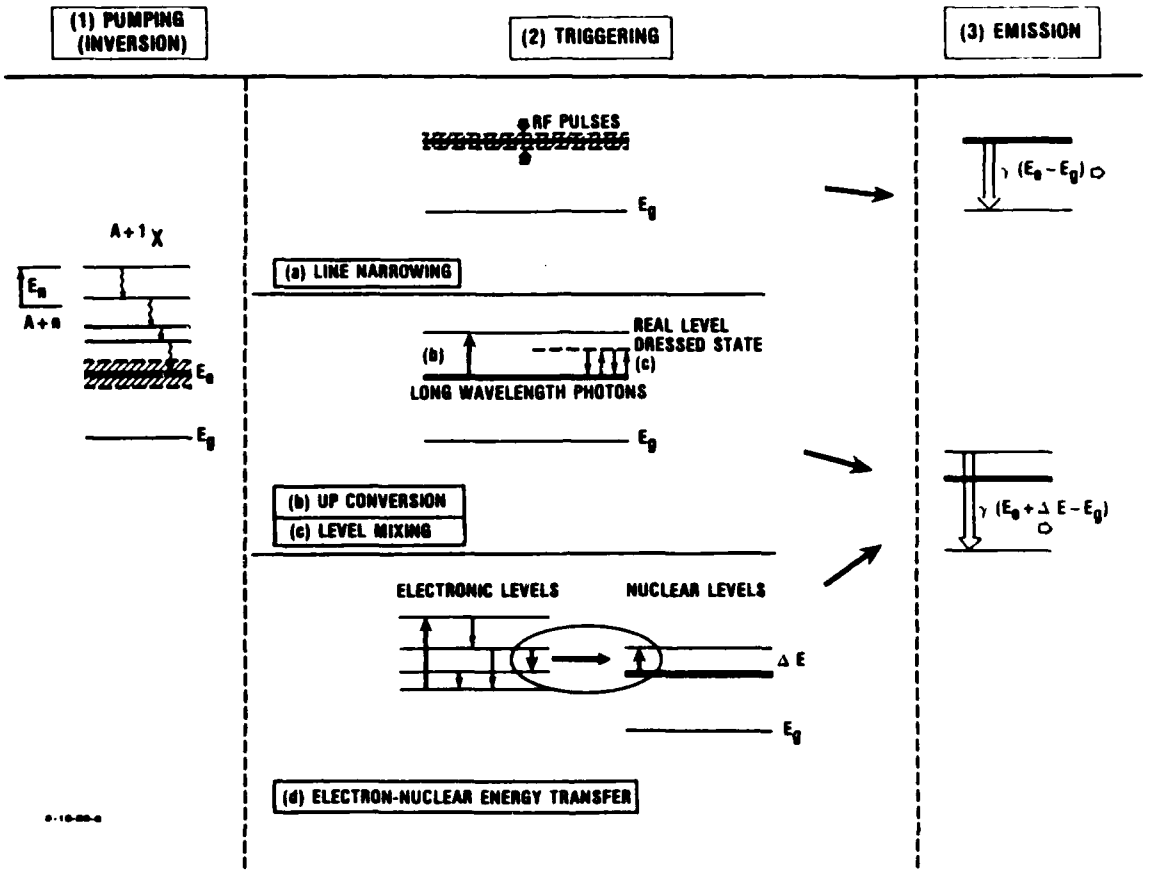

FIGURE 1. Four concepts for employing long-lived isomers in the development of γ-ray lasers. In all four cases, step 1 is the inversion and step 3 the stimulated emission. Intermediate step 2, which deals with the line-broadening problem, is different for each case. Step 2 involves, in case (a), line-narrowing and restoration of resonance through RF techniques, in case (b) incoherent direct electromagnetic (EM) pumping of near-lying short-lived level, in case (c) coherent direct (EM) preparation of a dressed nuclear state, and in case (d) atomic excitation and subsequent nuclear pumping by energy transfer through the interaction of the nuclear electrons.

shown in Fig. 1(c). The required nearby states have not been observed experimentally yet, although their existence is expected on the basis of theoretical models. It has also been reported that "dressed states" involving nuclear Zeeman levels can be prepared with available radio frequency (RF) fields (see Ref. 4).* In the fourth technique (Fig. 1(d)), upconversion is accomplished by electron-nuclear energy transfer.

CRITICAL ISSUES

The key problems associated with the four concepts described above are summarized in this subsection. The concepts identified at the workshop** and the critical issues specific to the implementation of each concept are as follows:

1. Line-narrowing of isomeric transition widths by RF pulses
   - Existence of long-lived or stable isotopes for manufacturing isomers
   - Suppression of inhomogeneous broadening in Mossbauer nuclei by RF pulses
   - Preparation of pure, defect-free host crystals with substitutionally implanted isomers
   - Meeting all threshold conditions for lasing
2. Incoherent Upconversion
   - Existence of nuclear levels within $nh\omega$ of a known isomer (ω = frequency of coherent radiation source)
   - Preparation of dressed states with coherent radiation
   - Preparation of host crystal, including isomeric nuclei
   - Meeting all threshold conditions for lasing

*Results are controversial. Most people in the field believe the experimental results are due to a magnetostrictive effect.

**IST/IDA Gamma-Ray Laser Workshop, IDA May 20-21, 1985, Proceedings published as an IDA Memorandum Report (Ref. 1).

3. Upconversion by optical or x-ray photons
    - Existence of nuclear levels within optical or x-ray energies of the isomeric level (missing nuclear data)
    - Availability of pumping power to achieve inversion of isomeric nuclei
    - Preparation of host crystals, including isomeric nuclei
    - Meeting all threshold conditions for lasing
4. Nuclear interlevel transfer by electronic transitions
    - Existence of proposed mechanisms and measurements of associated rates
    - Existence of suitable nuclear levels compatible with associated electronic pumping transitions
    - Suitable laser pumping sources
    - Meeting all threshold conditions for lasing

There are other critical issues associated with population inversion, energy release, and transport of radiation out of the medium--all of which are common to the four concepts. In particular, the use of the Borrmann effect for promoting selected transitions and reducing the linear extinction coefficient may be essential to all the concepts. Furthermore, the preparation of an active medium containing the required isotope in a structurally suitable condition (with a high recoilless fraction and other desirable properties which do not appreciably deteriorate during lasing) is essential to the four concepts. These problems must ultimately be addressed in a complete systems approach to the development of the laser.

II. SEARCH FOR NUCLEAR LEVELS FOR GAMMA-RAY LASER

A. INTRODUCTION

The concept of a gamma-ray laser extends the laser principle into the wavelengths of nuclear gamma rays. In such a laser, the lasing transition is a photon emitted in the decay of a nuclear level. A summary of the proposed schemes, their problems and advantages, has been set forth by Baldwin et al. among others (Ref. 1).

In orders of magnitude, the nuclear transitions cover the energy range of 10 to 10^6 eV. The useful range of a nuclear laser, however, will probably be in the range of 10 to 100 keV, a wavelength of about 10^{-8} to 10^{-9} cm. Transitions having an energy of the order of 10 keV or lower will preferentially decay by means other than photon emission, while transitions with energy much greater than 100 keV will cause difficulties with the laser design.

All the proposed schemes for a gamma-ray laser have one thing in common--they all involve a nucleus with a metastable excited state, i.e., a nuclear isomer. In some schemes, this is the state from which the lasing gamma ray is emitted. The gamma-ray leaves the nucleus either in its ground state or in another excited state. Other schemes use the metastable or isomeric state as a storage level from which the nucleus is "pumped" by some means or other to a lasing state. Again, after emitting the lasing transition the nucleus is left in either the ground state or another excited state. Figure 2 illustrates the two processes.

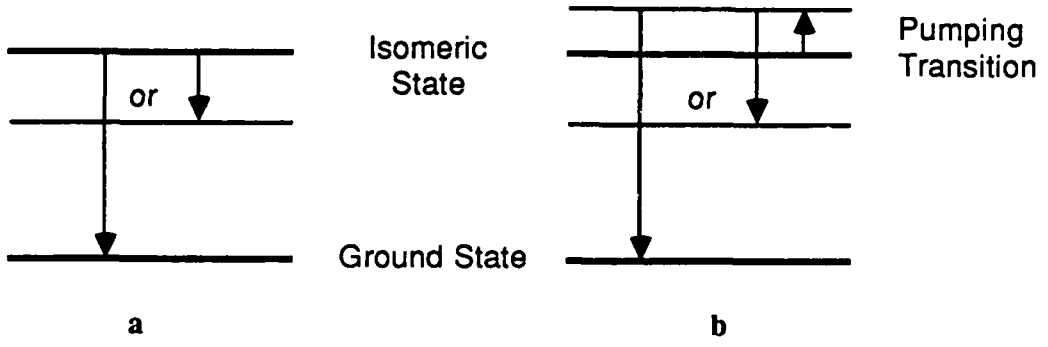

FIGURE 2. Energy-Level Diagrams Demonstrating Two Generic Lasing Schemes

Another feature common to all the proposed schemes is that they deal with hypothetical nuclei. It is therefore obvious that the first step in investigating the merits of the various schemes is to survey the field of known nuclei and to use the properties of real nuclei in the calculations. To do that, the available information on nuclear structure must be thoroughly explored to locate the levels which best qualify for these processes.

This chapter is a compilation of information on nuclei with properties which best fit the requirements set forth by the proposed laser schemes.

B. NUCLEAR INFORMATION

The foremost source of information on nuclear structure is the National Nuclear Data Center (NNDC). The data evaluation and compilation for this organization is done by The International Network for Nuclear Structure Data Evaluation. The manuscripts are reviewed and edited by the Nuclear Data Project and published in the journal Nuclear Data Sheets, by Academic Press, New York, NY. The NNDC also maintains computer files of the

published information. Also compiled and published by NNDC in "Nuclear Data Sheets" are lists of references complete with keywords of articles published since the latest compilation on a particular nucleus was issued. This last feature is important, since, on the average, these evaluated compilations are updated every 6 to 8 years.

The information on nuclear structure is always a synthesized body of knowledge deduced from a large collection of data obtained from many different types of experiments. Much of this information is indirect, interpreted in the light of theoretical expectations, current nuclear models, and nuclear systematics. For this reason, it is important to be aware of and to understand on what theories, models, or systematics the values one uses are based.

One can assign four different confidence levels to the evaluated information in "Nuclear Data Sheets":

1. Adopted Values. These are the numerical values for nuclear properties adopted by compilers, and form the bases of their adopted level scheme. The compilers have evaluated all experimental data relevant to this nucleus, plus the relevant theories and nuclear systematics in order to reach their conclusions.
2. Compiled Data. These are the actual published results from which some nuclear level--or transition--property has been deduced. Or, it is information which suggests other levels or properties but for which not enough information is known to consider the data confirmed.
3. Unassigned Data. Data or information which was available to the compilers, but which did not fit into the adopted level scheme. The existence of unassigned data is a very likely indication that the proposed level scheme is incomplete.

4. Recent References. These contain references to original publications published since the latest compilation on this particular nucleus was issued.

Depending on the type of nuclear information one is seeking, one may stop at the Adopted Data, or go on to a search through the Recent References. If one is looking for long-lived, low-energy nuclear isomers, one can quite confidently stop with the Adopted Data. A listing of nuclear levels with certain half-lives from the computer tapes of NNDC will accomplish the goal. If only an approximate value for the level energy and half-life is needed, one may stop there. If one wants to be sure that one has the latest and best values for the energy and half-life, a survey of Recent References will complete the search. If, however, one is interested in more involved features of the level scheme, such as transition probabilities, multipolarities, or conversion coefficients, in most cases the Adopted Data is not enough. In this event, a manual search of the Compiled Data and perhaps even the Unassigned Data, can be more fruitful and efficient than a computer search.

Another type of search through the compiled and unassigned data in these compilations can be useful; that is the search for missing levels. If one suspects, either from theory, or from systematics, that a particular nuclear level has been missed, the unassigned data can sometimes be used either to support the possible existence, or nonexistence, of such a level.

In addition to the evaluated compilations produced by the NNDC, the most notable other compilation is the "Table of Isotopes" prepared at Lawrence Berkeley Laboratory, University of California, Berkeley, and published by John Wiley & Sons, New York, NY. This compilation, which is issued periodically (every 6 to 8 years), offers compactness at the expense of completeness. It generally presents the Adopted Data from the "Nuclear Data Sheets" updated with more recent information considered significant by the compilers.

C. NUCLEAR STRUCTURE

There are a number of nuclear properties whose values are crucial to the success of a γ-ray laser. Figure 3 shows a nuclear level scheme with standard representations.

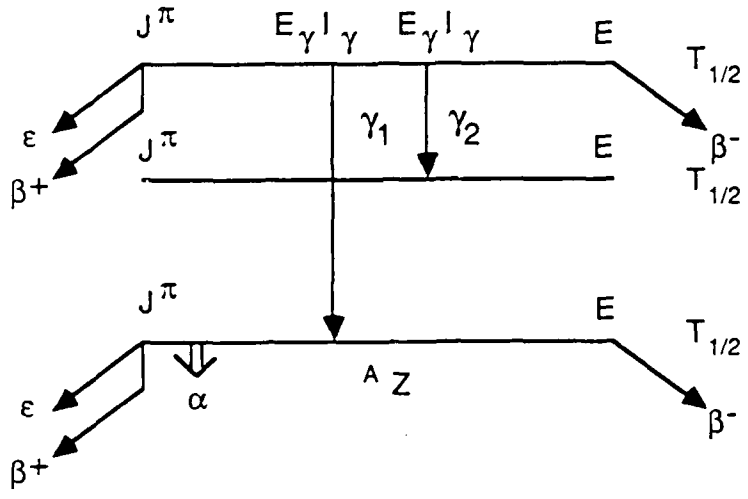

FIGURE 3. Nuclear Level Scheme Demonstrating Use of Symbols for Nuclear Transitions as Used in the Text

The following is a brief description of these properties and the definitions of symbols used to denote them. A nucleus is defined by its atomic number, Z (element name) and by its Mass number, A.

The level scheme of a nucleus, showing a sequence of energy levels, is generally deduced from a self-consistent arrangement of observed nuclear transitions (β^-, γ, β^+, ε). The nuclear reaction experiments [N(x,y)M where N and M are nuclei and x and y the incident and ejected particle, respectively] do give a direct energy spectrum of nuclear levels, but generally do not have the resolution necessary to give the detail obtainable from nuclear transition experiments.

A nuclear level can undergo spontaneous decay to a system with lower energy in many ways:

α	-decay	to a nucleus $^{A-4}(Z-2)$
$\beta-$	-decay	to a nucleus $^{A}(Z+1)$
e	electron capture	to a nucleus $^{A}(Z-1)$
β^+	positron emission	to a nucleus $^{A}(Z-1)$
γ	gamma-transitions	within the nucleus.

Sometimes the term "gamma-ray" refers to the photons alone; sometimes it is used to indicate the total transition of this energy, and includes both photons and internal conversion electrons. It is therefore important to know exactly what is meant by the term "gamma-ray" especially where intensities are concerned.

Nuclear levels are described by the following properties:

E Energy, measured from ground state of the nucleus. Generally deduced from transition energies.

$T_{1/2}$ Half-life. Sometimes meanlife, τ, defined by

$$\tau = T_{1/2}/\ln 2$$

is found more useful. From meanlife the level width, Γ, can be found

$$\Gamma = \hbar/\tau.$$

Since most nuclear levels decay by more than one mode,

$$\Gamma_{\text{total}} = \sum_i \Gamma_i.$$

The half-life is usually obtained by measuring the half-life of a transition and is therefore level-scheme dependent.

$J\pi$ Spin and parity of the level. (Spin = total angular momentum of the level.) Some spins of longer-lived nuclear levels have been measured directly. Most spins and all parity assignments, however, are indirectly deduced from transition properties, reaction data, and the level scheme. A "Summary of Basis for Spin and Parity Assignments" is published in the beginning of each issue of the journal Nuclear Data Sheets, outlining the spin assignment arguments which can be considered "strong" and those which are considered "weak."

In addition, nuclear levels can be described by their magnetic moments and by other, model-dependent, angular-momentum quantum numbers.

Nuclear transitions, γ-rays, are described by the following properties:

E Energy, measured directly.

$T_{1/2}$ Half-life is experimentally measured by either:

(a) following the decay of the transition, in which case the half-life is actually that of the level, or

(b) by photon transition probability measurements which lead to the partial half-life of the photon.

$$1/T_{1/2}(\text{level}) = \sum_i 1/T_{1/2}(i)$$

where i denotes all modes of decay.

The half-life of an electromagnetic transition can also be estimated theoretically using the well-known Weisskopf single-particle estimate:

$$T_{1/2w}(E) = 0.190 \left(\frac{L}{L+1}\right)\left(\frac{3+L}{3}\right)^2 \frac{[(2L+1)!!]^2}{A^{2L/3}} \left(\frac{164.44}{E(\text{MeV})}\right)^{2L+1} \times 10^{-21} \text{ s.}$$

$$T_{1/2w}(M) = 3.255\ A^{2/3}\ T_{1/2w}(E)$$

for nuclear radius $1.2A^{1/3} \times 10^{-13}$ cm. E and M refer to electric and magnetic multipole transitions, respectively.

Although transitions in real nuclei are seldom pure single-particle transitions, it has been found that the Weisskopf estimate can give a useful order-of-magnitude estimate for the various L values. (For comparison of the Weisskopf estimate with empirical data, see "Summary of Bases for Spin and Parity Assignments," found in the Introduction to each issue of the Nuclear Data Sheets.)

Branching ratio--sometimes denoted by β and defined as the ratio of the particular transition in question to total decay of the level. If one deals with the decay of an isomer, %IT is often quoted. This is the percent of total decay of this level proceeding within the nucleus, i.e., percent of isomeric transition. In the level scheme in Fig. 3, this is then the fraction of the decay proceeding through the gamma transitions (photons and conversion electrons)

$$\%IT = (N_{\gamma 1} + N_{ce1} + N_{\gamma 2} + N_{ce2})/(\text{All decay from level}) \times 100.$$

Obtained from measured intensities and level scheme.

Gamma-ray multipolarity, Λ--Λ gives information about the angular momentum, L, carried away by the transition and about the relative parities of the two states involved. The selection rule governing angular momentum change is:

$$|J_i - J_f| \leq L \leq |J_i + J_f| \ .$$

The transition can be either electric (E) or magnetic (M), depending on whether or not the nuclear states involved have the same or opposite parity. The rules for parity change are:

$$\text{Electric transition } \Delta\pi = (-1)^{L}$$
$$\text{Magnetic transition } \Delta\pi = (-1)^{L+1} .$$

The following table gives the multipolarities for the various angular momentum and parity changes:

L	$\Delta\pi$	
	+1	-1
1	M1	E1
2	E2	M2
3	M3	E3
4	E4	M4
5	M5	E5

The highest multipolarity observed has L = 5.

Since the transition probability is strongly dependent on L (see Weisskopf estimate, above), the transitions tend to be of the lowest order possible, i.e., $L = |J_i - J_f|$. Two major exceptions to this are: (1) some transitions where strongly enhanced E2 competes with M1 (for example, the transitions within rotational and vibrational bands in deformed nuclei); and (2) transitions where $J_i = J_f$. Here $J_i - J_f = 0$, and since L = 0 photons do not exist, the L = 1 photons are competing with the L = 0 internal conversion transition. If $J_i = J_f = 0$, then the only isomeric transition possible has L = 0, and the decay

can only go by internal conversion for $E < 2m_e$ and by internal conversion and pair production if $E \geq 2\ m_e$. The multipolarity is generally deduced from internal conversion coefficients and ratios. It can also be deduced from spins and parities of the levels involved. However, in that case the assumption is made that the transition is of pure multipolarity, and this may or may not be true.

Internal conversion coefficient α is defined by

$$\alpha = N_{ce}/N_{photon} \cdot$$

The transition can be converted in any of the atomic shells which contain electrons. Thus,

$$\alpha_{total} = \alpha_K + \alpha_{L1} + \alpha_{L2} + \alpha_{L3} + \alpha_{M1} + \text{etc.}$$

The conversion coefficients are obtained from the experimental relative intensities of the conversion electron lines and photons. Since the photons and conversion electrons cannot be measured in the same experiment, a calibration of some sort is always involved in the measurement of αs. The ratios α_K/α_L, α_{L1}/α_{L2}, etc., however, can be measured directly. Theoretically, the internal conversion process is a many-body, model-dependent problem involving the nucleus and all the atomic electrons. Various calculations have been carried out, and the results have been tabulated. These results show that, in general, the internal conversion coefficients (1) increase with increasing Z, (2) increase with increasing L, (3) decrease with increasing E, and (4) and the magnetic transitions have larger conversion coefficients than the electric transitions of same L.

Photon intensity, I_γ.

Although the relative photon intensity is a directly measured quantity, the absolute intensity of photons per decay of level depends on the level scheme and other above-mentioned quantities.

Thus the photon intensity (I_{photon}) for a transition is given by

$$I_{photon} = I_{transition}/(1 + \alpha)$$

or

$$I_{photon} = [\beta/(1 + \alpha)]\ I_{transition}$$

where β = branching ratio.

D. COMPILATIONS

As pointed out in the Introduction, all laser schemes require the existence of a nuclear metastable level, an isomer. The two types of schemes, however, require isomers with different properties. Therefore, the compilation is prepared in two parts: subsection E forms the data base for laser schemes shown in Fig. 2(a).

E. SELECTED ISOMERIC TRANSITIONS

The Table of Selected Isomeric Transitions (Table 1) was prepared in three steps. Each step resulted in a separate compilation, providing a starting point for any necessary additions and/or refinements. The three steps are as follows:

Step 1: Identification and selection of isomers*

Step 2: Collection of nuclear information*

Step 3: Compilation of data--Table 1 Selected Isomeric Transitions.

---

*This compilation not included here because of its size. It is on file at IDA.

TABLE 1. SELECTED ISOMERIC TRANSITIONS

ISOMER	INITIAL LEVEL			FINAL LEVEL			GAMMA-RAY					PARENT		
A Z	E (keV)	Jπ	T½/a (sec)	E (keV)	Jπ	T½/a (sec)	IT (%)	E (keV)	Mult.	ICC	Iγ (%)	A Z	T½/a	SIGMA(N,G) IB+BB
34,vCl	146.36 3	3+	1.920E+3 2	0	0+	1.526 3	46.9 10	146.36 3	M3	0.172	40	33Cl	2.511s	
44m,Sc	271.13 11	6+	2.110E+5 4	0	2+	1.414E+4 3	98.8	271.24	M4	0.1367	87	43Sc	3.89h	
45m,Sc	12.40 2	3/2+	0.316 9	0	7/2+	STABLE	100	12.40 2	M2	568	0.2	44Sc	3.93h	
46m,Sc	142.528 3	1-	18.70 5	0	4+	7.243E+6 2	100	142.528 3	E3	0.61	62	45Sc	STABLE	10+17
50m,Sc	256.895 10	2+,3+	0.35 3	0	5+	102.6 5	98.7 13	256.894 10	M3	0.0367	95	49Sc	57.4m	
58mvCo	24.89 2	5+	3.29E+4 4	0	2+	6.119E+6 3	100	24.89 2	M3	2.71E+3	0.037	57Co	271d	
60mvCo	58.59 1	2+	628 2	0	5+	1.6624E+8 1	99.76 3	58.603 7	M3+(E4)	48	2.0	59Co	STABLE	20+17
68mvCu	721.6 7	(6-)	225 3	610.5 6	(5-)		76	111.3 7	(M3)	3.67	16	67Cu	61.92h	
73mvGe	66.72 2	1/2-	0.449 11	13.275 17	5/2+	2.95E-6 2	100	53.440 9	M2	8.67	10.3	72Ge	STABLE	1.0
75mvGe	139.68 3	7/2+	47.7 7	0	1/2-	4.967E+3 2	99.970 6	139.68 3	E3	1.576	39	74Ge	STABLE	0.16+0.36
77mvGe	159.7 1	1/2-	52.9 6	0	7/2+	4.068E+4 4	21 2	159.7 1	E3	0.87	11.2	76Ge	STABLE	0.09+0.06
79mvGe	185.95 4	(7/2+)	39.0 10	0	(1/2-)	19.1 3	4 1	186.02 7	(E3)	0.432	2.8	78Ge	88m	
73mvSe	25.71 4	3/2-	2.39E+3 8	0	9/2+	2.57E+4 3	73 3	25.71 4	E3	5.51E+3	0.013	72Se	8.40d	
77mvSe	161.97 6	7/2+	17.45 10	0	1/2-	STABLE	100	161.9223 7	E3	0.907	52.4	76Se	STABLE	21+64
79mvSe	95.73 3	1/2-	235 3	0	7/2+	≤2.0E+12	100	95.73 3	E3	9.56	9.5	78Se	STABLE	0.32+0.2
81mvSe	102.97 5	7/2+	3.437E+3 3	0	1/2-	1.107E+3 7	99.95 1	102.97 5	E3+M4	9.2	9.8	80Se	STABLE	0.07+0.54
76mvBr	102.38 3	(4)+	1.31 2	48.47 2	(2)-	1.13E-9 6	>99.4	57.11 2	M2	9.65	9.4	75Br	97m	
77mvBr	105.68 15	9/2+	237 6	0	3/2-	2.0933E+5 2	100	105.87 10	E3	6.38	13.6	76Br	16.2h	
79mvBr	207.1 4	9/2+	4.86 4	0	3/2-	STABLE	100	207.2 4	E3	0.32	76	78Br	6.46m	
80mvBr	85.845 4	5-	1.591E+4 4	37.054 3	2+	7.43E-9 6	100	48.786 5	M3	308	0.32	79Br	STABLE	2.5+8.2
82mvBr	46 2	2-	368 5	0	5-	1.271E+5 1	97.6	46 2	M3	395	0.25	81Br	STABLE	2.4+0.26
79mvKr	129.77 5	7/2+	50 3	0	1/2-	1.261E+5 4	100	129.72 10	E3	2.68	27	78Kr	STABLE	0.17+6
81mvKr	190.57 4	1/2-	13 1	0	7/2+	6.7E+12 7	99.994 2	190.43 7	E3	0.491	67	80Kr	STABLE	4.6+8
83mvKr	41.56 2	1/2-	6.59E+3 7	9.40 1	7/2+	1.47E-7 4	100	32.16	E3	1.9E+3	0.05	82Kr	STABLE	16+ 20
81mvRb	86.29 6	9/2+	1.83E+3 2	0	3/2-	1.647E+4 2	97.7 11	86.28 11	E3	17.82	5.2	80Rb	34s	
84mvRb	464.3 3	6-	1.229E+3 10	248.2 2	(3)-	3.1E-10 6	64	216.1 3	(M3+E4)	0.9	34	83Rb	86.2d	
90mvRb	106.9 2	(4-)	258 5	0	(1-)	153 3	4.3	106.9 2	(M3)	11	0.36	89Rb	15.2m	
83mvBr	259.3 1	1/2-	4.95 12	0	7/2+	1.166E+5 7	100	259.3 1	E3	0.184	84	82Br	35.4d	
85mvBr	238.68 9	1/2-	4.060E+3 4	231.70 5	7/2+		86	(6.94)	(E3)	2.19E+7	3.9E-6	84Br	STABLE	0.53+0.27
85mvBr	238.68 9	1/2-	4.060E+3 4	0	9/2+	5.602E+6 2	1.0	238.6 2	M4	2.012	0.3			
86mvY	218.3 3	(8)+	2.88E+3 6	208.1 3	(5)-		99.31	10.2 1	E3	2.4E+6	4.1E-5	85Y	2.68h	
93mvY	758.4 6	(9/2)+	0.82 4	590.0 3	(3/2)-		100	168.4	E3	0.95	91	92Y	3.54h	
85mvZr	292.2 3	(1/2-)	10.9 3	0	(7/2-)	472 2	100	292.2 3	E3	0.097	<91	84Zr	28m	
87mvZr	335.9 4	(1/2-)	14.0 2	200.9 2	(7/2-)		100	135.1 2	(E3)	2.67	27	86Zr	16.5h	
90mvZr	2319.10 15	5-	0.809 2	2186.50 15	2+	8.4E-14 7	18	132.60 3	E3	2.9	4.6	89Zr	78.4h	
91m,Nb	104.49 9	(1/2)-	5.36E+6	0	9/2+	3E+11	95 2	104.5 1	(M4)	171	0.55	90Nb	14.6h	
93m,Nb	30.4 3	1/2-	4.29E+8 9	0	9/2+	STABLE	100	30.4 3	M4	1.93E+5	5E-4	92Nb	3.5E+7y	
94m,Nb	40.95 2	3+	375.6 6	0	(6)+	6.4E+11 5	99.50 6	40.94 3	M3	1.36E+3	0.07	93Nb	STABLE	1.15
95m,Nb	235.68 2	1/2-	3.12E+5 3	0	9/2+	3.021E+6 3	94.4 6	235.68 2	M4	2.92	24	94Nb	2.0E+4y	0.6+14.8
93mvMo	2425.2 6	(21/2)+	2.47E+4 2	2162.1 5	(13/2)+		99.88	263.1	E4	0.72	58	92Mo	STABLE	<0.3

TABLE 1. (Continued)

ISOMER		INITIAL LEVEL			FINAL LEVEL			GAMMA-RAY					PARENT		
A	Z	E (keV)	J^π	$T_{1/2}$ (sec)	E (keV)	J^π	$T_{1/2}$ (sec)	IT (%)	E (keV)	Mult.	ICC	$I_{\gamma\gamma}$ (%)	A Z	$T_{1/2}$	SIGMA(N,G) IS+BS
95	43Tc	38.93 4	1/2⁻	5.27E+6 9	0	9/2⁺	7.20E+4 4	4 1	38.9 1	M4	5.44E+4	7.4E-5	94Tc	4.88h	
96	43Tc	34.17 5	4⁻	3.09E+3 6	0	7⁺	3.70E+5 6	98.0 5	34.20 5	M3	3.94E+3	0.025	95Tc	20h	
97	43Tc	96.59 7	1/2⁻	7.82E+6 9	0	9/2⁺	8.2E+13 13	100	96.5 4	M4	317	0.31	96Tc	4.28d	
99	43Tc	142.63 3	(1/2)⁻	2.167E+4 7	0	9/2⁺	6.72E+12 16	1.7	142.63 3	M4	41	0.04	98Tc	4.2E+6y	0.9+?
99	43Tc	142.63 3	(1/2)⁻	2.167E+4 7	140.508 4	(7/2)⁺	1.96E-10 10	98.3	2.17 1	E3			98Tc	4.2E+6y	0.9+?
96	45Rh	52.0 1	2⁺⁺	90.6 12	0	5⁺⁺	594 6	60 5	52.0 1	M3	654	0.09	95Rh	5.02m	
97	45Rh	258.8 3	(1/2)⁻	2.66E+3 5	0	(9/2)⁺	1.87E+3 5	4.9 5	258.7 3	M4	2.60	1.4	96Rh	9.6m	
100	45Rh	339.5	(5⁺)	282	74.8	2⁺	2.14E-7	93	264.7	M3	0.53	61	99Rh	16.1d	
101	45Rh	157.32 4	9/2⁺	3.750E+5 8	0	1/2⁻	1.04E+8 10	7.7 6	157.32 3	M4	29.7	0.25	100Rh	20.8h	
103	45Rh	39.756 6	7/2⁺	3.367E+3 1	0	1/2⁻	STABLE	100	39.757 6	E3	1.462E+3	0.068	102Rh	2.9y	
104	45Rh	128.956 10	5⁺	260 3	51.422 2	2⁺	2.6E-9 2	95.6	77.53 1	E3	43.9	2.1	103Rh	STABLE	11+134
104	45Rh	128.956 10	5⁺	260 3	97.114 3	2⁺	<6E-10	4.0	31.8 2	M3	6.846E+3	5.8E-4	103Rh	STABLE	11+134
105	45Rh	129.781 4	1/2⁻	45	0	7/2⁺	1.273E+5 2	100	129.782 4	E3	4.00	20	104Rh	42.3s	
107	46Pd	214.9 5	11/2⁻	21.3 5	0	5/2⁺	2.05E+14 9	100	214.9 5	E3	0.455	69	106Pd	STABLE	0.013+0.28
109	46Pd	188.990 10	11/2⁻	281.4 6	0	5/2⁺	4.93E+4 4	100	188.990 10	E3	0.81	55	108Pd	STABLE	0.19+8
111	46Pd	172.2 1	11/2⁻	1.98E+4 4	0	5/2⁺	1.404E+3 12	73 3	172.18 8	E3	1.18	33.5	110Pd	STABLE	0.02+0.21
101	47Ag	274.0 7	1/2⁻	3.10 10	98.1 2	7/2⁺		100	176.2 5	E3	1.113	47	100Ag	2.0m	
102	47Ag	9.2 4	2⁻	462 30	0	5⁺	774 18	49 5	(9.2)	(M3)	1.40E+7	3.5E-6	101Ag	11.1m	
103	47Ag	134.44 4	1/2⁻	5.7 3	0	7/2⁺	3.94E+3 4	100	134.44 5	E3	3.70	21	102Ag	12.9m	
104	47Ag	6.9 4	2⁻	2.01E+3 12	0	5⁺	4.15E+3 6	33 5	6.9 4	M3	7.3E+7 7	4.5E-7	103Ag	65.7m	
105	47Ag	25.472 12	7/2⁺	434 10	0	1/2⁻	3.567E+6 6	99.66 7	25.48 2	E3	2.2397E+4	4.2E-3	104Ag	69.2m	
107	47Ag	93.13 2	7/2⁺	44.3 2	0	1/2⁻	STABLE	100	93.12 2	E3	20.4	4.7	106Ag	24.0m	
108	47Ag	109.472 7	6⁺	4.0E+9 7	79.140 2	2⁻	1.2E-9 4	8.7 6	30.332 8	M4	4.57E+5	2E-5	107Ag	STABLE	0.35+38
109	47Ag	88.0341 11	7/2⁺	39.6 2	0	1/2⁻	STABLE	100	88.04 5	E3	26.7	3.6	108Ag	2.37m	
110	47Ag	117.59	6⁺	2.1579E+7 3	1.113	2⁻	6.6E-7 4	1.36 6	116.48 5	M4	168.3	8.0E-3	109Ag	STABLE	4.6+87
111	47Ag	59.82 4	7/2⁺	64.8 8	0	1/2⁻	6.44E+5 1	99.3 2	59.77 4	E3	186	0.53	110Ag	24.6s	
													110mAg	249.76d	80
113	47Ag	43.2 10	(7/2)⁺	68.7 16	0	1/2⁻	1.93E+4 2	80	43.2 10	E3	1.10E+3	0.073	112Ag	3.14h	
111	48Cd	396.22 3	11/2⁻	2.92E+3 2	245.42 1	5/2⁺	8.50E-8 7	100	150.825 15	E3	2.30	30	110Cd	STABLE	0.10+11
113	48Cd	263.59 12	11/2⁻	4.45E+8 16	0	1/2⁺	2.9E+23 6	0.14	263.7 3	E5	5.1	0.02	112Cd	STABLE	?+2.2
112	49In	156.5 1	4⁺	1.254E+3 12	0	1⁺	864 12	100	155.5 2	M3	6.80	12.8	111In	2.83d	
114	49In	190.34 6	5⁺	4.278E+6 1	0	1⁺	71.9 1	95.7 3	190.29 3	E4	5.21	15	113In	STABLE	8+3.9
116	49In	289.660 6	8⁻	2.18 4	127.267 6	5⁺	3.249E+3 4	100	162.390 3	E3	1.73	37	115In	STABLE	87+75+41
118	49In	200	(8⁻)	8.5 3	60	(5⁺)	267 3	98.5	138.2 5	E3	3.60	21	117In	43.8m	
113	50Sn	77.39 2	7/2⁺	1.28E+3 2	0	1/2⁺	9.944E+6 3	91 2	77.38 2	M3+E4	181 5	0.50	112Sn	STABLE	0.30+0.7
117	50Sn	314.58 4	11/2⁻	1.176E+6+3	158.56 2	3/2⁺	2.79E-10 9	100	156.02 3	M4	46.4 3	2.1	116Sn	STABLE	0.006+0.1
119	50Sn	89.530 13	11/2⁻	2.53E+7 1	23.870 8	3/2⁺	1.81E-8 1	100	65.66 1	M4	5.00E+3	2.0E-2	118Sn	STABLE	0.05+0.2
121	50Sn	6.30 8	11/2⁻	1.73E+9 16	0	3/2⁺	9.74E+4 1	78 2	6.29 8	(M4)	9.4E+10		120Sn	STABLE	0.001+0.16
128	50Sn	2091.48 12	(7⁻)	6.5 5	2000.35 7	(4⁺)		100	91.15 10	E3	26.6	3.6	127Sn	2.10h	
129	50Sn	35.2 3	(11/2⁻)	402 24	0	(3/2⁺)	130 2	2E-4	35.2 3	(M4)	2.53E+5	8E-10	128Sn	59.1m	
122	51Sb	163 1	(8⁻)	252 12	137.50 5	(5)⁺	5.3E-4 3	100	25	E3	3.9E+4	2.6E-3	121Sb	STABLE	0.05+6.2
124	51Sb¹	10.8633 11	5⁺	93 5	0	3⁻	5.201E+6 3	75 5	10.8630 11	(M2)	2.46E+4	0.003	123Sb	STABLE	0.02+0.04+4.1
124	51Sb²	36.846 2	8⁻	1.21E+3 2	10.8633 11	5⁺	93 5	100	25.981 3	E3	3.23E+4	0.003	123Sb	STABLE	0.02+0.04+4.1
126	51Sb¹	17.7 3	(5⁺)	1.14E+3 2	0	(8⁻)	1.07E+6 1	14 4	17.7 3	E3	3.19E+5	4E-5	125Sb	2.73y	
126	51Sb²	40.4 3	(3⁻)	11	17.7 3	(5⁺)	1.14E+3 2	100	22.70 7	M2	744	0.13	125Sb	2.73y	

TABLE 1. (Continued)

ISOMER	INITIAL LEVEL			FINAL LEVEL			GAMMA-RAY					PARENT		
A Z	E (keV)	Jπ	$T_{1/2}$ (sec)	E (keV)	Jπ	$T_{1/2}$ (sec)	IT (%)	E (keV)	Mult.	ICC	$I_{\gamma\gamma}$ (%)	A Z	$T_{1/2}$	SIGMA(N,G) IB+GB
^{121m}Te	293.98 3	11/2⁻	1.33E+7 6	212.19 3	3/2⁺	6.2E-11 15	88.6 11	81.788 15	M4	1.785E+3	0.05	120Te	STABLE	0.3+2
^{123m}Te	247.46 6	11/2⁻	1.034E+7 1	158.99 3	3/2⁺	1.96E-10 9	100	88.46 3	M4	1.152E+3	0.09	122Te	STABLE	3
^{123m}Te	247.46 6	11/2⁻	1.034E+7 1	0	1/2⁺	4.1E+20	0.003	247.5 2	E5	8.3	3E-4	122Te	STABLE	3
^{125m}Te	144.722 14	11/2⁻	5.01E+6 9	35.499 10	3/2⁺	1.48E-9 1	100	109.27 2	M4	353	0.28	124Te	STABLE	0.04+7
^{125m}Te	144.722 14	11/2⁻	5.01E+6 9	0	1/2⁺	STABLE	1E-4	144.78 3	E5	252	4E-7	124Te	STABLE	0.04+7
^{127m}Te	88.26 8	11/2⁻	9.4E+6 2	0	3/2⁺	3.37E+4 3	97.6 2	88.26 8	M4	1.167E+3	0.08	126Te	STABLE	0.13+0.9
^{129m}Te	105.50 5	11/2⁻	2.903E+6 9	0	3/2⁺	4.18E+3 2	64 7	105.50 5	M4	439	0.15	128Te	>8E+24y	0.015+0.20
^{131m}Te	182.25 2	11/2⁻	1.08E+5 7	0	3/2⁺	1.500E+3 6	22 2	182.25 2	M4	25.8	0.82	130Te	2.5E+21y	0.02+0.22
^{130m}I	48.2	2⁻	540 6	0	5⁺	4.450E+4 4	83	48.2	M3	1.895E+3	0.04	129I	1.6E+7y	20+10
^{132m}I	120	(8⁻)	5.02E+3 10	22	(5⁺)		86 2	98.0 10	E3	21.8	3.8	131I	8.04d	80
^{133m}I	1634.21	(19/2⁻)	9	1560.2	(15/2⁻)		100	73	(M2)	25	3.8	132I	2.30h	
^{134m}I	316.3 4	8⁻	221 4	44.4 2	5⁺	<10E-9	97 4	271.9 3	E3	0.23	79	133I	20.8h	
^{125m}Xe	252.6 1	(9/2)⁻	57 1	111.8 1	(3/2)⁺		100	140.8 1	E3	4.09	20	124Xe	STABLE	28+140
^{127m}Xe	297.1 2	(9/2⁻)	69.2 9	124.81 12	(3/2⁺)	0.28E-9 1	100	172.5 3	E3	1.638	38	126Xe	STABLE	0.4+3
^{129m}Xe	236.14 5	11/2⁻	7.68E+5 2	39.578 2	3/2⁺	1.01E-9 4	100	196.56 3	M4	20.75	4.6	128Xe	STABLE	0.5+4
^{131m}Xe	163.93 1	11/2⁻	1.03E+6 1	0	3/2⁺	STABLE	100	163.930 8	M4	50.0	2.0	130Xe	STABLE	0.4+5
^{133m}Xe	233.5	11/2⁻	1.89E+5 3	0	3/2⁺	4.571E+5 9	100	233.5	M4	9.0	10	132Xe	STABLE	0.05+0.4
^{134m}Xe	1965.5 5	7⁻	0.29 2	1731.16 3	4⁺		100	232.9 15	E3	0.45	69	133Xe	5.245d	200
^{123m}Cs	159 1	(11/2⁻)	1.60 15	94.5 6	(5/2⁺)	9E-9 3	100	63.9 6	(E3)	241.5	0.4	122Cs	4.5m	
^{124m}Cs	462.54 9	(7)⁺	6.3 2	301.10 6	(4)⁻	6.9E-8 3	2.2	161	(E3)	2.33	0.66	123Cs	5.87m	
^{124m}Cs	462.54 9	(7)⁺	6.3 2	397.65 8	(5)⁻		98	64.90 5	M2	47.8	2.0	123Cs	5.87m	
^{134m}Cs	138.747 3	8⁻	1.048E+4 4	0	4⁺	6.50E+7 2	0.52 5	138.72 2	M4	132	4E-3	133Cs	STABLE	2.6+27
^{136m}Cs	138.747 3	8⁻	1.048E+4 4	11.246 2	5⁺	4.6E-8 1	100 2	127.502 2	E3	6.89	13	135Cs	STABLE	2.6+27
^{138m}Cs	79.9 3	(6⁻)	174 6	0	3⁺⁻¹	1.932E+3 6	81 3	79.9 3	M3	218	0.37	137Cs	30.17y	
^{129m}Ba	8.42 5	(7/2)⁺	7.81E+3 14	0	1/2⁺	8.0E+3 4	<100	(8.42 5)	(E3)	4.83E+7	<2E-6	128Ba	2.43d	
^{131m}Ba	187.5 2	9/2⁻	876 12	108.5 2	3/2⁻		100	79.05 12	E3	83	1.2	130Ba	STABLE	2.5+9
^{133m}Ba	288.38	11/2⁻	1.400E+5 4	12.29	3/2⁺	8.1E-9 20	99.99	276.09	M4	4.72	17	132Ba	STABLE	0.6+7
^{135m}Ba	268.24 3	11/2⁻	1.033E+5 7	0	3/2⁺	STABLE	100	268.238 10	M4	5.40	16	134Ba	STABLE	0.16+2
^{136m}Ba	2030.5 8	7⁻	0.37 5	1866.6 8	4⁺		100	163.89 5	E3	2.258	31	135Ba	STABLE	0.14+6
^{129m}La	173.7 3	(11/2⁻)	0.56 5	68.9 2	(5/2⁻)		100	104.8 2	E3	20.3	4.7	128La	5.0m	
^{132m}La	188.7 10	6⁻	1.46E+3 3	0	2⁻	1.73E+4 7	3.0	188.7	E4	7.6	0.35	131La	59m	
^{132m}La	188.7 10	6⁻	1.46E+3 3	135.2 10	3⁻		73	53.5	M3	1.74E+3	0.042	131La	59m	
^{135m}Ce	445.4	(11/2⁻)	20 1	296.1	(5/2⁻)		100	150.2 2	E3	3.7	21	134Ce	75.9h	
^{137m}Ce	254.29 5	11/2⁻	1.24E+5 1	0	3/2⁻	3.24E+4 11	99.22 3	254.29 5	M4	8.08	11	136Ce	STABLE	1+6
^{142m}Pr	3.683 4	5⁻	876 30	0	2⁻	6.883E+4 14	100	(3.683 4)	(M3)	2E+10		141Pr	STABLE	3.9+7.5
^{144m}Pr	59.03 3	3⁻	432 18	0	0⁻	1.037E+3 3	99.96	59.03 3	M3	1.258E+3	0.08	143Pr	13.58d	
^{137m}Nd	519.6 5	11/2⁻	1.60 15	286.0 2	5/2⁺		100	233.6 3	E3	0.372	64	136Nd	50.65m	
^{139m}Nd	231.15 5	11/2⁻	1.98E+4 7	0	3/2⁺	1.78E+3 3	12 2	231.15 5	M4	14.79	0.76	138Nd	5.04h	
^{139m}Pm	188.7 3	11/2⁻	0.18 2	0	(5/2)⁺	249 3	100	188.7 3	E3	1.512E+3	0.07	138Pm	3.24m	
^{148m}Pm	137.0 1	6⁻	3.567E+6 10	75.7 1	2⁻		4.6 5	61.30 5	E4	1.36E+4	3.4E-4	147Pm	2.62y	85+97
^{139m}Sm	457.8 4	(11/2⁻)	9.5 10	267.4 4	(5/2⁺)		93.7	190.1 3	E3	1.536	37	138Sm	3.0m	
^{141m}Sm	175.8 3	11/2⁻	1.356E+3 12	1.58 4	3/2⁺		0.31 3	174.2 2	M4	69.8	4.4E-3	140Sm	14.82m	
^{141m}Eu	96.4 2	(11/2)⁻	3.3 3	0	(5/2)⁺	40.0 7	33 8	96.4 2	E3	47.1	0.69	140Eu	20s	
^{152m}Eu	147.81 11	(8)⁻	5.76E+3 6	108.1148 4	(5)⁺	≤2.0E-8	100	39.75 10	E3	7.71E+3	0.013	151Eu	STABLE	4+3300+5900

TABLE 1. (Continued)

ISOMER	INITIAL LEVEL			FINAL LEVEL			GAMMA-RAY					PARENT		
A Z	E (keV)	Jπ	T½ (sec)	E (keV)	Jπ	T½ (sec)	IT (%)	E (keV)	Mult.	ICC	Iγ (%)	A Z	T½	SIGMA(N,G) IS+GS
152₆₅Tb	501.7 2	(8)+	258 12	342.15 16	(5)-		78.9 8	159.39 10	E3	3.95	16	151Tb	17.6h	
158₆₅Tb	110 1	0-	10.5 2	0	3-	4.7E+9 9	100	109.9 15	M3	112.5	0.9	157Tb	150y	
146₆₆Dy	2935.6 7	(10+)	0.15 2	2808.8 7	(7-)		43	127.0 3	E3	13.56	3.0	145Dy	18s	
149₆₆Dy	2661.3 4	(27/2-)	0.51 1	2550.4 3	(21/2-)		100	110.9 3	E3	27.6	3.3	148Dy	3.1m	
165₆₆Dy	108.160 3	1/2-	75.5 4	0	7/2+	8.40E+3 2	97.76 8	108.160 3	E3	31.5	3.0	164Dy	STABLE	1700+1000
158₆₇Ho	67.25 5	2-	1.62E+3 12	0	5+	678 24	75	67.25 5	E3	481	0.16	157Ho	12.6m	
159₆₇Ho	205.7 2	1/2+	8.30 8	0	7/2-	1.98E+3 2	94.4	205.9 1	E3	1.382	40	158Ho	11.3m	
159₆₇Ho	205.7 2	1/2+	8.30 8	165.9 2	7/2+		5.6	39.5 3	M2	2.35E+4	2.4E-4	158Ho	11.3m	
160₆₇Ho	59.98 3	2-	1.81E+4 2	0	5+	1.54E+3 2	65 3	59.98 3	E3	910	0.07	159Ho	33m	
161₆₇Ho	211.14 3	1/2+	6.73 10	0	7/2-	8.9E+3 2	100	211.15 3	E3	1.20	45	160Ho	25.6m	
162₆₇Ho	106	6-	4.02E+3 6	96.1 1	5+		63 4	10	E3	3.2E+7		161Ho	2.48h	
163₆₇Ho	297.88 8	(1/2)+	1.09 3	0	(7/2)-	1.0E+9 7	100	297.88 8	E3	0.291	77	162Ho	15m	
164₆₇Ho	140 1	6-	2.25E+3 9	94.0 1	5+		100	46	E3	4.54E+3	0.02	163Ho	>10y	
167₆₈Er	207.801 5	1/2-	2.28 3	0	7/2+	STABLE	100	207.801 5	E3	1.40	42	166Er	STABLE	15+5
169₇₀Yb	24.201 2	1/2-	46 2	0	7/2+	2.7667E+6 7	100	24.20 2	E3	2.66E+5	4E-4	168Yb	STABLE	23E+2
176₇₀Yb	1050.7 7	(8)-	11.4 5	954.6 6	8+	4E-12 1	100	96.1 3	E1	0.382	72	175Yb	4.19d	
177₇₀Yb	331.5 3	1/2-	6.41 2	104.5 2	7/2+	4.48E-9 8	100	227.0 2	M3	7.1	12	176Yb	STABLE	3
166₇₁Lu	34.37	(3-)	85 6	0	(6-)	159 6	42 5	34.37	(M3)	3.5E+4	1.2E-3	165Lu	12m	
169₇₁Lu	29.0 5	1/2-	160 10	0	7/2+	1.22AE+5 2	100	29.0 5	E3	9.75E+4	1E-3	168Lu	5.5m	
170₇₁Lu	93.0	4-	0.67 10	44.52	2+	3.00E-9 6	100	48.42	M2	240	0.4	169Lu	34.06h	
171₇₁Lu	71.3 2	1/2-	79 2	0	7/2+	7.12E+5 3	100	71.1 2	E3	484	0.21	170Lu	2.00d	
172₇₁Lu	41.86 4	(1-)	222 30	0	(4-)	5.79E+5 3	100	41.86 4	M3	2.8E+4	3.6E-3	171Lu	8.24d	
174₇₁Lu	170.86 4	(6-)	1.23E+7 2	111.78 4	(3-)		89	59.08 2	M3	3.32E+3	0.03	173Lu	1.37y	
174₇₁Lu	170.86 4	(6-)	1.23E+7 2	44.70 3	(2-)		10	126.2	(E4)	266	0.04	173Lu	1.37y	
177₇₁Lu	970.15 5	23/2-	1.390E+7 3	854.32 2	17/2+		100	115.83 4	E3			176Lu	3.6E+10y	5 +2300
177₇₂Hf[A]	1315.4 1	23/2+	1.08 6	1086.9 1	19/2+		100	228.44 6	E2	0.19	84	176Hf	STABLE	26
177₇₂Hf[B]	2740.0 3	37/2-	3.08E+3 3	2526.0 2	31/2+		100	214.0 1	E3	1.5	40	176Hf	STABLE	26
178₇₂Hf	1147.44 3	8-	4.0 2	1058.52 2	8+		100	88.878 15	E1	0.55	65	177Hf	STABLE	1.0+370
179₇₂Hf[A]	374.8	(1/2)-	18.68 6	214.3	(7/2)-	1.86E-9 5	99.98	160.7	M3	34.8	2.8	178Hf	STABLE	50+30
179₇₂Hf[B]	1105.7	(25/2-)	2.17E+6 3	848.3	(19/2+)		5.3	257.3 2	E3	0.65	3.2	178Hf	STABLE	50+30
179₇₂Hf[B]	1105.7	(25/2-)	2.17E+6 3	1084.7	(21/2+)		(95)	21.03 14	(M2)	1.2E+4	8E-3	178Hf	STABLE	50+30
180₇₂Hf	1141.56 6	8-	1.98E+4 4	1084.02 3	8+		86.4	57.549 1	E1	0.33	65	179Hf	STABLE	0.45+ 41
182₇₂Hf	1172.9	(8-)	3.69E+3 9	1122.1	8+		21	50.9 2	E1	0.43	15	181Hf	42.39d	
182₇₃Ta	16.5 4	5+	0.283 3	0	3-	9.94E+6 2	100	16.5 4	M2	1.5E+4	7E-3	181Ta	STABLE	0.11+ 20.5
182₇₃Ta	519.7 4	10-	950 6	334.8 4	7+		98	184.951 15	E3	3.3	23	181Ta	STABLE	0.11+ 20.5
179₇₄W	221.9	(1/2-)	384 18	0	(7/2-)	2.25E+3 3	99	221.5 2	M3	10.8	8	178W	21.7d	
183₇₄W	309.491 4	(11/2)+	5.15 3	99.078 1	5/2-	8.6E-10 6	2.6	210.3 1	(E3)	1.89	0.9	182W	STABLE	21
183₇₄W	309.491 4	(11/2)+	5.15 3	207.010 2	7/2-		97	102.481 3	M2	40.3	2.3	182W	STABLE	21
185₇₄W	197.41 4	11/2+	100 2	65.86 3	9/2-		90	131.55 2	E3	19.75	4.3	184W	>3E+17y	0.002+1.8
185₇₄W	197.41 4	11/2+	100 2	173.68 2	7/2-	<1.5E-9	6.7	23.54	(M2)	8.69E+3	7E-4	184W	>3E+17y	0.002+1.8
185₇₄W	197.41 4	11/2+	100 2	187.88 2	(5/2-)		3.3	(9.53)	(E3)	4.13E+7		184W	>3E+17y	0.002+1.8
184₇₅Re	188.01 4	8+	1.43E+7 4	0	3-	3.28E+6 4	0.6	188.01	(E5)	237	2.5E-3	183Re	70.0d	
184₇₅Re	188.01 4	8+	1.43E+7 4	104.729 4	4-		74.1	83.28 4	M4	1.36E+4	5E-3	183Re	70.0d	
186₇₅Re	150	8+	6E+12	99.362	(3)-		100	50	E5	1E+6		185Re	STABLE	111
188₇₅Re	172.069 9	(6)-	1.116E+3 6	156.047 4	(3)-		100	15.93 10	M3	2.3E+7	4E-6	187Re	5E+10y	2.8+75
190₇₅Re	173	(6)-	1.15E+4 7	119.12 5	(3)-		45 3	(54)	(M3)	8.8E+3		189Re	24.3h	

TABLE 1. (Continued)

ISOMER	INITIAL LEVEL			FINAL LEVEL			GAMMA-RAY					PARENT		
A Z	E (keV)	J^{π}	$T_{1/2}$ (sec)	E (keV)	J^{π}	$T_{1/2}$ (sec)	IT (%)	E (keV)	Mult.	ICC	$I_{\gamma\gamma}$ (%)	A Z	$T_{1/2}$	SIGMA(N,G) IS+GS
$^{183m}_{76}$Os	170.72 9	(1/2$^-$)	3.56E+4 11	0	(9/2$^-$)	4.7E+4 2	16	170.72 9	M4	230	0.07	182Os	21.5h	
$^{189m}_{76}$Os	30.83 3	9/2$^-$	2.09E+4 4	0	3/2$^-$	STABLE	100	30.82 4	M3	3.17E+5	3.2E-4	188Os	STABLE	5
$^{190m}_{76}$Os	1705.4 2	10$^-$	594 6	1666.5 2	8$^-$		100	38.9 1	M2+E3	1.24E+3	0.08	189Os	STABLE	0.26mb+20
$^{191m}_{76}$Os	74.38 1	3/2$^-$	4.72E+4 2	0	9/2$^-$	1.33E+6 1	100	74.38 1	M3+E4	1.355E+3	0.07	190Os	STABLE	9+4
$^{192m}_{76}$Os	2015.4 2	(10$^-$)	5.9 1	1968.0 2	(7$^-$)		11	(47.4 2)	(E3)	7.76E+3	1E-3	191Os	15.4d	400
$^{190m}_{77}$Ir^{1}	26.3 1	(7)$^+$	4.32E+3	0	(4)$^+$	1.018E+6 9	100	26.3 1	M3	9.74E+5	1E-4	189Ir	13.2d	
$^{190m}_{77}$Ir^{2}	175.0 1	(11)$^-$	1.15E+4 7	26.3	(7)$^+$	4.32E+3	5.6 10	148.7 1	M4	493	0.011	189Ir	13.2d	
$^{191m}_{77}$Ir	171.29 2	11/2$^-$	4.94 3	129.396 7	5/2$^+$	8.9E-11 2	100	41.85 1	E3	1.744E+4	0.006	190Ir	11.78d	
$^{192m}_{77}$Ir^{1}	58.0 4	1$^{(-)}$	87 3	0	4$^{(-)}$	6.3790E+6 7	99.9825	58.0 4	E3	2.55E+3	0.04	191Ir	STABLE	0.2+310+630
$^{192m}_{77}$Ir^{2}	155.16 12	(9$^+$)	7.6E+9 3	0	4$^{(-)}$	6.3790E+6 7	100	155.16 12	(E5)	1.026E+3	0.10	191Ir	STABLE	0.2+310+630
$^{193m}_{77}$Ir	80.24 4	11/2$^-$	9.16E+5 9	0	3/2$^+$	STABLE	100	80.27 4	M4	2.19E+4	0.005	192Ir	73.831d	1400
$^{195m}_{77}$Ir	120	(11/2$^-$)	1.37E+4 7	0	(3/2$^+$)	9.0E+3 11	4 2	120	(M4)	1.70E+3	0.002	194Ir	19.15h	
$^{193m}_{78}$Pt	149.78 4	(13/2)$^+$	3.74E+5 3	14.28 1	(5/2)$^-$	2.52E-9 5	100	135.50 3	M4	905	0.11	192Pt	STABLE	1+9
$^{195m}_{78}$Pt	259.4 2	13/2$^+$	3.473E+5 9	129.757 15	9/2$^-$	6.7E-10 3	100	129.5 2	M4	1.18E+3	0.08	194Pt	STABLE	0.10+1.1
$^{191m}_{79}$Au	266.2 4	(11/2$^-$)	0.92 11	252.5 2	(5/2)$^+$		100	13.7 6	(E3)	1.19E+7	8E-6	190Au	42.8m	
$^{192m}_{79}$Au	431.7	(11)$^-$	0.167	371.9	(8)$^+$		100	59.8	E3	2.49E+3	0.04	191Au	3.18h	
$^{193m}_{79}$Au	290.2 2	(11/2$^-$)	3.9 3	257.97 4	(5/2)$^+$	4.5E-11 20	99.97	32.2 1	E3	9.55E+4	1E-3	192Au	4.94h	
$^{194m}_{79}$Au^{1}	107.4 7	(5$^+$)	0.600 8	80.52 16	3$^-$		100	26.9 5	(M2)	7.814E+3	0.013	193Au	17.65h	
$^{194m}_{79}$Au^{2}	475.8 15	(10$^-$)	0.420 10	406.8 9	(8$^-$)	2.9E-9 4	100	69.0 7	(M2)	108	0.92	193Au	17.65h	
$^{195m}_{79}$Au	318.59 7	11/2$^-$	30.5 2	261.77 5	5/2$^+$	5.4E-11 10	99.46	56.80 3	E3	3.364E+3	0.03	194Au	39.5h	
$^{196m}_{79}$Au^{1}	84.66 2	5$^+$	8.1 2	0	2$^-$	5.342E+5 9	100	84.66 2	E3	334	0.30	195Au	186d	
$^{196m}_{79}$Au^{2}	595.66 4	12$^-$	3.49E+4 4	420.75 3	8$^-$	2.0E-9 2	100	174.91 2	M4	236	0.42	195Au	186d	
$^{197m}_{79}$Au	409.2 2	11/2$^-$	7.8 1	279.0 1	5/2$^+$	1.86E-11 15	99.5	130.2 1	E3	30.3	3.2	196Au	6.183d	
$^{198m}_{79}$Au	811.7 15	(12$^-$)	1.99E+5 3	696.5 2	(8$^-$)		100	115.2 15	(M4)	2.59E+3	0.04	197Au	STABLE	0+98.7
$^{193m}_{80}$Hg	141.0	13/2$^+$	4.25E+4 7	39 49 3	5/2$^-$	0.63E-9 3	8	101.5	M4	6.29E+3	1.3E-3	192Hg	4.85h	
$^{195m}_{80}$Hg	176.08 4	13/2$^+$	1.50E+5 3	53.30 3	5/2$^-$	7.2E-10 3	54 2	122.78 3	M4	1.92E+3	0.03	194Hg	520y	
$^{197m}_{80}$Hg	298.95 9	13/2$^+$	8.57E+4 4	133.98 5	5/2$^-$	8.1E-9 2	93.0 7	164.97 7	M4	348	0.27	196Hg	STABLE	120+3100
$^{195m}_{81}$Tl	482.7 2	9/2$^-$	3.6 4	383.64 15	3/2$^+$		100	99.0 6	E3	160	0.62	194Tl	33.0m	
$^{196m}_{81}$Tl	394.7 7	(7$^+$)	5.08E+3 7	274.6 6	(3$^-$)		4.5	120.1 3	M4	2.4E+3	1.9E-3	195Tl	1.16h	
$^{197m}_{81}$Tl	608.3 2	9/2$^-$	0.54 1	385.85 10	3/2$^+$		100	222.45 5	E3	2.28	30	196Tl	1.84h	
$^{198m}_{81}$Tl	543.7 4	7$^+$	6.73E+3 11	282.8 2	3$^-$		46 2	260.9 3	M4	35.2	1.3	197Tl	2.84h	
$^{197m}_{82}$Pb	319.3 7	13/2$^+$	2.68E+3 5	84.9 2	5/2$^-$		19 2	234.4 7	M4	63.8	0.29	196Pb	37m	
$^{202m}_{82}$Pb	2169.79 12	9$^-$	1.30E+4 1	2040.34 7	5$^-$		24	129.2 1	E4	524	0.045	201Pb	9.33h	
$^{203m}_{82}$Pb^{1}	825.2 1	13/2$^+$	6.3 2	820.3 3	(7/2)$^-$		6	4.9 2	(E3)	5.9E+9	1E-9	202Pb	5.3E+4y	
$^{203m}_{82}$Pb^{2}	2949.3 3	29/2$^+$	0.48 2	2796.1 2	(23/2)$^+$		81	153.4 2	E3	15.81	4.8	202Pb	5.3E+4y	
$^{198m}_{83}$Bi	248.5 5	(10$^-$)	7.7 5	0	(7$^-$)	711 11	100	248.5 5	E3	1.567	39	197Bi	?	
$^{203m}_{83}$Bi	1098.15 9	1/2$^+$	0.303 5	908.64 7	7/2$^-$		90	189.51 8	E3	5.75	13	202Bi	1.72h	
$^{203m}_{83}$Bi	1098.15 9	1/2$^+$	0.303 5	893.50 8	(5/2)$^-$		10	204.65 7	E3+(M2)	4.9 2	1.7	202Bi	1.72h	
$^{207m}_{84}$Po	1383.2 1	19/2$^-$	2.8 2	1115.07 2	13/2$^+$	4.9E-5 4	100	268.1 1	E3	1.19	46	206Po	8.8d	
$^{237m}_{94}$Pu	145.544 10	1/2$^+$	0.18 2	0	7/2$^-$	3.91E+6 2	100	145.552 12	E3	52.9	1.9	236Pu	2.851y	
$^{242m}_{95}$Am	48.63 5	5$^-$	4.45E+9 6	0	1$^-$	5.767E+4 7	99.54 1	48.63 5	E4	6.9E+5	1.4E-4	241Am	432.2y	50+550

The definitions, policies, and symbols used in the Nuclear Data Sheets are followed throughout this work.

1. Scope

This compilation includes all known isomers which have a half-life (level) $\geq$ 0.1 seconds, a de-exciting γ-ray with energy $\leq$ 300 keV, and for which the branching ratio and multipolarity of this transition are known, or can be estimated.

References 5 through 10 were used as sources for this compilation.

F. EXPLANATION OF TABLE

The table lists 199 isomers with 215 transitions and was prepared from information, described in step 2, Section E (p. 17). The primary sources for the data and the policies for selection of this information are explained in the introductions to the Appendices.

The following shorthand is used throughout the table: Powers of ten are expressed in the form E ± x and the uncertainty in the last significant figure(s) is shown following the number. Thus, $3.12 \pm 0.03 \times 10^5$ is given as 3.12E + 5 3.

The information in this table falls into five groups:

1. Information on the isomeric state
   A, Z, E, J pi, and $T_{1/2}$--self-explanatory.
2. Information on the final level of the transition
   E, J pi, and $T_{1/2}$--self-explanatory.
3. Isomeric Transition Branching Ratio--IT(%)
   This is the percent of branching of this particular transition (photons + conversion electrons).
4. Gamma-ray properties--Properties of the transition in question.

E(keV) Transition Energy.

Occasionally, the energy given in this column does not agree exactly with the difference between the

energies given for the two nuclear levels involved. This is understandable, because the energy given here is the adopted transition energy obtained from gamma-ray and/or internal conversion electron measurements, while the adopted level energies are derived values based on all measurements leading to these particular levels.

Mult.-Gamma-ray multipolarity.

A mixture of multipolarities is given only if it has been shown experimentally that the transition is of mixed multipolarity.

ICC-Internal conversion coefficient I_{ce}/I_{γ}.

The value adopted by the Nuclear Data Sheets is given. If no value was given in Nuclear Data Sheets, then a theoretical value was obtained by interpolation from either Ref. 9 or 10.

I_{γ}(%)-Photon intensity.

Percent of decay of level by photons of this energy.

5. Properties of the parent for the production of the isomer by neutron capture.

AZ	Target for neutron capture
$T_{1/2}$	Half-life of the target nucleus
σ(N,G)	Neutron capture cross section
IS+GS	In several cases, cross sections are given for the production of three different isomeric states [i.e., IS(1) + IS(2) + GS].

III. STUDY OF THE PHOTON GAIN CONDITION FOR LONG-LIVED NUCLEAR ISOMERIC TRANSITIONS

A. INTRODUCTION

The proposed methods for making a γ-ray laser (Ref. 3 and 11) all require the preparation of nuclei in excited states. Additionally, the proposed concepts require a sufficiently large cross section for stimulated emission of photons that a coherent γ-ray pulse is produced. Together, these two factors enter into the threshold condition for lasing discussed by Baldwin (Ref. 3) and others (Ref. 12 and 13). This threshold condition is an essential, but not sufficient, requirement (Ref. 14) in the development of a γ-ray laser. We use this condition to study candidate nuclei. Other requirements concern the temporal evolution of the γ-ray pulse.

The difficulties with most γ-ray laser schemes are summarized by Baldwin (Ref. 3). In summary, shorter-lived nuclear electromagnetic transitions (half-life $t_{1/2} \leq 1$ μsec) demand very stringent pumping requirements to attain the necessary population inversion. On the other hand, transitions involving longer-lived excited nuclear states (isomers with $t_{1/2} > 1$ sec) are more readily pumped to large population inversions. Unfortunately, the natural linewidth for resonant photon absorption is so narrow that inhomogeneous broadening effects lead to prohibitively great reductions in the resonant absorption cross section.

In previous reports (Ref. 1), parametric studies of certain isotopes were undertaken to determine the extent to which physical conditions had to be controlled to obtain a positive laser gain. The effects of inhomogeneous line broadening and

some details of the pumping requirements were particularly addressed. However, for the isotopes identified and studied, the internal conversion coefficients were high and prevented gain, even though the other parameters were near favorable. After a thorough search of isomers, those with the largest gain coefficients were selected and calculations performed to determine the conditions required for lasing to be feasible.

Approximately 2600 nuclides have been identified (Ref. 5 through 10). The proton numbers (Z) and total nucleon numbers (A) for these nuclides range in values from Z = 0 to Z = 107 and A = 1 to A = 263, including stable and unstable ground states, isomers, and fission isomers. Of these nuclides, 279 are stable isotopes of 80 elements. We count 400 excited state isomers, of which we find around 310 with half-lives greater than one second. Since we are primarily interested in γ-rays with energies less than approximately 100 keV, we limit our study to 183 of the identified isomers, or 194 actual transitions. We additionally study some hypothetical isomeric transitions.

B. BACKGROUND: NUCLEAR ISOMERS

The structure of atomic nuclei is basically understood in terms of the nuclear shell model (Ref. 15). The illustrative single-particle levels are depicted in Fig. 4. Nuclear states near closed shells can have significantly differing angular momentum, which leads to isomers (Ref. 16). Many isomers originate from other mechanisms, as described in more suitable models -- we use the convention adopted in the Table of Isotopes, Ref. 7) in distinguishing the isomers as "isomers" (spin, shape, etc.) or "fission isomers."

C. THE THRESHOLD CONDITION FOR LASER GAIN

The photon gain condition in a laser is met when the rate of addition of photons to a radiation mode is greater than the rate of removal. This condition (Ref. 11 and 14) is expressed as

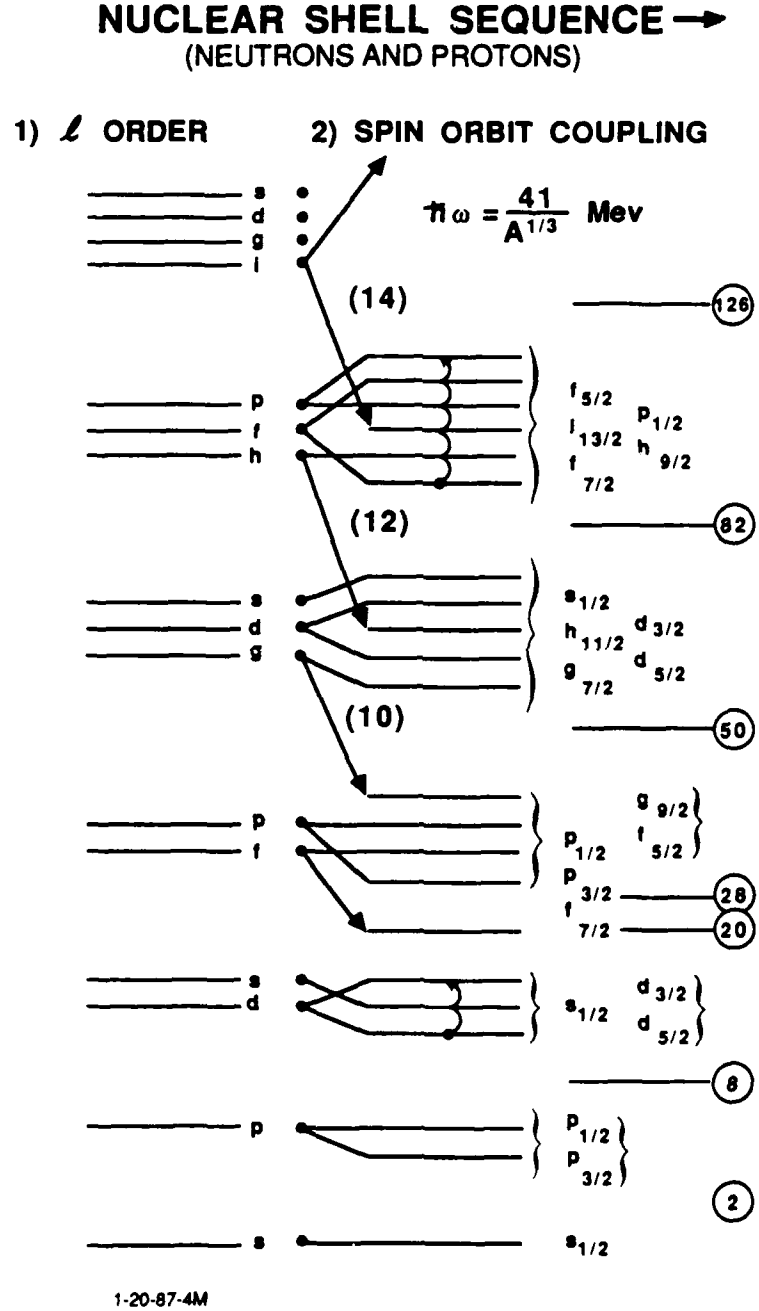

FICURE 4. Nuclear shell model levels

$$\sigma_R n^* \geq \sigma_a n_o \quad , \tag{1}$$

where σ_R is the cross section at resonance for the radiation-induced transition, σ_a is the total non-resonant photon removal cross section, n_o is the total atom density, and n^* is the statistically weighted population inversion. Here,

$$n^* = n_e - \frac{g_e n_g}{g_g} \quad , \tag{2}$$

where n_e and n_g are the excited state and lower state nuclear number densities, respectively; g_e and g_g are the spin degeneracies of the excited and lower nuclear states. It is convenient to introduce a coefficient μ (cm^{-1}) which includes all photon loss terms due to non-nuclear effects. The gain coefficient, K, is defined as

$$K = \sigma_R n^* - \mu \quad . \tag{3}$$

The gain coefficient can be positive or negative. For lasing to occur, K must be positive. The loss coefficient μ is, in a simple approximation, a product of μ_e, the linear extinction coefficient, and the laser operating mode M. The quantity M is discussed by Trammell and Hannon (Ref. 17). Balko and Wasylkiwskyj (Ref. 11) point out that for steady state operation M=1, for pulsed operation M=21, and in the Dicke superradiator mode M = ln (n*V), where V is the active volume of participating nuclei.

We consider the Schawlow-Townes threshold condition in this study. That is, we restrict ourselves to eq. (3). We intend to further address superradiant pulse formation in future work.

In eq. (3) the resonance cross section σ_R is given by

$$\sigma_R = \frac{2\pi\lambda^2 \beta \, f g}{(1+\alpha)(1+a)} \left(\frac{\Gamma_\gamma}{\Gamma_\gamma + \Gamma_g} \right) , \tag{4}$$

where the terms are defined as follows:

$\lambda\!\!\!^{-}$ is the nominal wavelength of the emitted photon divided by 2π

α is the internal conversion coefficient

β is the branching ratio for the nuclear decay of interest

Γ_γ is the natural radiation linewidth of the nuclear transition energy E_o

Γ_g is the natural radiation linewidth of the ground state

a is the inhomogeneous line-broadening factor. This line broadening is due to various effects, such as hyperfine electric monopole interactions (isomer shift), magnetic dipole interactions (Zeeman-shift), and electric quadrupole interactions due to electric field gradients. These and other contributors to inhomogeneous broadening are discussed in Ref. 3, 11, 12, and 14.

f the recoilless fraction, is given by:

$$f = \exp\left\{\left(\frac{-3R}{2k\theta_{eff}}\right)\left[1+\frac{2}{3}\left(\frac{\pi T}{\theta_{eff}}\right)^2\right]\right\}. \qquad (5)$$

This factor gives the fractional number of photons per decay emitted and absorbed without loss of energy to the lattice. The quantity R is the recoil energy of the nucleus, θ_{eff} is the effective Debye temperature of the solid and T is the absolute equilibrium temperature of the system.

g is a coupling factor of the nuclei to the radiation mode.

The linear extinction coefficient $\mu_e = \sigma_a n_o$, where σ_a is the cross section for non-resonant photon absorption or scattering. Photon absorption or scattering occurs due to the photoelectric, Compton, and pair production processes.

As will be seen, on the nuclear level (unlike the atomic level) the gain due to stimulated emission of photons is about six to nine orders of magnitude smaller than the loss of photons, ($\sigma_R n^*/\mu_e \approx 10^{-6} - 10^{-9}$). Therefore, under usual conditions, lasing is strongly inhibited. Special conditions and nuclear transitions with specific and unusual characteristics are required to obtain lasing. Actual nuclei are examined in Subsection D.

D. THRESHOLD GAINS ($\sigma_R n^*$) FOR ISOMERIC TRANSITIONS

Equation (3) of the previous section can be used to examine the properties of real nuclei. Since many parameters enter into eq. (3), such a study could be quite extensive. We consider here the ordering of isomeric transitions in terms of the positive part of the gain term, $\sigma_R n^*$. Nuclear data was obtained from Ref. 5 through 10. The types of data obtained from these sources is listed below. For a detailed discussion refer to A. Artna-Cohen, Chapter II.

- Excited state energy (keV)
- Excited state half-life (s)
- Excited state spin (integral or half integral quantum number)
- Lower state energy (keV)
- Lower state half-life (s)
- Lower state spin (integral or half integral quantum number)
- Branching ratio (ratio of decay rates)
- Internal conversion coefficient (ratio of e/γ)
- Approximate thermal neutron absorption cross section (barns)

The specific nuclei which are examined comprise the isomeric transitions listed in Table 2. Isomers other than those listed have γ-ray energies greater than 100 keV. We do not study these latter transitions here. Some transitions with energies greater than or near 100 keV are included as examples.

TABLE 2. ISOMER LIST

List of isomeric nuclides from ref.(7). Long-lived isomers which we study in this report are highlighted in bold type. Notes are included at the bottom summarizing the notation used throughout the list.

Na	24m						
Al	24m	26m					
Cl	34m	38m					
K	38m						
Sc	42m	44m	45m	46m	50m		
Mn	50m	52m					
Fe	53m						
Co	53m	54m	58m	60m	62(g)	62(m)	
Cu	68m	70(g)	70(m)				
Zn	69m	71m					
Ga	74m						
Ge	73m	75m	77m	79m			
Se	73m	77m	79m	81m	83m		
Br	74m	77m	79m	80m	82m	84m	
Kr	79m	81m	83m	85m			
Rb	78m	81m	82m	84m	86m	90m	
Sr	83m	85m	87m				
Y	85(g)	85(m)	86m	87m	89m	90m	91m
	93m	97(g)	97(m)				
Zr	85m	87m	89m	90m			
Nb	90m	91m	92m	93m	94m	95m	97m
	98m	99m					
Mo	91m	93m					
Tc	93m	94m	95m	96m	97m	99m	102m
Ru	93m						
Rh	95m	96m	97m	98(g)	98(m)	99m	100m
	101m	102m	103m	104(1,2)m		105m	106m
Pd	107m	109m	111m				
Ag	101m	102m	103m	104m	105m	106m	107m
	108m	109m	110m	111m	113m	116m	118m
	120m						
Cd	111m	113m	115m	117m	119m		
In	105m	107m	109m1	109m2	111m	112m	113m
	114m	115m	116m1	116m2	117m	118m	119m
	121m	123(g)	123(m)				

Sn	113m	117m	119m	121m	123m	125m	127m
	128m	129m	130m				
Sb	116m	118m	122m	124m1	124m2	126m1	126m2
	128(g)	128(m)					
Te	119m	121m	123(1,2)m		125(1,2)m		127m
	129m	131m	133m				
I	118m	120m	130m	132m	133m	134m	
Xe	125m	127m	129m	131m	133m	134m	
	135m						
Cs	123m	124(1,2)m		134(1,2)m		135m	136m
	138m						
Ba	129m	131m	133m	135m	136m	137m	
La	129m	132(1,2)m					
Ce	135m	137m	139m				
Pr	138m	142m	144m				
Nd	137m	139m	141m				
Pm	140m	148m					
Sm	139m	141m	143m				
Eu	141m	152m1	152m2	154m			
Gd	145m						
Tb	149m	152m	154m1	154m2	156m	158m	
Dy	147m	165m					
Ho	158m1	158m2	159(1,2)m		160m	161m	162m
	163m	164m	166m				
Er	167m						
Tm	162m	163m	164m				
Yb	169m	176m	177m				
Lu	166m1	166m2	168m	169m	170m	171m	172m
	174(1,2)m		176m	177m	178m		
Hf	177m1	177m2	178m1	178m2	179m1	179m2	180m
	182m						
Ta	180(g)	180(m)	182m1	182m2			
W	179m	183(1,2)m		185(1,2,3)m			
Re	184(1,2)m		186m	188m	190m		
Os	183m	189m	190m	191m	192m		

TABLE 2. (Continued)

Ir	**190m1**	**190m2**	**191m**	**192m1**	**192m2**	**193m**	**194m**
	195m	**196m**					
Pt	**193m**	**195m**	197m	**199m**			
Au	189m	191m	**193m**	**195m**	**196m1**	**196m2**	**197m**
	198m	200m					
Hg	185(g)	185(m)	<191m1	<191m2	**193m**	**195m**	**197m**
	199m						
Tl	185m	186m	187m	193m	194m	195m	196m
	197m	198m	206m	207m			
Pb	197m	199m	201m	202m	203m1	203m2	204m
	207m						
Bi	191m	193m	195m	197m	198m	199(g)	199(m)
	200m	201m	210m	212m1	212m2		
Po	195(g)	195(m)	197m	199m	201m	203m	**207m**
	211m	212m					
At	198m	200(g)	200(m)	212m	216m		
Rn	201(g)	201(m)	202m	203m			
Fr	214m						
Ra	213m						
Ac	216m	222m					
Th							
Pa	234m						
U	235m	235f	236f	238f			
Np	237f	238f	240m				
Pu	235f	236f1	236f2	237m	237f1	237f2	238f1
	238f2	239f1	239f2				
	240f1	240f2	241f1	241f2	242f1	242f2	243f
	244f						
Am	235f	236f	237f	238f	239f	240f	241f
	242m	242f	243f				
	244m	244f	245f	246f			
Cm	240f	241f	242f1	242f2	244f1	244f2	
Bk	242f1	242f2	243f	244f	245f		
Cf	246f						
Es	254f	250m					
Md							
No	254m						
Lr							

Z	104	260m	
Z	105	260m	261m
Z	106		
Z	107		

Notes

1. The symbols of the form "m1" and "m2" refer to more than one metastable state for a given isotope.
2. The symbol "<" signifies metastable states of elements for which the atomic mass is unknown.
3. The symbols "f", "f1", etc. refer to fission isomers.
4. The symbols "(1,2)" refer to more than one transition studied for a given isomer.
5. Isomers in bold type are studied in this report as discussed in the text.
6. The symbols (g) and (m) appear within sets of isomers for which the ground state is uncertain but most likely the state denoted.
7. Elements "Z" are currently not named.

We now discuss particular aspects of the data which we use. Where known, experimental values for internal conversion coefficients are used. In some cases, estimates using Ref. 6 and 9 are used in analyzing partial experimental data. In cases where no experimental data are known, we estimate the internal conversion coefficients solely from theoretical curves.

The recoilless fraction is discussed in Ref. 3. The Debye temperatures used are listed in Table 3; we assume elemental forms in all cases (Ref. 18 and 19). For elements showing allotropy we list the higher of the Debye temperatures. For the elements whose Debye temperatures were not found, we assumed a Debye temperature of 300K. In the overall analysis, this assumption applies to the metals Sc, Y, Tc, Po, Pu, Am, Es, and rare earth metals, excluding Gd. For the general survey, we assume an equilibrium temperature of 10K, which is quite low relative to typical metallic Debye temperatures. As seen from eq. (5), the recoilless fraction is less sensitive to the exact Debye temperature at low equilibrium temperatures.

For small doping concentrations, the effective Debye temperature is approximated by:

$$\theta_{eff} = \sqrt{\frac{M_H}{M_I}}\,\theta_H \quad . \tag{6}$$

The mass of the isomer in all cases is taken to be the integral atomic mass number (M_I). Here M_H and θ_H are the host mass and Debye temperature, respectively. Density and mass data for elements of terrestrial isotopic composition were obtained from Ref. 20. This density information is used in calculating effective Debye temperatures in doped crystalline materials. Thus, for dopings of the isomer in natural hosts of terrestrial isotopic abundance, very small shifts in θ_{eff} are insignificant with respect to expected errors in θ_{eff}, so that the computed recoilless fractions are applicable even to high population inversions.

TABLE 3. DEBYE TEMPERATURES

Element	Debye Temp. (^{o}K)	Atomic Wt.	Atomic Number
Be	1100	9	4
Na	150	24	11
K	100	40	19
Rh	385	104	45
Co	385	60	27
Ag	215	108	47
Cd	172	110	48
Ne	63	20	10
Ar	85	40	18
Kr	63	83.8	36
Xe	55	131.3	54
Li	277	6.94	3
Rb	58	85.4	37
Cs	42	132.9	55
Cu	304	63.5	29
Au	155	197	79
Ca	220	40.1	20
Sr	148	87.6	38
Ba	115	137.4	56
Al	375	27	13
Th	145	232	90
C	1800	12	6
Si	505	28.1	14
Ge	211	72.6	32
Sn	260	118.7	50
Pb	68	207.2	82
V	300	51	23
Nb	252	92.9	41
Ta	230	181	73
N	68	14	7
Cr	405	52	24
Mo	360	96	42
W	270	183.9	74

(continued)

TABLE 3. DEBYE TEMPERATURES (Continued)

Element	Debye Temp. (^{o}K)	Atomic Wt.	Atomic Number
Mn	350	54.9	25
Fe	355	55.9	26
Ni	375	58.7	28
Pd	263	106.4	46
Ir	285	192.2	77
Pt	225	195.1	78
He	28.4	4.003	2
H	105	1.008	1
Mg	290	24.3	12
Zn	200	65.4	30
Hg	37	200.6	80
La	132	138.9	57
Gd	152	157.3	64
U	200	238.1	92
B	1250	10.8	5
Ge	125	69.7	31
In	78	114.8	49
Tl	96	204.4	81
Ti	342	47.9	22
Zr	250	91.2	40
Hf	213	178.5	72
Sn	163	118.7	50
As	224	74.9	33
Sb	140	121.8	51
Bi	62	209	83
O	91	16	8
Se	135	79	34
Te	120	127.6	52
Re	275	186.2	75
Cl	115	35.5	17
Br	110	79.9	35
I	106	126.9	53
Ru	400	101.1	44
Os	250	190.2	76

The recoil energy used is given by the expression:

$$R = (5.32 \times 10^{-4}) E_o^2 / M \quad \text{in eV} \tag{7}$$

for E_o in keV and M in atomic mass units (Ref. 3). The operating mode has no effect on the positive gain terms discussed in this section. Other operating modes affect the photon loss term discussed in Subsection E.

The linear extinction coefficient is found using the empirical relations (Ref. 3):

$$\sigma_{cs} = 0.658 \; Z \exp [-2.95 \times 10^{-3} \; E_o] \quad \text{barns} \tag{8}$$

for the Compton scattering cross section, and

$$\sigma_{ph} = \kappa Z^{4.5} E_o^{-3.0} \quad \text{barns} \tag{9}$$

for the photoelectric cross section. Here κ is approximately 8.5 for $E_K < E_0$, 0.7 for $E_L < E_0 < E_K$, and 0.115 for $E_0 < E_L$ where E_K and E_L are the electron K and L shell-binding energies. These latter binding energies are approximately given by:

$$E_K = 9.67 \; (Z/30)^{2.16} \quad \text{keV} \tag{10}$$

and

$$E_L = 1.18 \; (Z/30)^{2.6} \quad \text{keV.} \tag{11}$$

(Pair production does not contribute at energies below 1.02 MeV.)

In the first analysis of the 196 candidate isomers we choose to fix the population inversion at 100 percent ($n^* = n_e$). In Subsection F we evaluate n^* from neutron pumping kinetics. We fix the initial equilibrium temperature at 10 K. The

temperature dependence is further discussed in Subsection E. We vary the inhomogeneous broadening parameter a from 1 to 10^{10} in our study--a significant range of inhomogeneous line broadening. The ordering in the inhomogeneous line-broadening parameter a does not affect the identification of the top isomer candidates, since the a dependence enters as a simple 1/(1+a) factor in the positive gain term [see eq. (4)]. For neutron pumping calculations (Subsection F) we use the one-neutron absorption cross section σ for the production of the isomer from the nuclide having one less neutron. This value is the average thermal neutron absorption cross section. Such neutron cross sections are further discussed in Ref. 16. For unrecorded cross sections, we assume a value of one barn, which is a conservative estimate.

The top isomers in natural hosts are listed in Table 4. Of these isomers, ^{105}Rh and ^{192}Ir are discussed by Balko (Ref. 10). Of the 18 isomers listed, 7 have naturally occurring precursors with 4 having large notable neutron absorption cross sections (> 10 barns). It is interesting to find one of these four, ^{60}Co, at the top of the list. Only one isomer, ^{165}Dy, has an average neutron absorption cross section (as defined in Ref. 16) greater than 1000 barns (1700 barns). If one incorporates the candidate isomer in a 1:100 number ratio in a natural Be host, the maximum attainable population inversion decreases, although the marked improvement in effective Debye temperature increases the number of candidate isomeric nuclei. In such cases, the recoilless fraction approaches 1.0. These isomers are listed in Table 5.

E. PARAMETERS REQUIRED FOR A POSITIVE GAIN CONDITION IN REAL NUCLEI

A positive laser gain coefficient, $K = \sigma_R n^* - \mu$, is a necessary but insufficient condition for operation of a γ-ray laser. This coefficient can be computed as a function of the temperature T and the inhomogeneous line-broadening parameter a. These

TABLE 4. ISOMERS IN NATURAL HOSTS

*	60Co27	*	182m1Ta73
†	126m2Sb51		96Rh45
	58Co27		113Ag47
	105Rh45	*	165Dy66
	111Ag47		96Tc43
	103Rh45	*	124Sb51
	109Ag47		171Lu71
	107Ag47	*	113Sn50
*	94Nb41	*	192Ir77

*Indicates isomers with naturally occurring precursors.
†The symbols m1 and m2 denote metastable states in nuclei having more than one isomer.

TABLE 5: ISOMERS IN Be HOST

†	126m2Sb51		13Rh45
*	60Co27		68Cu29
	79Se34	*	94Nb41
	109Ag47	*	124Sb51
	107Ag47	*	165Dy66
	82Br35		113Ag47
	111Ag47	*	182m1Ta73
	58Co27	*	113Sn50
	77Br35		96Tc43

*Indicates isomer has naturally occurring precursor.
†The symbols m1 and m2 denote metastable states in nuclei having more than one isomer.

are two of the key physical parameters affecting the threshold operating region where lasing action could conceivably occur.

In view a of Figs. 5 through 12, we show results from the analysis of seven isotopes of choice, and one hypothetical isotope corresponding to a long-lived ^{57}Fe isomeric state with half-life 1000 sec and neutron absorption cross section of 1000 barns. We plot $\log_{10}(\sigma_R n^*)$ versus $\log_{10}(a)$ for temperatures of 10 K and 100 K and for values of $\log_{10}a$ from 1 to 10. In these figures, the horizontal axis intersects the vertical axis at $\log_{10}\mu$. Thus, the region of the graph above the horizontal axis and below the plotted curve represents combinations of a and T for which we find a net positive laser gain. Recall that $\mu = \mu_e M$. Clearly, any change in μ only adjusts the positioning of the horizontal axis. The details of the operating modes will be further studied in an ongoing investigation.

Another set of plots, Figs. 13 through 20, depicts the effects of including the isomer of choice in a Be substrate. Temperature plays a less important role due to the increased effective Debye temperature. Thus, although the gain is reduced because of the smaller population inversion, the gain curves are less temperature-sensitive. The possibility exists for improving the value of μ over its calculated value; for example, through the use of the Borrmann effect. Consequently, we display plots (view b of Figs. 5 through 12) with $\mu = 0.1\ \mu_a$.

F. DYNAMICS OF POPULATION INVERSION

The previous calculations all represent a simple treatment of threshold conditions in a laser. We now consider a calculation of the flux of neutrons necessary to prepare a sufficient population inversion of the isomeric state to obtain a positive gain coefficient. The following approach is used to compute the number of precursor nuclei (n_i), the number of isomeric nuclei (n_e), and the number of lower state nuclei (n_g). We assume the level system shown in Fig. 21. The precursor

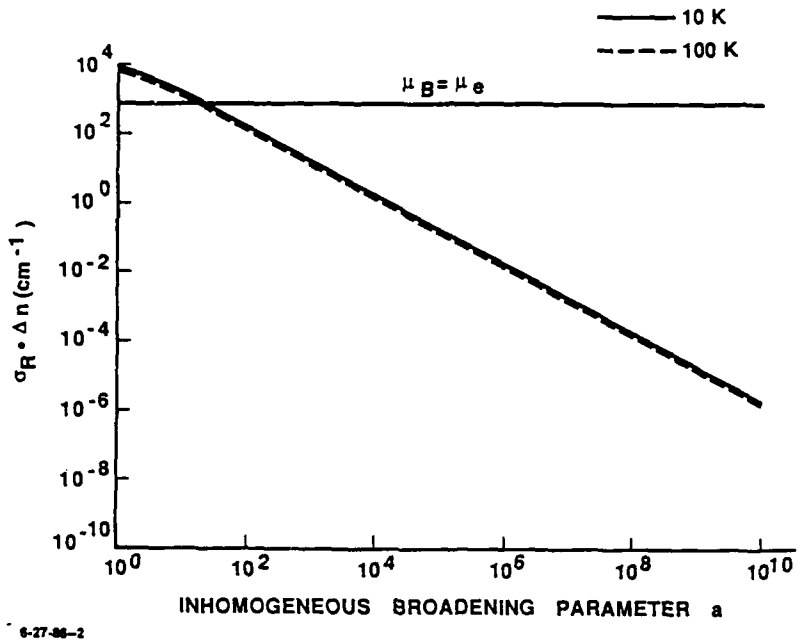

FIGURE 5a. The laser gain coefficient as a function of the inhomogeneous line-broadening parameter for an illustrative "^{57}Fe" nucleus. The nucleus is assumed to have a 1000-second lifetime and to have been produced from ^{56}Fe with a neutron absorption cross section of 1000 barns.

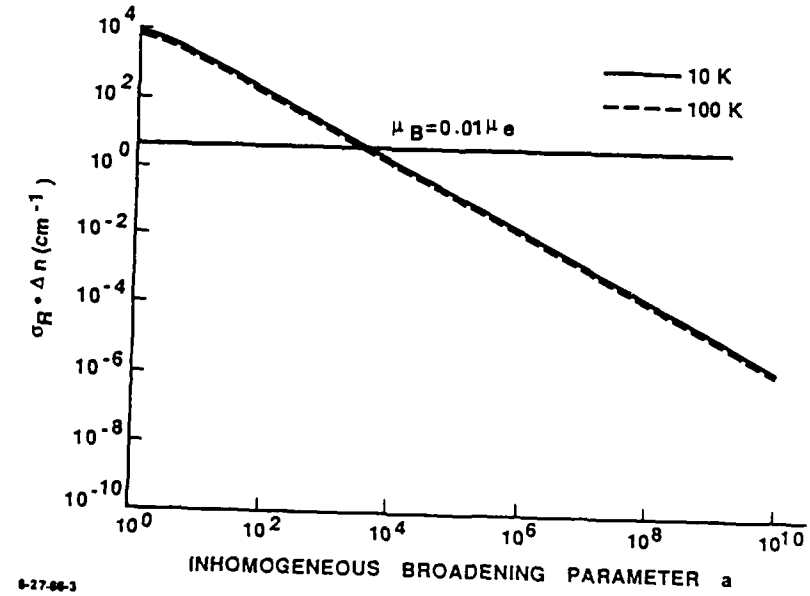

FIGURE 5b. The laser gain coefficient as a function of the inhomogeneous line-broadening parameter with an assumed Borrmann effect.

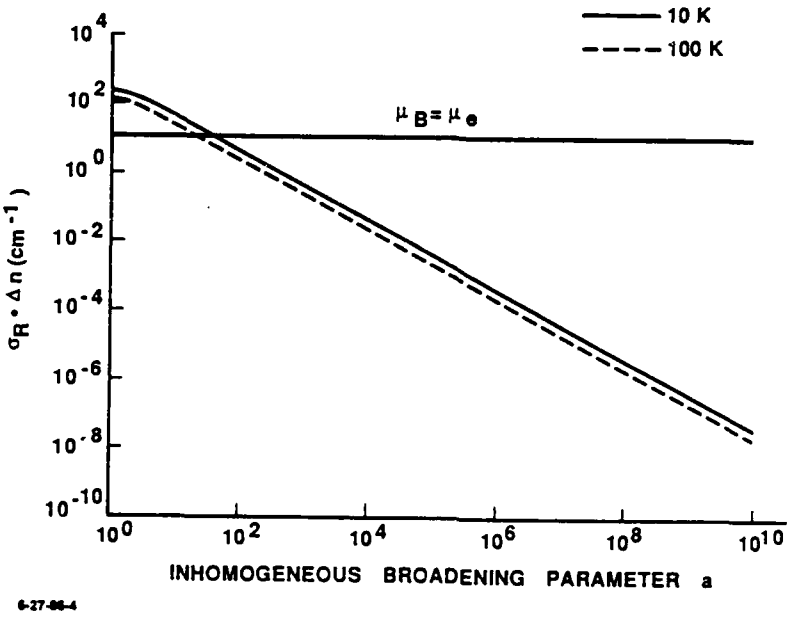

FIGURE 6a. The laser gain coefficient as a function of the inhomogeneous line-broadening parameter for ^{60}Co.

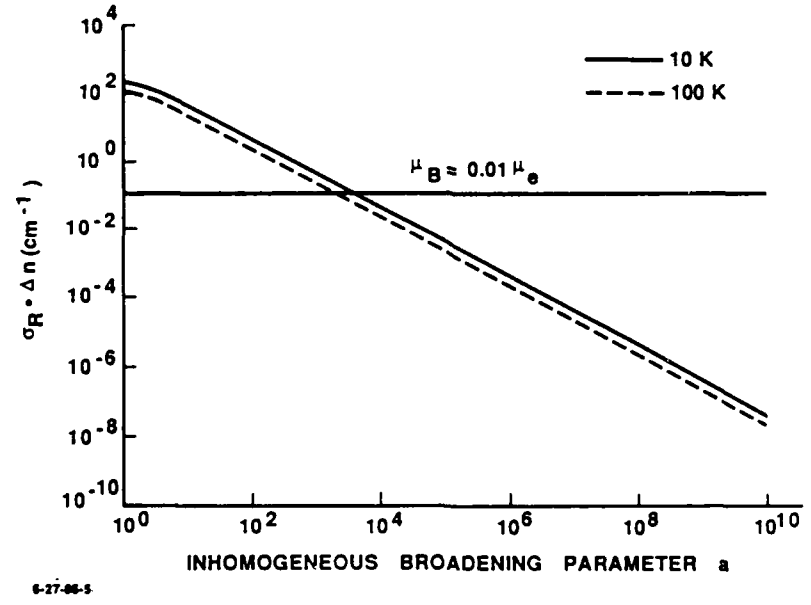

FIGURE 6b. The laser gain coefficient as a function of the inhomogeneous line-broadening parameter for ^{60}Co and an assumed Borrmann effect.

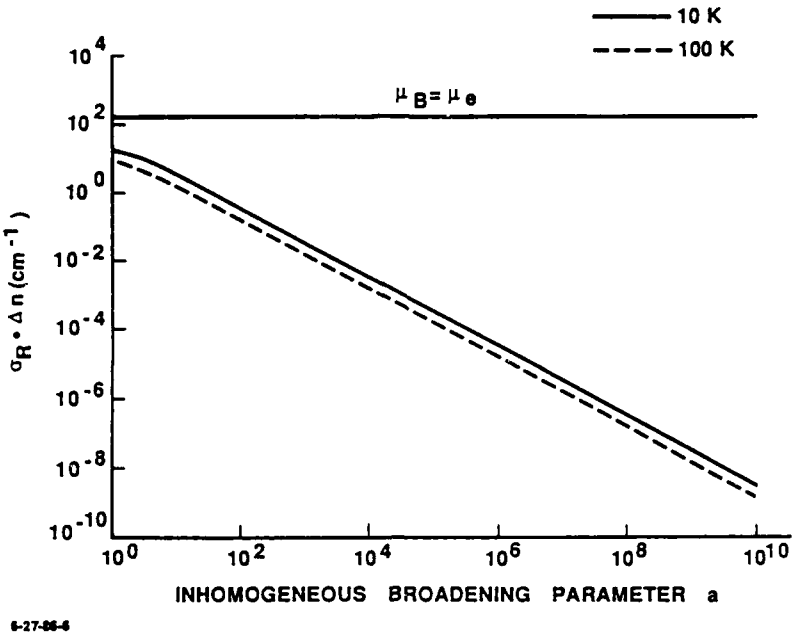

FIGURE 7a. The laser gain coefficient as a function of the inhomogeneous line-broadening parameter for ^{94}Nb.

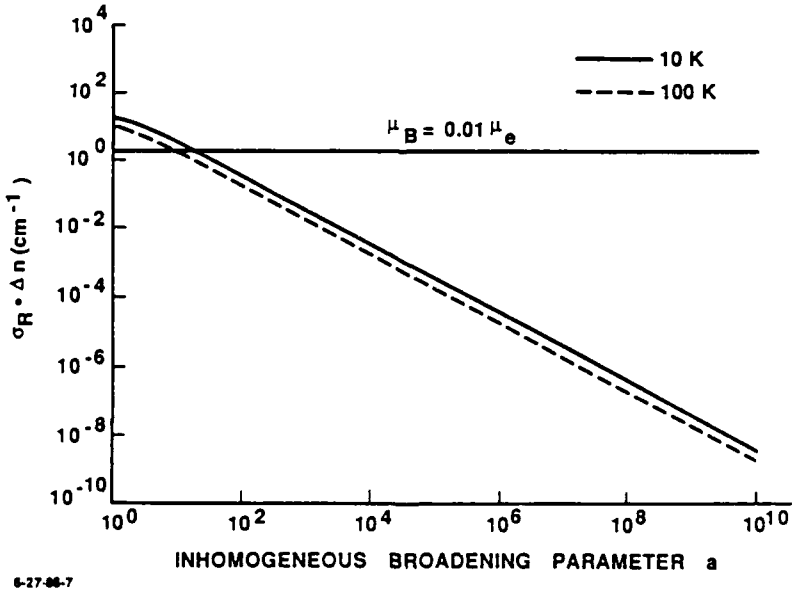

FIGURE 7b. The laser gain coefficient as a function of the inhomogeneous line-broadening parameter for ^{94}Nb with an assumed Borrmann effect.

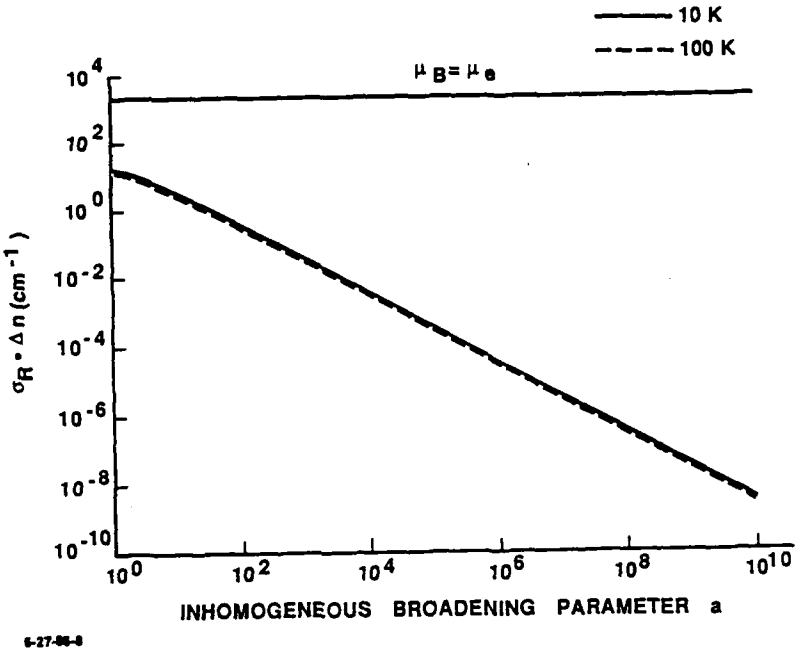

FIGURE 8a. The laser gain coefficient as a function of the inhomogeneous line-broadening parameter for the first metastable state of ^{182}Ta.

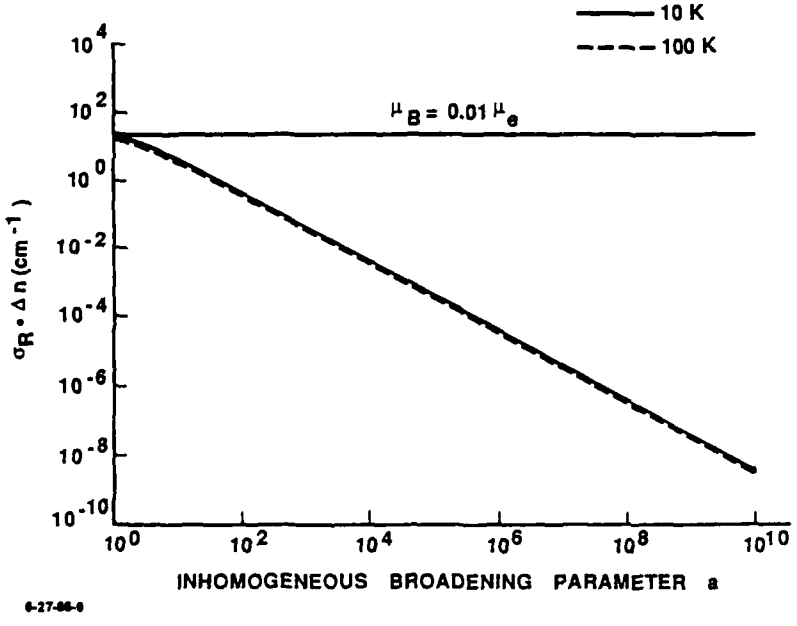

FIGURE 8b. The laser gain coefficient as a function of the inhomogeneous line-broadening parameter for the first metastable state of ^{182}Ta and an assumed Dorrmann effect.

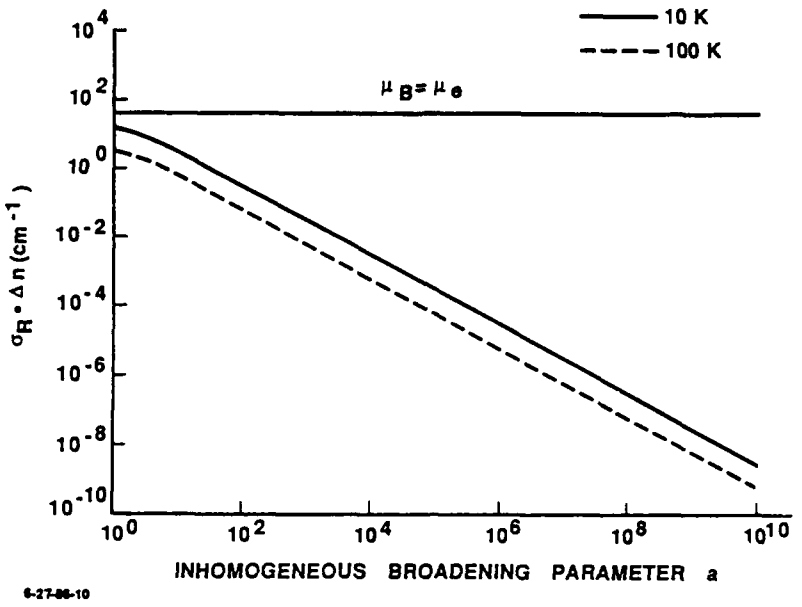

FIGURE 9a. The laser gain coefficient as a function of the inhomogeneous line-broadening parameter for ^{165}Dy.

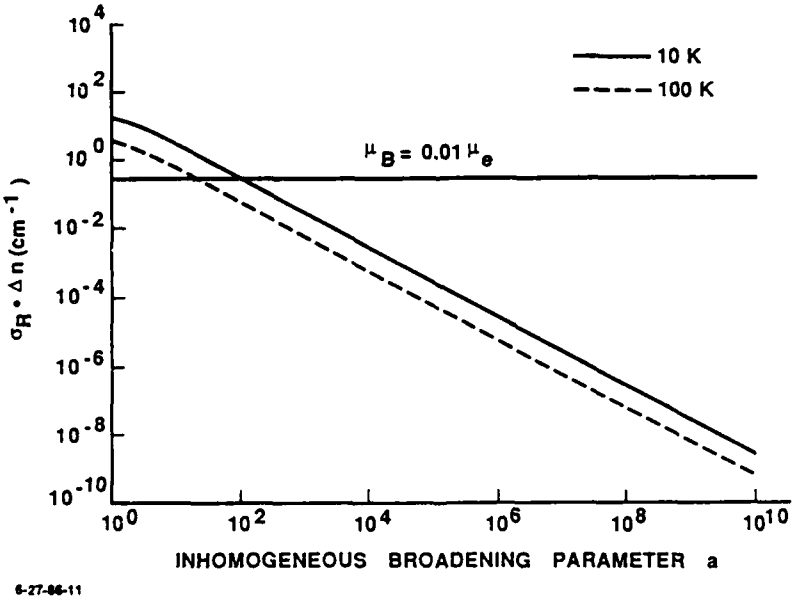

FIGURE 9b. The laser gain coefficient as a function of the inhomogeneous line-broadening parameter for ^{165}Dy with an assumed Borrmann effect.

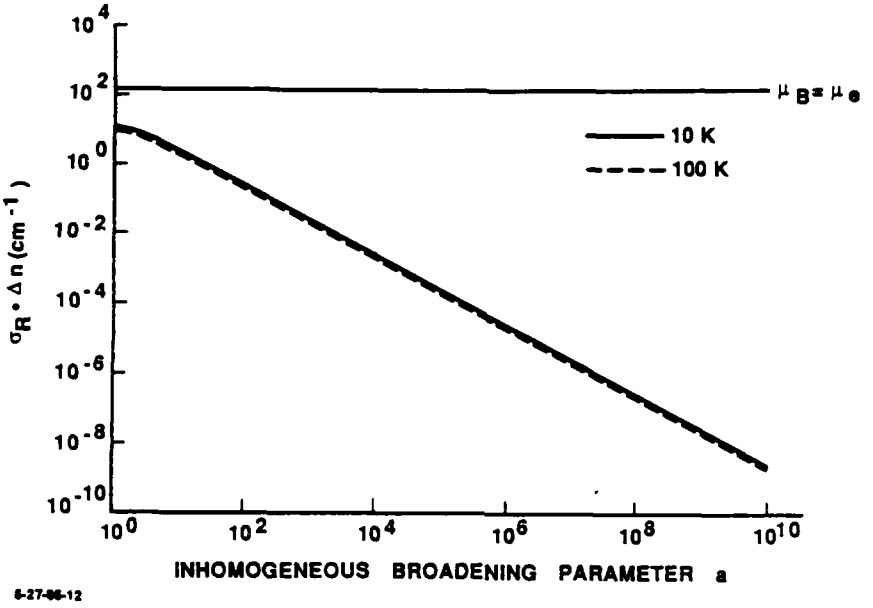

FIGURE 10a. The laser gain coefficient as a function of the inhomogeneous line-broadening parameter for $^{124m}2Sb$ (the second metastable state).

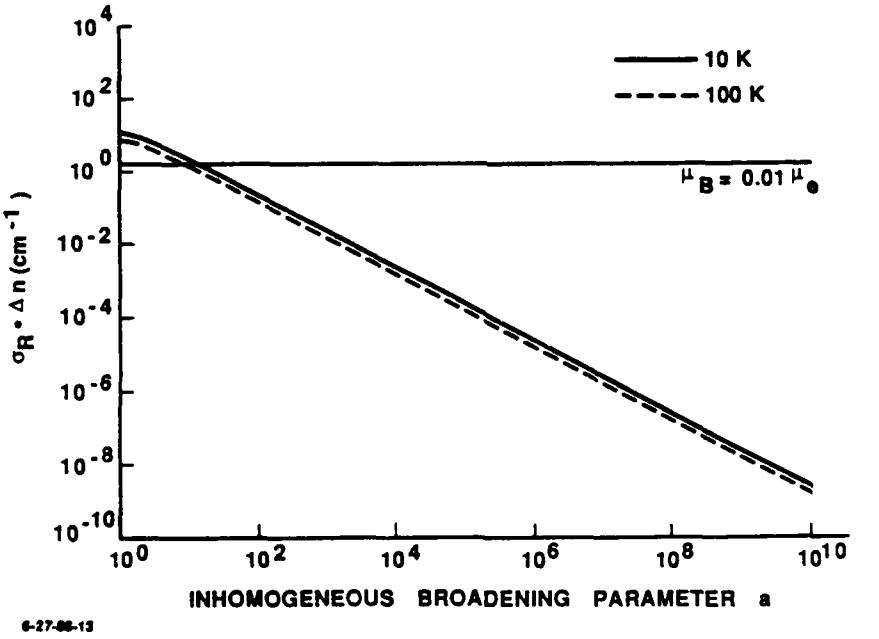

FIGURE 10b. The laser gain coefficient as a function of inhomogeneous line-broadening for $^{124m}2Sb$ and an assumed Borrmann effect.

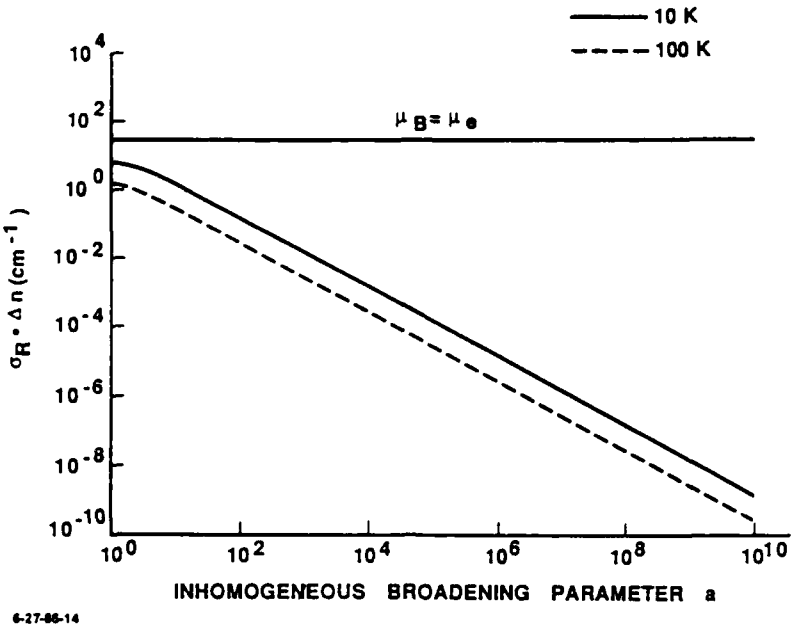

FIGURE 11a. The laser gain coefficient as a function of inhomogenecus line-broadening for ^{113}Sn.

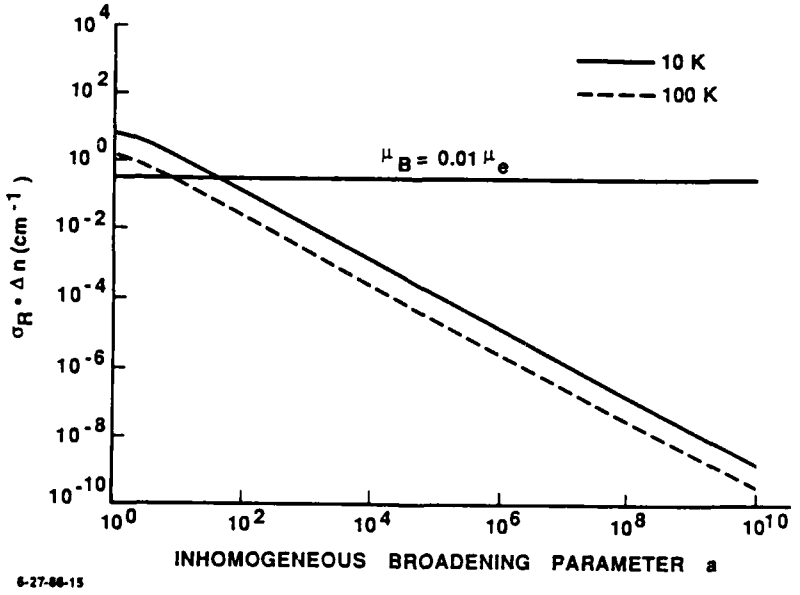

FIGURE 11b. The laser gain coefficient as a function of the inhomogeneous line-broadening parameter for ^{113}Sn and an assumed Borrmann effect.

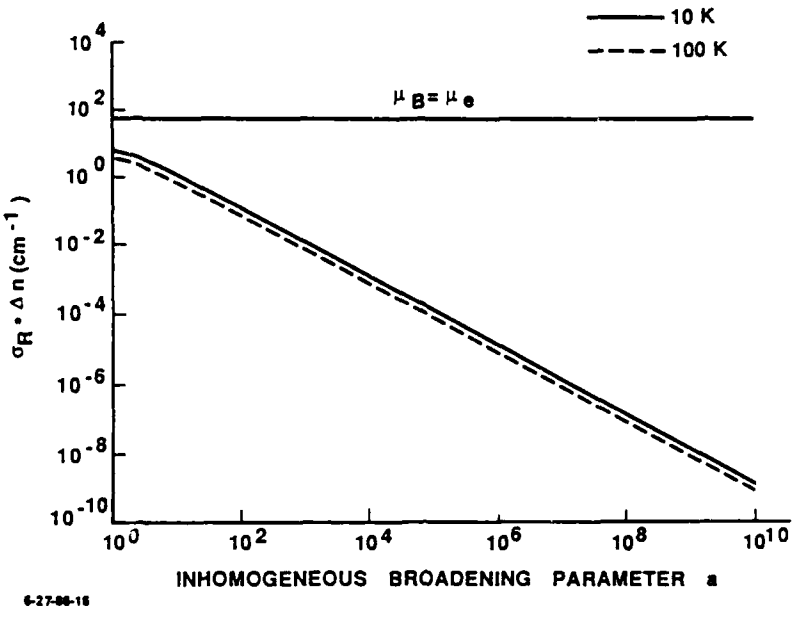

FIGURE 12a. The laser gain coefficient as a function of inhomogeneous line-broadening parameter for ^{192}Ir.

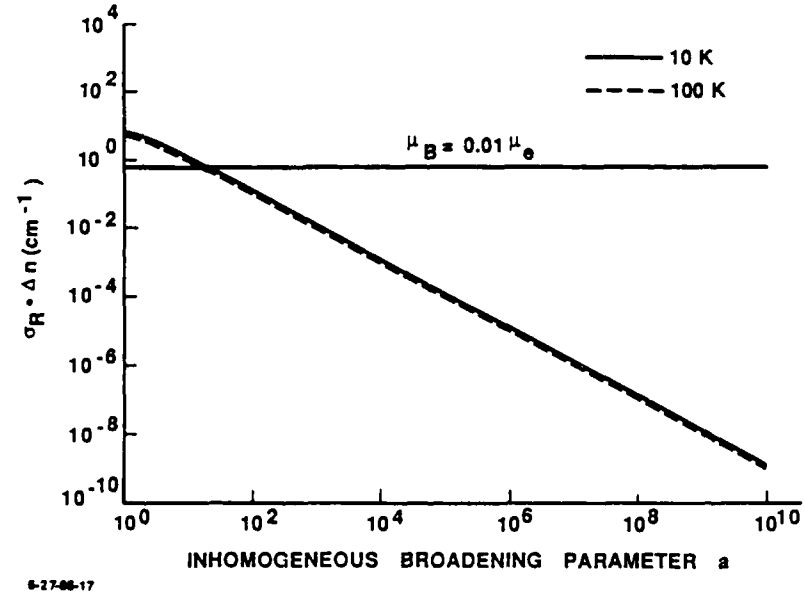

FIGURE 12b. The laser gain coefficient as a function of the inhomogeneous line-broadening parameter for ^{192}Ir with an assumed Borrmann effect.

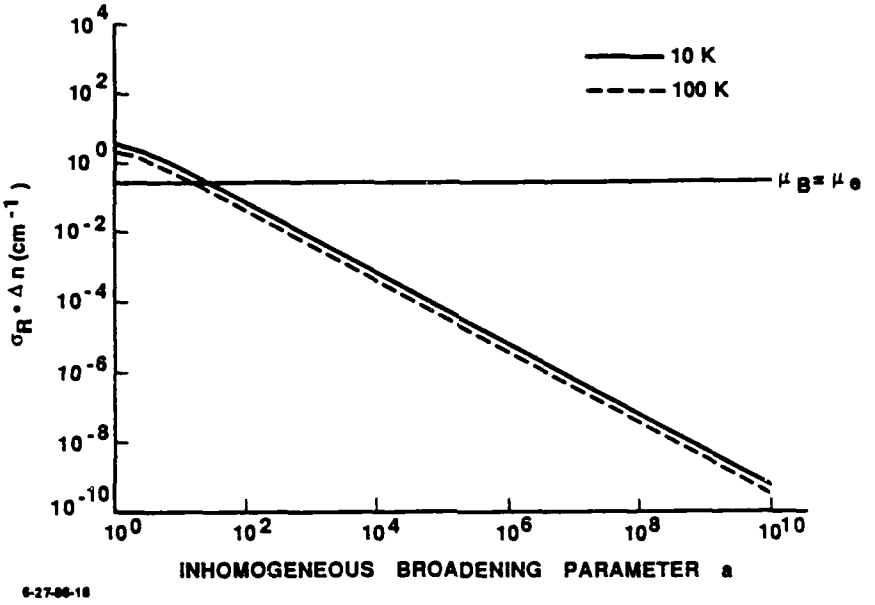

FIGURE 13. Gain for ^{60}Co in a Be host.

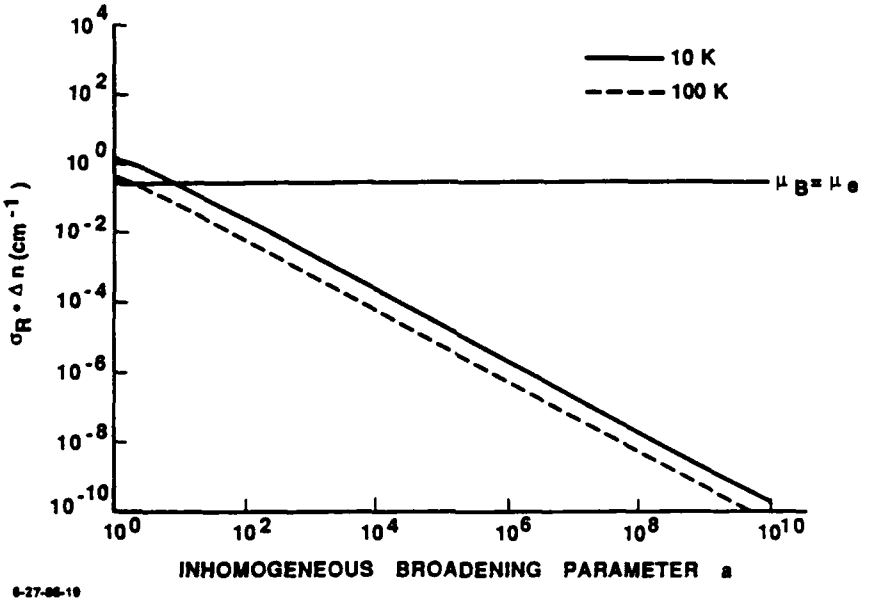

FIGURE 14. Gain for ^{79}Se in a Be host.

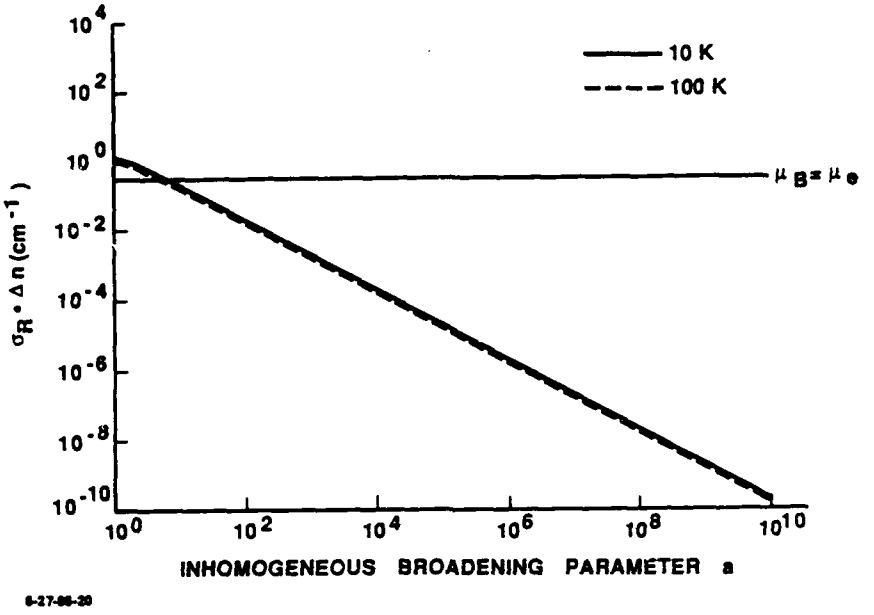

FIGURE 15. Gain for ^{82}Br in a Be host.

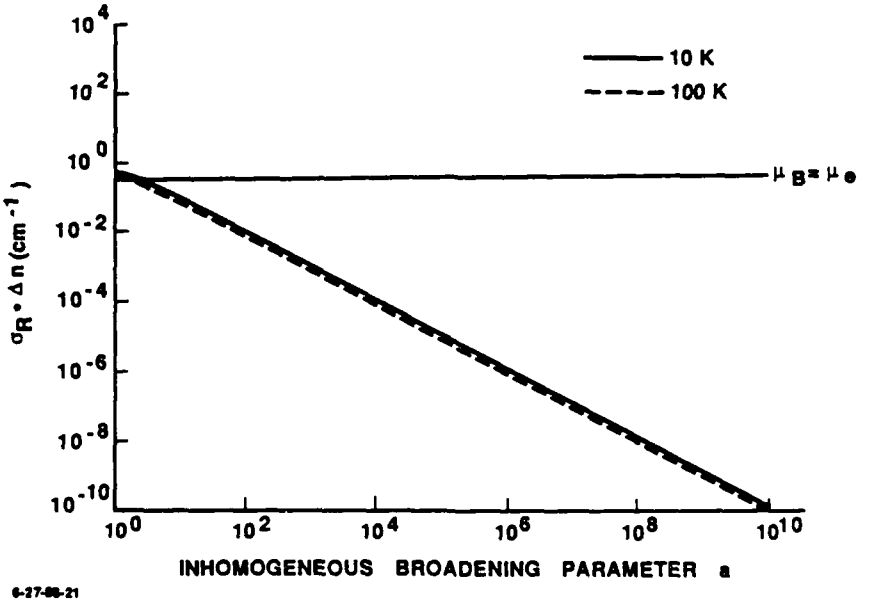

FIGURE 16. Gain for ^{94}Nb in a Be host.

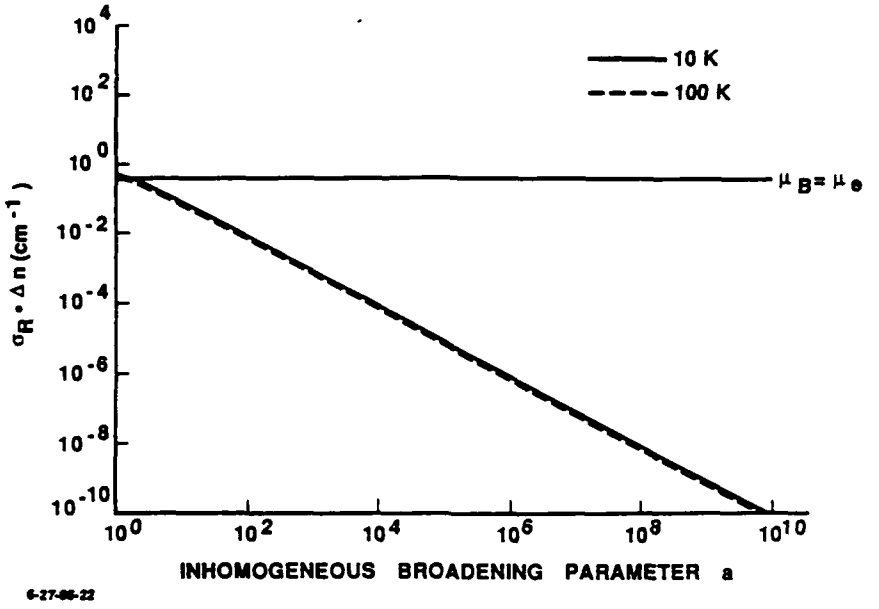

FIGURE 17. Gain for ^{124}Sb in a Be host.

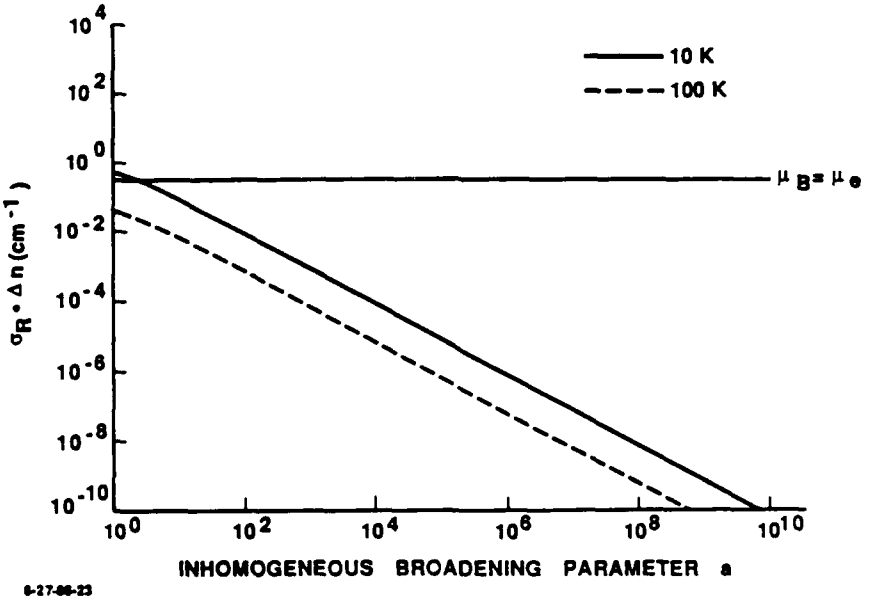

FIGURE 18. Gain for ^{165}Dy in a Be host.

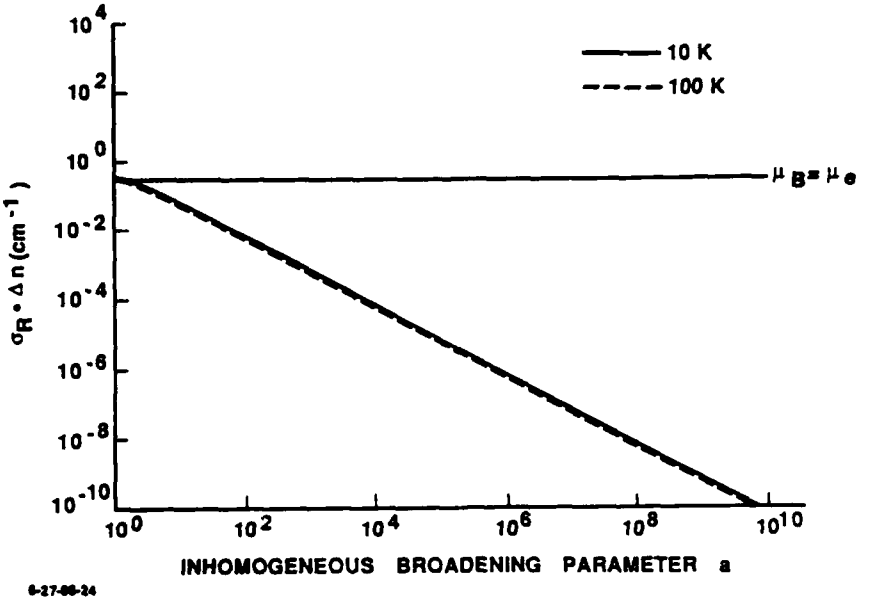

FIGURE 19. Gain for the first metastable ^{182}Ta level in a Be host.

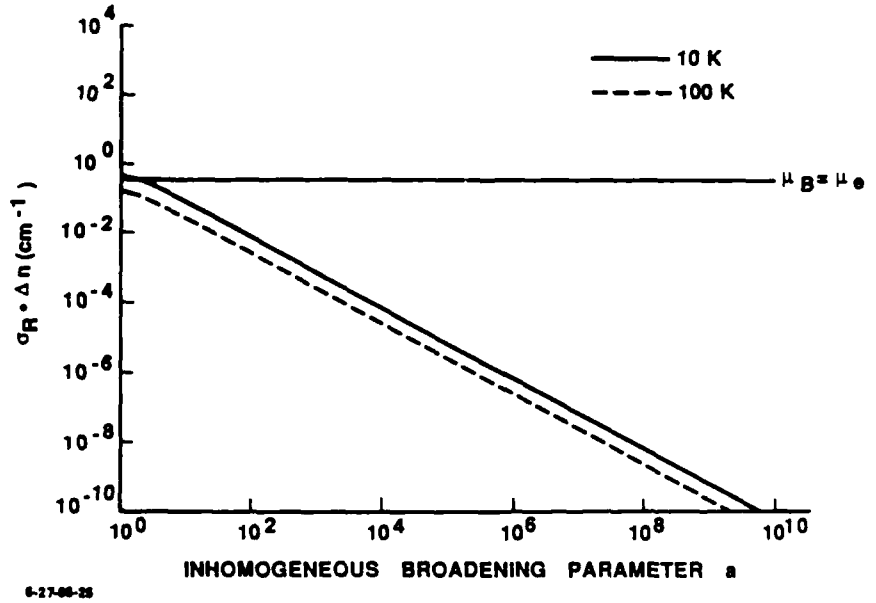

FIGURE 20. Gain for ^{113}Sn in a Be host.

nuclei (i) with neutron absorption cross section σ are pumped by a neutron flux ϕ, yielding nuclei (e) in excited isomeric states. These nuclei decay at the spontaneous rate λ, to the state (g). In most cases, (g) is the ground state, if so, its spontaneous decay rate $\lambda_g = \infty$. In general, the decay rate λ_g is non-zero.

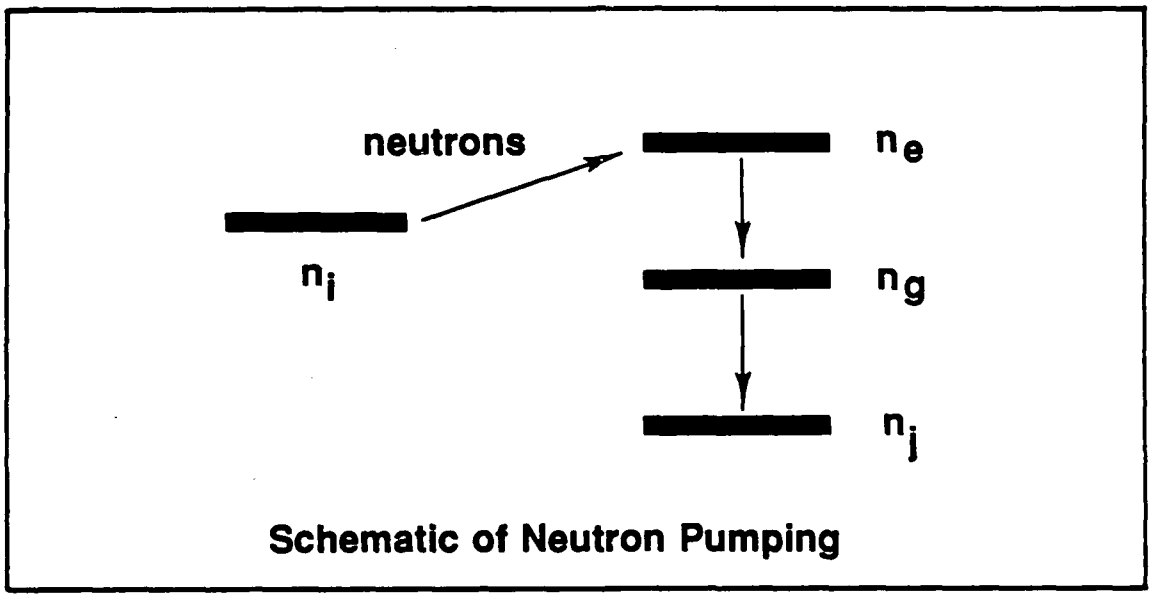

FIGURE 21. Schematic of Neutron Pumping

In this model, $n_e + n_i + n_g + n_j = N$, where N is the total number of nuclei per cubic centimeter, initially in state (i). The number densities of all states of interest are then given by:

$$n_i(t) = N_e^{-\sigma\phi t}$$

$$n_e(t) = \frac{\phi\sigma N}{(\lambda-\sigma\phi)}\left(e^{-\sigma\phi t} - e^{-\lambda t}\right)$$

$$n_g(t) = \frac{\lambda\phi\sigma N}{(\lambda-\sigma\phi)}\left[\frac{e^{-\sigma\phi t} - e^{-\lambda t}}{(\lambda_g-\sigma\phi)} - \frac{}{(\lambda_g-\lambda)}\right] + \tag{12}$$

$$+ \left[\frac{\lambda\phi\sigma N}{(\lambda_g-\sigma\phi)(\lambda_g-\lambda)}\right] e^{-\lambda_g t} \quad .$$

In this simple picture, σ is an average thermal neutron absorption cross section (cm^2, 1 barn = 10^{-24} cm^2), ϕ is an appropriate neutron flux (neutrons/cm^2-sec), λ is the decay rate (sec^{-1}) of the isomeric state (prior to any pulse), and λ_g is the decay rate (sec^{-1}) of the lower state.

Using this dynamic model we compute the population inversion n* and from it estimate the energy available in a γ-ray pulse. For this purpose we approximate:

$$E_{out} = E_o V(n^* - \mu/\sigma_R) \quad , \tag{13}$$

where $n^*\sigma_R-\mu > 0$, as assumed in Ref. (11) and Subsection E, and and the volume V is fixed at 1 cm^3. The results for the best isomeric candidates are shown in Figs. 22 through 30. These figures present the time- and flux-dependent available energy for chosen inhomogeneous line-broadening parameters and total extinction lengths. Note that current reactor designers are aiming for a flux of 10^{18} cm^2/sec with fluxes of 10^{16} cm^2/sec presently available (personal communication, R.D. Cheverton, Oak Ridge National Laboratory).

G. CONCLUSIONS

As a result of a systematic investigation of known properties of real nuclei and their properties, the "best" long-lived isomeric γ-ray laser candidates were identified. Lasing, even with the best candidates, requires stressing physical conditions. The analysis of doped substrates indicates that doping increases the number of available candidates, but decreases the magnitude of the positive laser gain term. For the best isomer, the

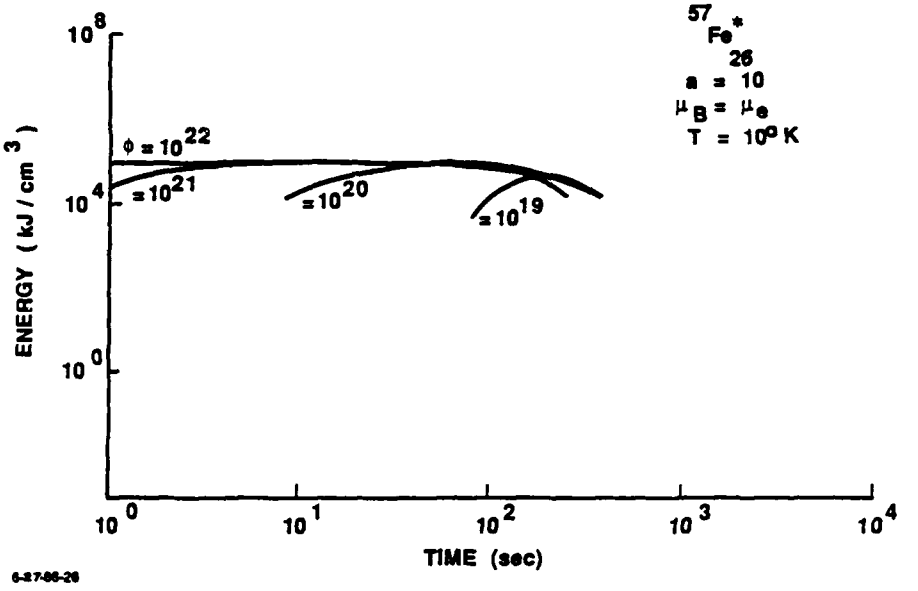

(a)

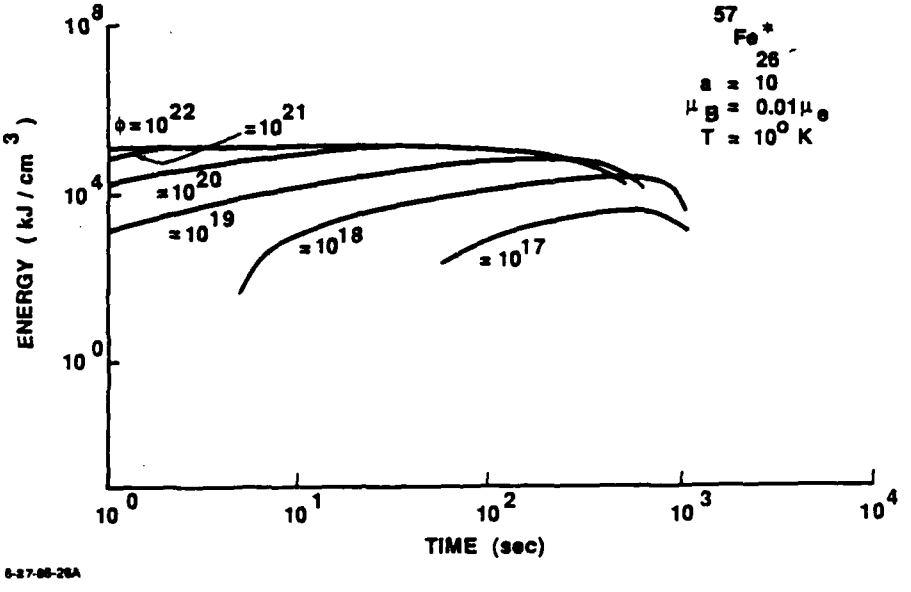

(b)

FIGURE 22. The log of the available energy output [log (kJ/cm^3] as a function of pumping time [log (seconds)] for various neutron fluxes (neuts/cm^2-sec) for the case of $^{57}Fe^*26$. $^{57}Fe^*26$ is a hypothetical nuclear isotope with all the properties of ^{57}Fe, except that its lifetime is assumed to be 1000 sec and the thermal neutron cross section 1000 barns. In part (a), the empirical linear extinction coefficient for iron, is assumed. In part (b), results are shown for a linear extinction coefficient improved by a factor of one hundred.

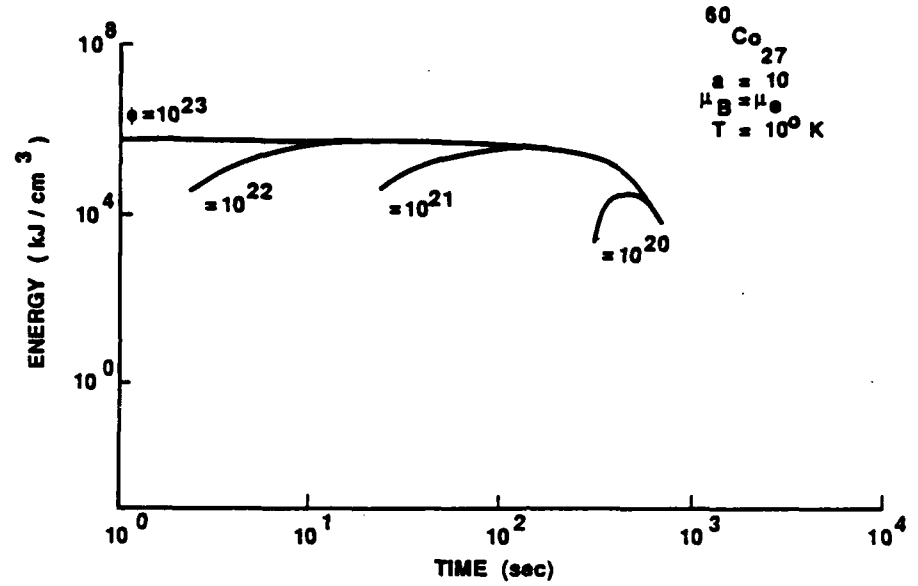

(a)

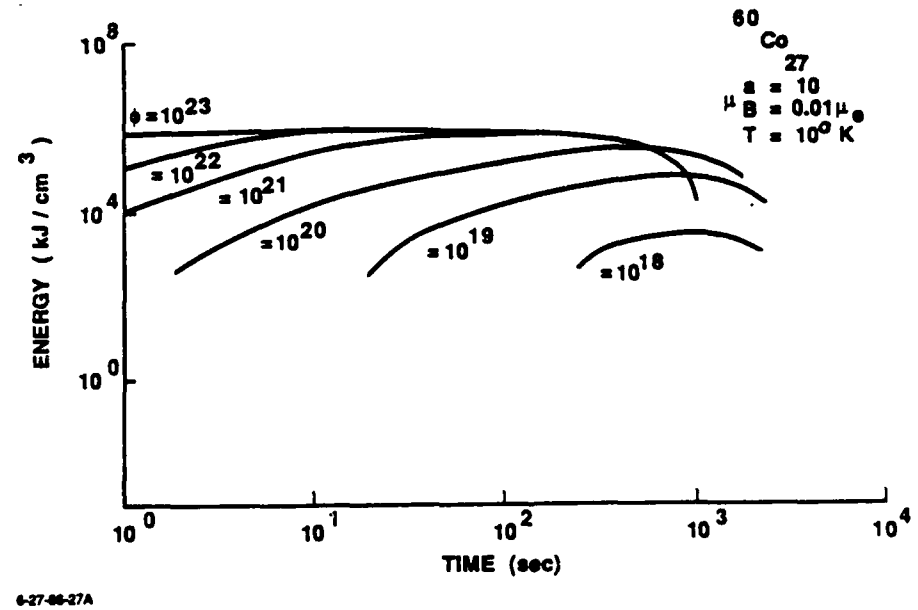

(b)

FIGURE 23. Energy output as a function of pumping time and neutron flux for the case of ^{60}Co. The neutron absorption cross section is taken to be 20 barns in views (a) and (b). In view (b), an improvement of 100 on the linear extinction coefficient is assumed. This is currently the best long-lived isomer candidate.

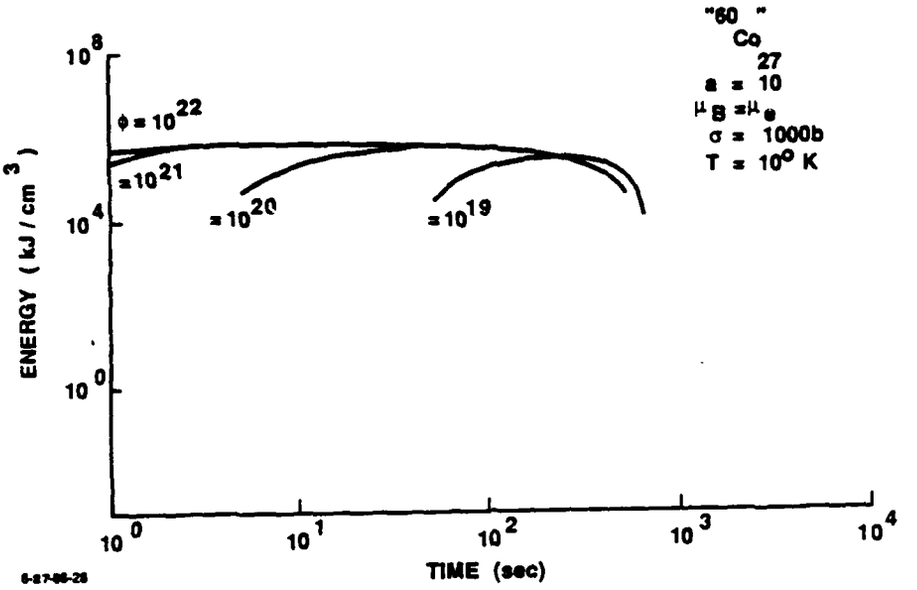

(a)

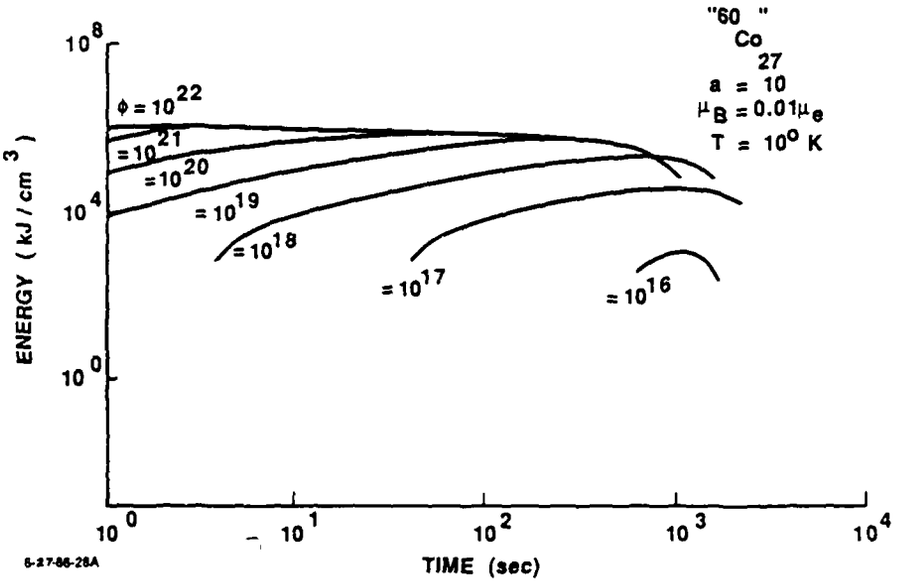

(b)

FIGURE 24. The energy output from "^{60}Co" increases at lowering neutron fluxes if the neutron absorption cross section is increased to 1000 barns for the two cases discussed in parts (a) and (b). Such neutron absorption cross sections are typical of some other isotopes.

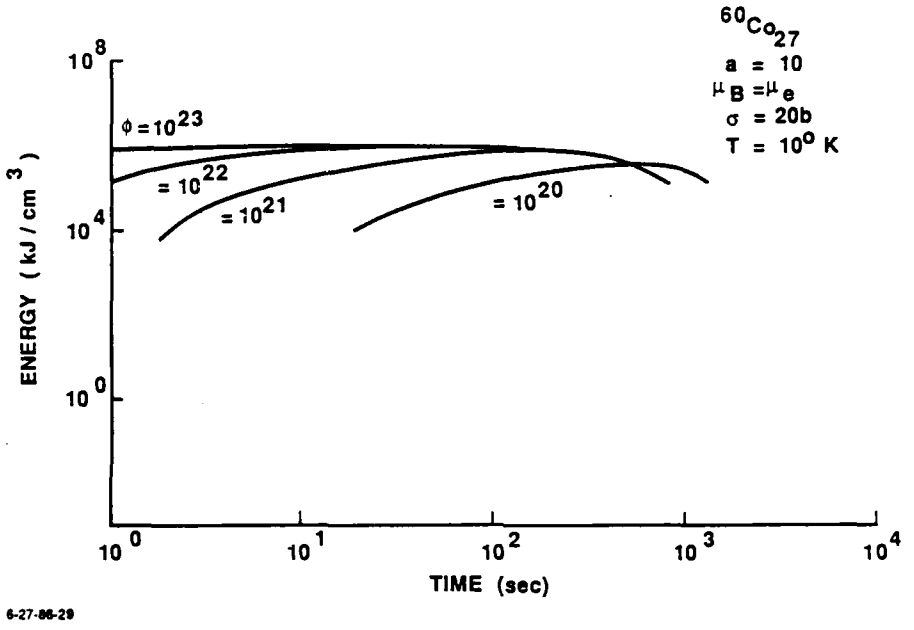

FIGURE 25. The effects of increasing the inhomogeneous line-broadening by a factor of ten from 10 to 100 are depicted here; where otherwise all parameters are the same as Fig. 23(a). The applicable gain curve is given in Fig. 6(b), in which it is seen that for a = 100 a positive gain coefficient is still seen.

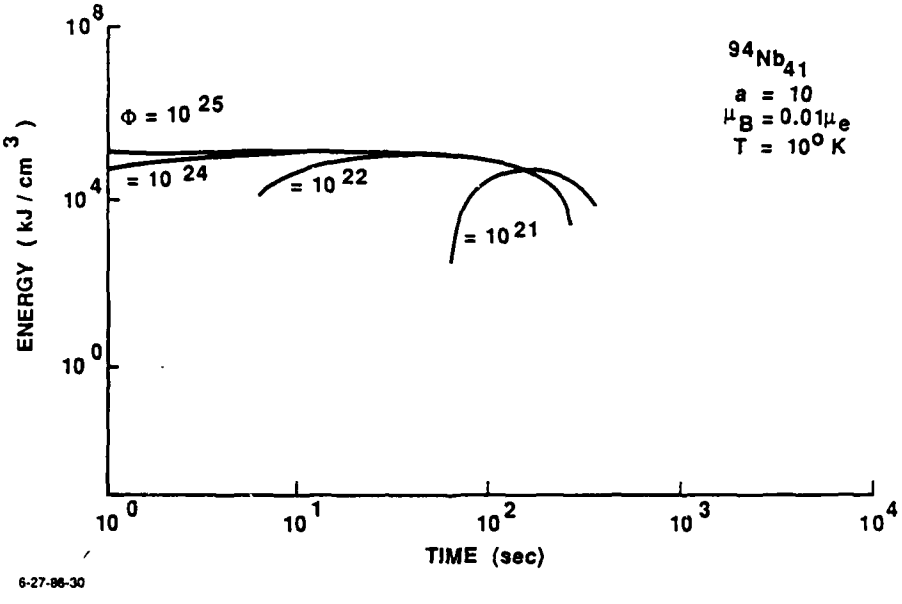

FIGURE 26. Energy available using ^{94}Nb. A positive gain coefficient is achieved only for improved values for the linear extinction coefficient; thus, the case $\mu_B = 0.01\ \mu_e$ is depicted.

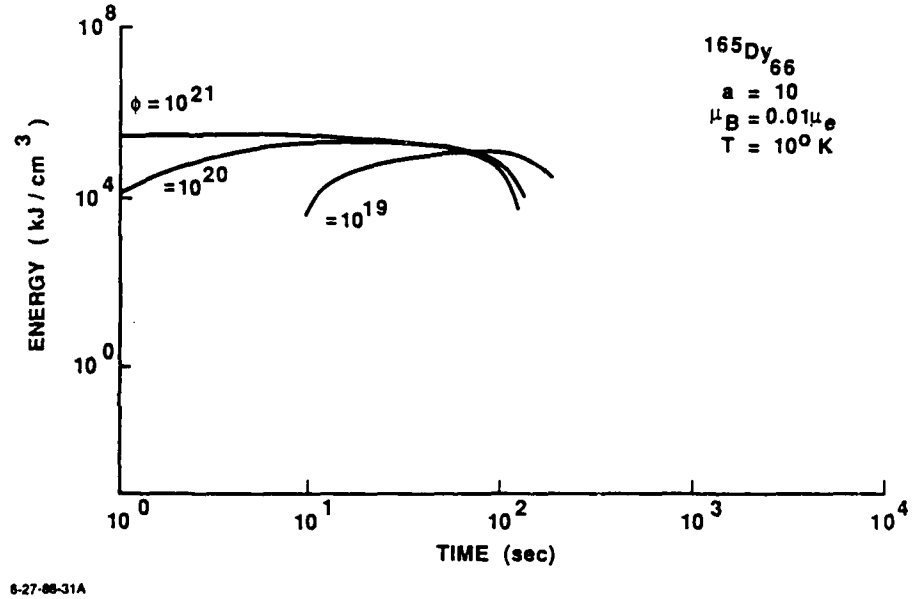

FIGURE 27. Available energy from the ^{165}Dy isomer, using an improved linear extinction coefficient.

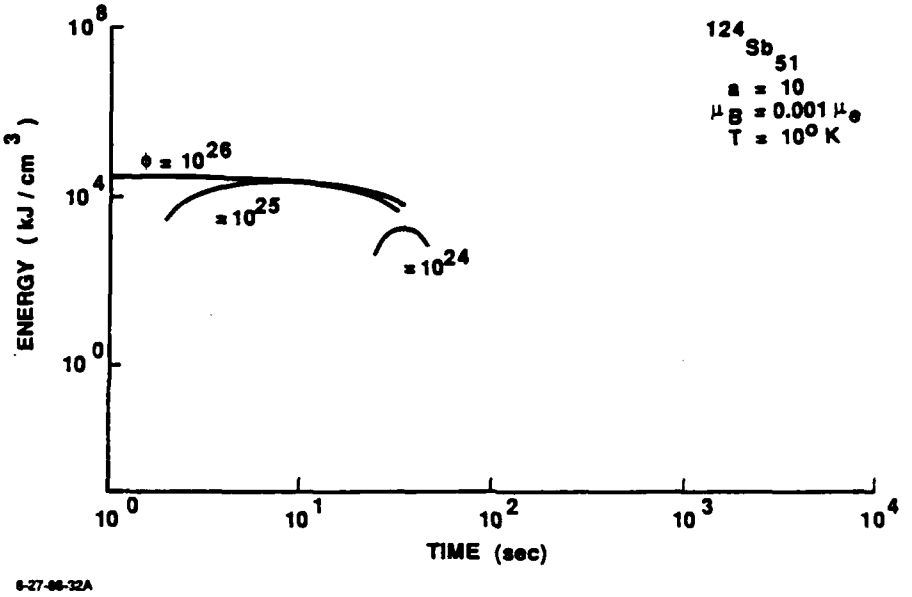

FIGURE 28. Available energy from the ^{124}Sb isomer using an improved linear extinction coefficients.

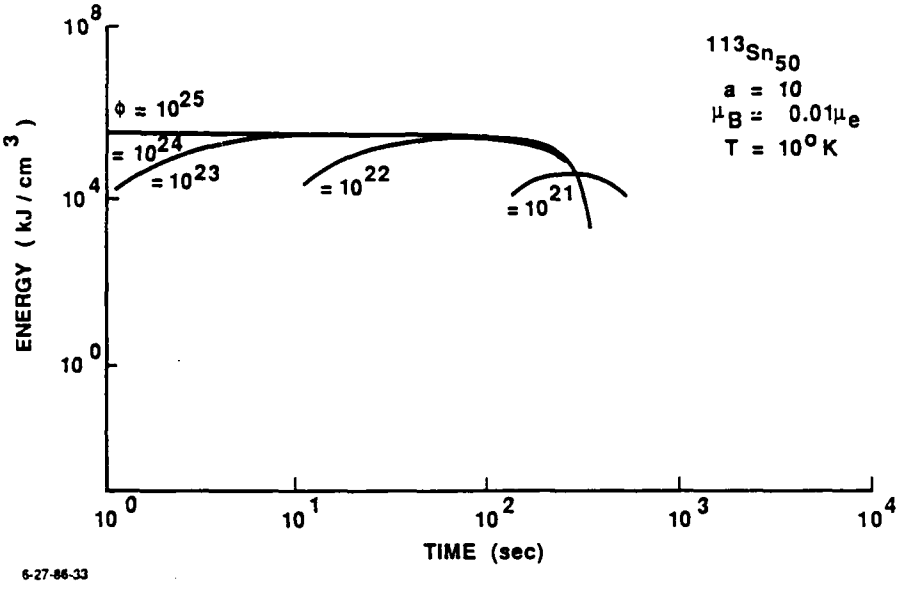

FIGURE 29. Available energy from the ^{113}Sn isomer with an assumed one-hundred-fold improvement in the linear extinction coefficient.

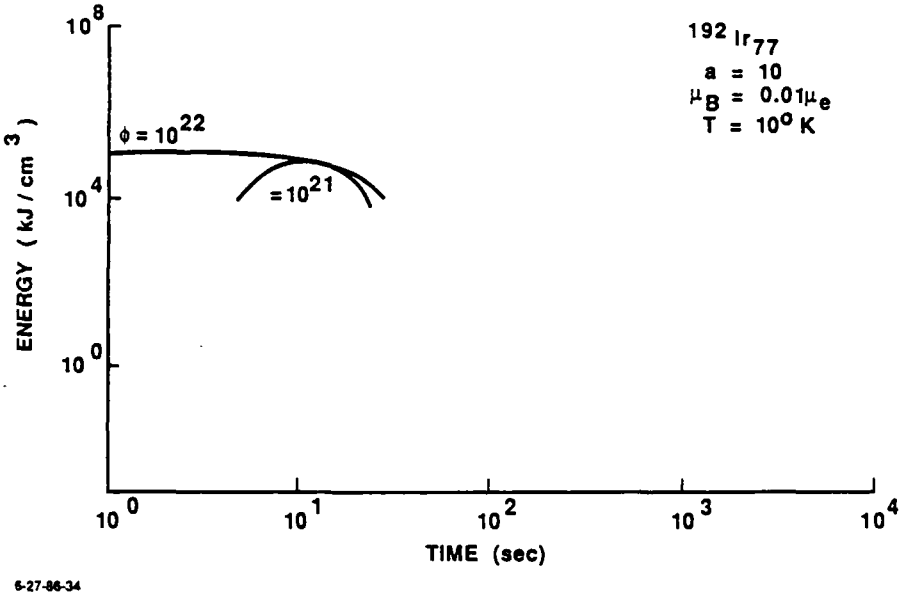

FIGURE 30. Available energy from the ^{192}Ir isomer with an assumed one-hundred-fold improvement in the linear extinction coefficient.

maximum permissible value of the inhomogeneous line-broadening parameter which will give a net positive laser gain condition is approximately 10^2. If the linear extinction coefficient is improved by a factor of 10^2, then the inhomogeneous line broadening parameter can be as great as 10^4. The parameters associated with the best nucleus found (^{60}Co) are: M3 transition, 628 sec half-life, and $\alpha = 48.3$; for an odd-odd nucleus--close to the ideal parameters suggested for the most successful γ-ray laser candidate (Ref. 3 and 11).

The laser gain condition is one basic requirement for lasing to occur. It is clearly useful in a first examination of γ-ray laser prospects involving real nuclei. The critical improvement needed for a positive gain condition appears to be the elimination of inhomogeneous line broadening--the nemesis of the long-lived isomer lasing concept. We are currently attempting to determine the extent of this problem. One additional question involves the time evolution of a γ-ray pulse and the time required to eliminate inhomogeneous line broadening. This problem concerns fundamental uncertainty relationships and the rate at which the superradiant pulse evolves. The possibility of eliminating inhomogeneous line broadening by radio-frequency electromagnetic pulses also exists. We intend to pursue both the duration and the radio frequency pulse questions.

Other γ-ray laser concepts have been proposed in addition to the long-lived isomer concept. The alternative picture of a Dicke super-radiator can also be addressed. Our summary of properties of nuclear isomeric states is of use in pursuing a study of these other concepts.

In conclusion, we report on the identification of those real isomers having the best computed gain conditions. Having identified these real nuclear levels, we describe the magnitudes of improvement required in certain physical parameters to achieve the lasing regime in the long-lived isomer concept, both under static threshold conditions and dynamic neutron

pumping conditions. Many simplifying assumptions were noted. Line narrowing and temporal problems remain. This study serves to highlight the difficulties associated with the long-lived isomer concept. Shorter lived isomeric transitions or pumped isomer concepts (Chapter V) may provide more attractive schemes. We are pursuing such analyses.

IV. LINE NARROWING OF INHOMOGENEOUSLY BROADENED ISOMERIC LEVELS

A. INTRODUCTION

One concept for producing a γ-ray laser is predicated on the ability to narrow inhomogeneously broadened nuclear resonance lines in an isomeric crystal, i.e., a crystal containing nuclei in an isomeric state. The narrowing has to be done in this crystal until resonance between levels destroyed by inhomogeneous broadening is recovered and threshold is achieved (Chapter III). The technique proposed for eliminating the effects of nuclear dipole-dipole interaction, a major contributor to the inhomogeneous broadening, is a well-known RF pulsing technique used in high resolution nuclear magnetic resonance (NMR) spectroscopy (Ref. 21) and shown to be applicable to Mössbauer spectroscopy (Ref. 22). Such techniques have been used to reduce the inhomogeneous broadening in NMR work by up to four orders of magnitude (Ref. 3).

It has been argued by other authors also in (Ref. 3) that time on the order of a lifetime of the nuclear isomeric state is required to achieve the desired narrowing, i.e., bring the effective linewidth close to the natural nuclear linewidth. It is claimed that the time required for any narrowing is at least as long as the inverse of the linewidth achieved, no matter what mechanism is used, and reference is made to the time frequency complementarity principle (Ref. 3, 23).

The author has determined that the nuclear lifetime is irrelevant and certainly not a bounding parameter in such methods, as far as the time required for line narrowing is concerned. Thus, to narrow an inhomogeneously broadened line and bring it close to the natural linewidth does not require time

on the order of a nuclear lifetime. In fact, the limitation is instrumental and not basic. Furthermore, under appropriate conditions one may not need to narrow the line close to the natural linewidth to achieve threshold, as discussed in Chapter III.

1. Inhomogeneous Broadening and Its Effect on Mössbauer Experiments

The interaction between a source and an absorber in a Mössbauer experiment can be described in terms of an emission line and an absorption cross section. If the source and absorber are stationary, and a detector is located as shown in Fig. 31, then

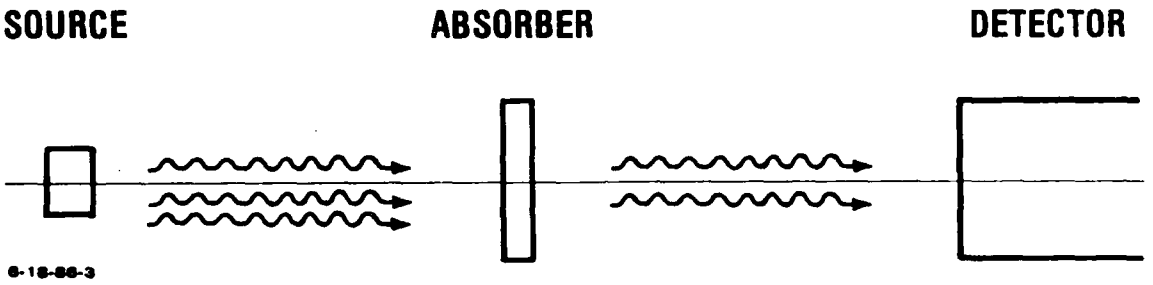

FIGURE 31. Mössbauer Transmission Experimental Geometry

the detected loss in the total photon count, I_D, during the time interval $t_2 - t_1$ because of the presence of the absorber is given by

$$I_D = \int_{t_1}^{t_2} dt \int_{-\infty}^{+\infty} I_s(E,E_s,f_s)\ \sigma_a(E,E_a,f_a)\ dE\ , \qquad (12)$$

where

$$I_S(E,E_S,f_S) = I_O \frac{(\Gamma_S/2)^2 f_S}{(E - E_S)^2 + (\Gamma_S/2)^2} \qquad (13)$$

is the same count rate per energy interval dE,

and

$$\sigma_a(E,E_a,f_a) = \sigma_O \frac{(\Gamma_a/2)^2 f_a}{(E - E_a)^2 + (\Gamma_a/2)^2} \qquad (14)$$

is the cross section for absorption of a photon of energy E.

$$\sigma_O = \frac{\lambda^2}{2\pi} \frac{2I_e + 1}{2I_g + 1} \frac{1}{1 + \alpha} \qquad (15)$$

The other parameters are defined as follows:

I_O is the flux of photons from the source per cm^2/sec, in the direction of the detector. It is assumed in equation (11) that the integration time is short enough that I_O can be taken as constant.

Γ_S, Γ_a are the natural linewidths of the source and absorber emissions, respectively.

f_S, f_a are the recoilless fractions of the source and absorber emissions, respectively, and are strong functions of temperature.

E_S, E_a are resonance energies of the source and absorber nuclei, respectively.

With I_e and I_g, the nuclear spin quantum number of the excited and ground states, α is the internal conversion coefficient of the transition, and λ the nominal wavelength of the γ-ray. Figure 32 is a schematic representation of these parameters. The integral over energy given in eq. (12) is represented by the shaded region in the figure.

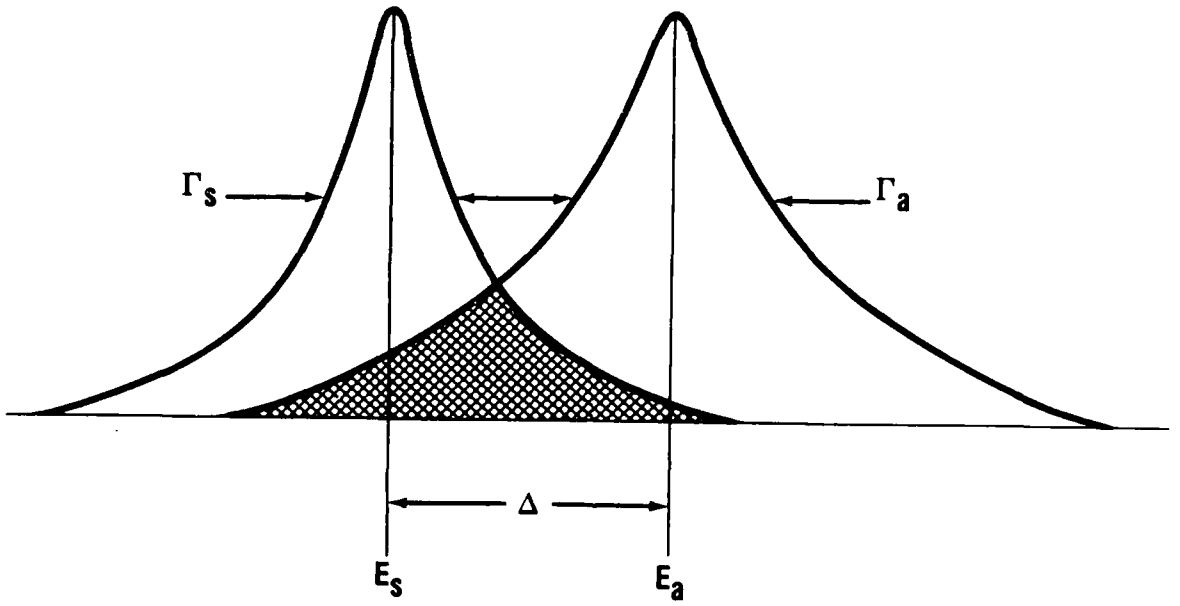

FIGURE 32. Resonance condition for source and absorber

The usual way of performing Mössbauer experiments is depicted in Fig. 31. One moves the source at predetermined velocities and counts the number of transmitted γ-photons through the absorber. The velocity of the source effectively doppler shifts the energy of the emitted photons to $E_s + \frac{v}{c} E_s$, where v is the source velocity and c the speed of light in vacuum. In this way a Mössbauer transmission spectrum is generated to obtain information about the nuclear electromagnetic interactions.

There are other ways of moving the resonances apart in a controlled fashion. One can introduce (1) external DC magnetic fields to shift the resonances; (2) vary the temperature of the samples and thus affect changes in f_a, f_s, and to a much smaller extent, E_s and E_a (second-order doppler shift); or (3) use RF fields to produce zero-order shifts in the energy of the nuclear levels and mix the nuclear states (produce dressed states of nuclei), as suggested by Collins et al. (Ref. 24).

If the absorber were composed of nuclei subjected to the same external fields at the same temperature, the result of the experiment would be essentially as described in eq. (12). The signal strength would be a function of the number of participating nuclei obtained by multiplying the result of eq. (12) by the number of nuclei in the path of the beam, or $\rho_a \times T \times A$, where ρ is the nuclear density in the absorber, T is the thickness of the absorber, and A the area of the absorber illuminated by the beam. This assumes no multiple scattering in the absorber and a thin sample, so that there would be no modification of the beam as it traverses the absorber (effects already well studied by other investigators) (Ref. 25). The actual experimental conditions are generally quite different. Nuclei imbedded in a solid host interact with the neighboring atoms and change this ideal situation drastically. The effect of impurities, crystal dislocations, and crystal boundaries is to introduce slightly different fields at nuclei located in different positions in the lattice and thereby shift the nuclear resonant energies.

Even if the crystal were perfect and we considered only those nuclei well within the regular structure, so that boundary effects were negligible, there would still be a slightly different resonance energy at different lattice sites. The nuclear spin-spin or magnetic dipole-dipole interaction between the emitting or absorbing nuclei and their nearest neighbors would be different due to random orientations of the magnetic moments of nearest neighbors. This is an inherently nuclear effect and

if it were possible to eliminate all the solid state and geometrical factors, this interaction would still remain.

The spin-spin interaction energy is given by

$$E_{d-d} = \frac{2\vec{\mu}_1 \cdot \vec{\mu}_2}{r^3} , \qquad (16)$$

where $\vec{\mu}_1$, $\vec{\mu}_2$ are the magnetic moments of the respective nuclei and r is the distance separating their centers. For ^{107}Ag, this energy has been estimated to be about 10^{-12} eV (Ref. 26). Such a weak interaction is not important in experiments with good Mössbauer nuclei, such as ^{57}Fe, which has a natural linewidth of 10^{-9} eV. This interaction, however, essentially destroys resonance between long-lived or isomeric nuclei such as ^{107}Ag or ^{109}Ag because the effective lineshape for the absorber and source is now smeared out over energies much larger than the natural linewidth, which is on the order of 10^{-17} eV.

Inhomogeneous broadening of resonance levels is depicted in Fig. 33, where the resonance condition for a good Mössbauer isotope ^{57}Fe is compared to the resonance condition for a poor Mössbauer isotope, ^{107}Ag.* In view a of Fig. 33, the resonances of the emitting and absorbing nuclei are separated by an energy, ΔE, which arises because of the slight difference in the local environment of the two nuclei. The natural linewidth, Γ_n of ^{57}Fe, is large enough that the overlap region provides a good resonance effect. On the other hand, as shown in view b of the figure, for the long-lived isotope with the very narrow natural line, the environmental difference between the nuclear sites, which induces the energy shift ΔE, destroys the resonance condition between emitter and absorber. To properly describe this situation, eq. (12) has to be rewritten as:

*For the moment, the difference in the recoilless fraction, f, between the two isotopes is ignored.

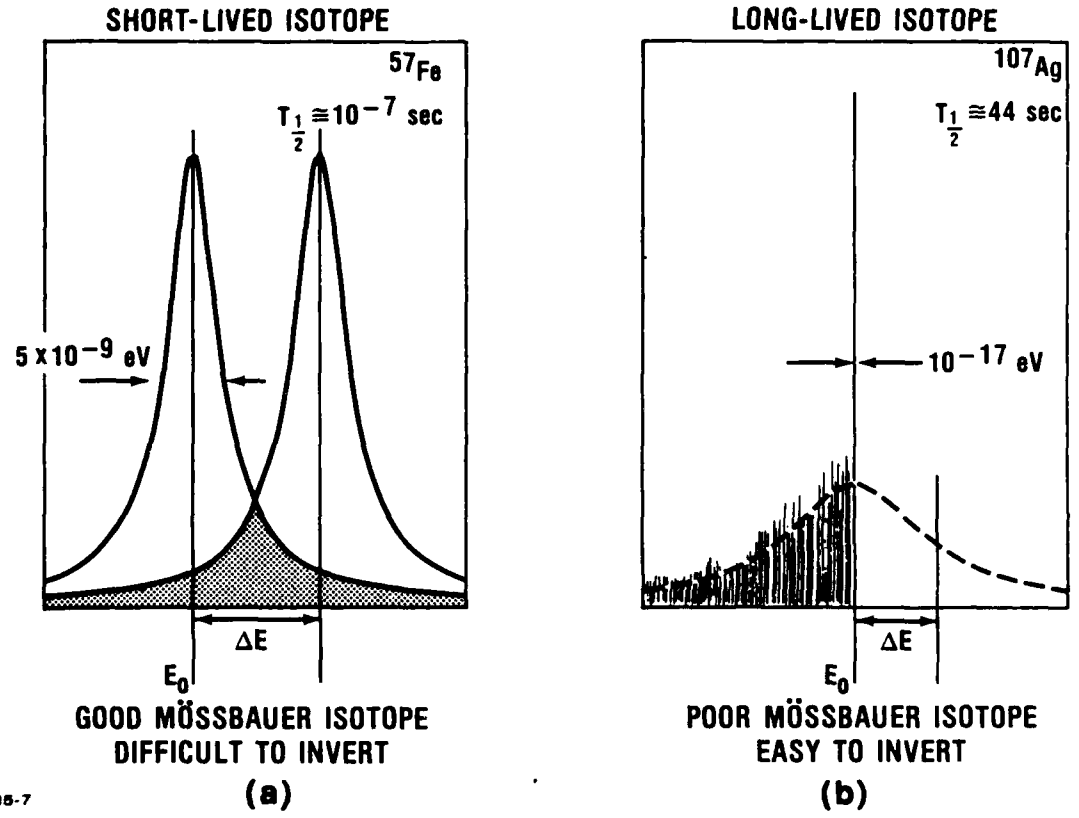

FIGURE 33. Resonance conditions for short- and long-lived isotopes.

$$I_D = \int_{t_1}^{t_2} dt \int_{-\infty}^{+\infty} dE \sum_{i=1}^{N} I_s' (E, E_{si}, f_s) \sum_{i=1}^{M} \sigma_a (E, E_{aj}, f_a) \quad , \quad (17)$$

with

$$E_{si} = E_s + \varepsilon_{ci} + \varepsilon_{ni}$$

$$E_{aj} = E_a + \varepsilon_{cj} + \varepsilon_{nj} \quad ,$$

where

ε_{ci} is the energy shift in the resonance of nucleus i due to crystal imperfections, impurities, boundary effects, and gravitational effects,

ε_{ni} is the energy shift in the resonance of nucleus i due to nuclear spin effects from neighboring nuclei.

The average effect of this inhomogeneous line broadening due to the energy shifts ε_{ci} and ε_{ni} can be approximated by an effective increase in the linewidth of the source or absorber by a factor (1 + a) where a is called the inhomogeneous broadening parameter (Ref. 3, 27). The effect on the threshold condition for lasing is drastic, because the factor 1 + a multiplies the linewidth of the nuclei in the lasing medium, thus effectively reducing the resonance cross section (Refs. 3, 27).

In the line-narrowing concept for developing a γ-ray laser (Ref. 22, 24), it is assumed that (1) the line-broadening terms due to crystal imperfections and impurities can be substantially reduced by proper geometry, size, and crystal preparation and that (2) the nuclear spin interaction term can be reduced by an appropriate sequence of RF pulses, as in high-energy resolution NMR. The total magnitude of the required effect is dependent on other isomer characteristics, as discussed in Ref. 27. In the rest of this paper we assume that condition (1) above can be met and concentrate only on condition (2) and the requirement for the reduction of the dipole-dipole interaction term, ε_{ni}.

This term will disappear naturally when either the ground or excited nuclear states have zero spin, because then either μ_1 or μ_2 will be zero. Also, in a totally inverted crystal the effect of this term will be greatly diminished in the early stages of pulse evolution because of the relatively small number of nuclei in the ground state.

2. The Time Required for the Reduction of Inhomogeneous Line Broadening

It is very difficult to reduce the inhomogeneous broadening in the source and absorber composed of long-lived isomeric nuclei, and at the same time to measure a Mössbauer line close to the natural linewidth in an experiment as depicted in Fig. 31. Best linewidths measured in this way are on the order of 10^{-10} eV (Ref. 28). However, to reduce the linewidth of radiating and absorbing nuclei in the same sample and to measure the reduction in the total emission from the sample because of increased resonant self-absorption seems to be much less difficult. This latter approach was taken by Wildner and Gonser (Ref. 29) and Bezina et al., (Ref. 26) in attempting to observe the resonance effect in ^{109}Ag and ^{107}Ag, respectively. It is also this kind of experiment that is more related to testing the requirements for developing a γ-ray laser.

In the operation of a γ-ray laser it is not necessary to measure a narrow nuclear lineshape. This requirement is the basis for Mössbauer spectroscopy but is not necessary for the operation of a γ-ray laser. A γ-ray laser can be developed and operated without the measurement of a narrow line. For the development of a γ-ray laser, all that is needed is a high recoilless fraction and a good resonance condition.

This leads to the second point. With the RF line-narrowing technique we are not narrowing the line of an individual nucleus which is homogeneously broadened. Instead, we are shifting the position of the resonance for an arbitrary emitter-absorber pair $E_{si} = E_s + \varepsilon_{ni}$ to $E_{si} = E_s$ by suppressing the dipole-dipole

coupling. This shift in energy has to be done in a time shorter than $\frac{h}{|H_{eff}|}$, where H_{eff} is the interaction Hamiltonian (personal communication, Douglas Burrum, Bruckner Instruments). For our case, this can be calculated from eq. 15). This requirement is similar to that found in the study of line narrowing by time-dependent hyperfine interactions. For example, it has been determined that in order to motionally narrow the Mössbauer (or NMR) line by a relaxation mechanism, the relaxation time has to be much less than the Larmour precession time of the interaction (Ref. 30).

Note that these statements make no reference to the nuclear lifetime. The nuclear lifetime is related to the natural linewidth and in this way sets the lower limit on linewidth* but not the minimum time for the operation of line narrowing.

It is true, however, that the pulsing sequence or any dynamic line-narrowing mechanism has to be continued for a time at least as long as the required measurement time or, in the case of the operation of the γ-ray laser, at least as long as it takes the pulse to be emitted. In the superradiance theory of pulse emission this time is expected to be much shorter than the actual lifetime (Ref. 31). Thus, the limitation on narrowing is not a basic physical limitation but a technological limitation. Basically, the relevant question is, how long an operating time at the required power can the line-narrowing apparatus sustain?

Consider for the moment that a linewidth measurement is essential to the application of the γ-ray laser. The relevant relationship then, is given by

$$\Delta\omega \quad \Delta t = \frac{1}{\sqrt{S/N}} ,$$

*This statement is not generally true, as lines narrower than the natural linewidth are expected under special conditions (see Ref. 25).

where $\Delta\omega$ is the minimum frequency variance that can be measured in the time Δt if the signal-to-noise is given by S/N. This expression is well known among radar engineers (Ref. 32). For S/N = 1 the relationship referred to by other authors is recovered.

Most Mössbauer work is done with 1 to 100 mCi sources. If one wants to measure a linewidth to a resolution of 10^{-9} eV in a time on the order of 10^{-8} s, at least 10^{12} photons/s/channel have to be detected. Whether such a strong source with the required narrow line can be prepared is a different matter. The point is that the previous uncertainty principle does not forbid the measurement.

B. CONCLUSIONS

(1) The inhomogeneous broadening of Mössbauer lines is due to slightly different resonance energies of different nuclei.

(2) To narrow the Mössbauer line, the resonant energies must be shifted so that a larger percentage of them overlap. This can be done by proper crystal preparation and a sequence of RF pulses which decouple the nuclear spins.

(3) The decoupling of the spins can be done in a time much much shorter than the nuclear lifetime for long-lived isomeric levels with lifetimes greater than 1 s and depends on the capabilities of the RF pulse generators.

(4) The measurement of the resulting narrow line close to the natural linewidth is not a requirement for the operation of the γ-ray laser.

(5) However, if such a line is to be measured in a time shorter than the lifetime, the complementarity principle requires that the signal-to-noise ratio in such a measurement be correspondingly high.

V. PROSPECTS FOR LASER-INDUCED GAMMA EMISSION

A. INTRODUCTION

The possibility of laser-induced gamma emission from nuclei has been discussed by others (Ref. 3, 24, 33). In particular, the anti-Stokes Raman process is discussed in Ref. 33. Here we additionally consider on- or near-resonant processes in anticipation of intense high-photon-energy lasers, using an approach similar to that of Ref. 33. The calculations here are used to investigate the feasibility of detecting laser-induced nuclear decays by pumping a nuclear isomer. We first calculate nuclear cross sections pertinent to the problem and then discuss the evaluation of the lifetimes of the nuclear states. In the final section, we consider the example of a nucleus similar to the case of ^{186}Re.

B. NUCLEAR CROSS SECTIONS

Consider the schematic energy level diagram of Fig. 34. State (a) with spin and parity $J_a\pi_a$ has energy E_a relative to the state (b). The state (c) differs by a small amount of energy (typically in the x-ray energy regime or lower) from state (a). This latter state is the state which is pumped in the anti-Stokes or resonant case and whose corresponding photon cross section is of key importance. In general, there can be any number of states between level (b) and level (e), depicted collectively as states (i) in Fig. 34. State (e) is the upper excited state of the lasing transition and state (g) is the ground state.

The photon energy of the pumping laser is denoted by E; E_o is the energy difference between states (c) and (a). The

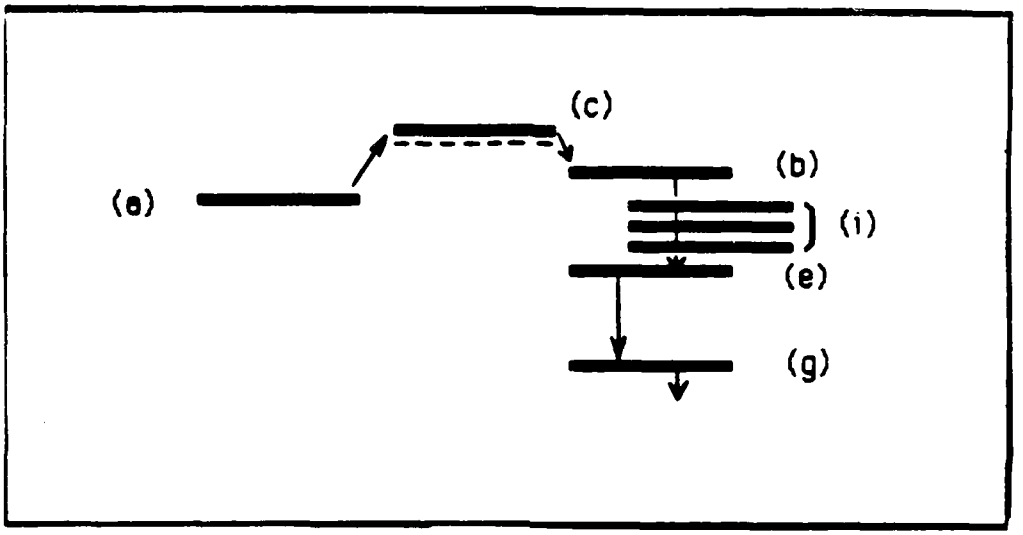

FIGURE 34. Schematic for gamma emission. State (a) is pumped resonantly (or off-resonantly, dashed line) to state (b) via state (c). Transitions through intermediate states (i) occur. Transition (e) to (g) is the lasing transition.

total lifetime of the excited state (c) is τ_t and its total width is denoted $\Gamma_t = h/\tau_t$. The partial width for the (c) to (a) electromagnetic transition is Γ_e. The absorption cross section for the (a) to (c) transition is given by:

$$\sigma_{a,c}(E) = \frac{g\, E^2 \Gamma_e \Gamma_t}{(E_o^2 - E^2)^2 + E^2 \Gamma_t^2} \frac{\lambda^2}{2\pi} , \qquad (18)$$

where g is a degeneracy factor and λ is the nominal photon wavelength such that $E_o = hc/\lambda$. The degeneracy factor $g = (2J_a + 1)/(2J_c + 1)$ accounts for angular momentum degeneracies. This general result, taken from Ref. 34, has a different energy dependence than the well-known Lorentzian lineshape. For near-resonant scattering one obtains the Lorentzian lineshape energy dependence of the Breit-Wigner cross section.

$$\sigma_{a,c} = \frac{\lambda^2}{2\pi} \left(\frac{g}{4}\right) \frac{\Gamma_e\ \Gamma_t}{(E-E_o)^2 + (\Gamma_t/2)^2} \qquad (19)$$

For $E << E_o$ (in eq. (18);

$$\sigma_{a,c} = \frac{\lambda^2}{2\pi} g \frac{E^2 \Gamma_e \Gamma_t}{E_o^4} , \qquad (20)$$

and for $E >> E_o$ in eq. (18);

$$\sigma_{a,c} = \frac{\lambda^2}{2\pi} g \frac{\Gamma_e \Gamma_t}{E^2} . \qquad (21)$$

From Ref. 33 we introduce the partial width for the decay of state (c) to state (b) as Γ_l. This width is visualized as the "tail of (c) in the decay to (b)." The complete cross section for the (a) to (b) transition is then given by:

$$\sigma^c_{a,b} = \sigma_{a,c} \frac{\Gamma_l}{\Gamma_t} = \frac{\lambda^2}{2\pi}\left(\frac{q}{4}\right) \frac{\Gamma_e \Gamma_l}{(E-E_o)^2 + (\Gamma_t/2)^2} \quad . \qquad (22)$$

Two items are noted:

1. First, if $E_b < E_a$ the direct decay of state (a) to state (b) must be suppressed relative to the rate of pumping determined by $\sigma^c_{a,b}$ in eq. (22) and the photon flux. This condition possibly arises when state (a) is a long-lived isomeric level. In such an instance, we would conclude that the states (a) and (b) are joined by an electromagnetic transition rate of high multipolarity or themselves lie very close together in energy. In the former case, the net sum multipolarities and parity product of transitions (a) to (c) and (c) to (b) must equal the multipolarity and parity change in the transition of (a) to (b); in the case of maximum multipolarity, difference of the spins of the states (a) and (b). In general, then, large multipolarities also arise in the (a) to (c) to (b) sequence. Consequently, the need for a hindered transition from (a) to (b) would, in general, lead to a hindered transition from (a) to (c) to (b). If we assume single-particle transitions (the Weisskopf single-particle limit) this will be the case (see Ref. 35). In the case of many real nuclei, other symmetries or selection rules will alter the single-particle Weisskopf picture. Such effects are important and will be discussed later. A low-energy spacing between state (a) and state (b) can also diminish the magnitude of the (a) to (b) transition, and such cases are also possible. We note

that single-particle transition rates are useful in addressing and understanding the roles that multipolarities and such energy differences play.

2. Second, the subsequent decay of state (b) to a state (e) is of further interest if (e) decays by a lasing or super-radiant transition. As such, it can decay to state (g) (which, in general, could also be unstable). In such a scheme the properties of the intermediate states (i) are critical in analysis of the temporal requirements for achieving a population inversion.

We can compute the population inversion required for a positive laser gain coefficient by assuming that the lifetimes of the intermediate states are negligible with respect to the lifetime of the state (b). Note that the decay of state (g) must be included in the computation of the population inversion. The laser gain is defined in more detail later in subparagraph C.

For convenience, we assume that the basic physics of the pumping and the physics of the lasing transition are essentially separate questions. We assume that these processes are analogously described by the same models descriptive of lower energy processes already observed.

We consider now two limiting cases of eq. (22) in the description of the pumping process. In the case of Raman scattering, the photon energy E is much less than the transition energy E_o, such that $|E - E_o| \approx E_o$ and

$$\sigma^{c}_{a,b} = \frac{\pi^2}{2\pi} \frac{q}{4} \frac{\Gamma_e \Gamma_1}{E_o^2} ,$$

as reported in Ref. (33). This latter expression is obtained from eq. (19), assuming $E \approx E_o$. Thus, treatment of the anti-Stokes Raman scattering cross section might better be

approached by eq. (24), obtained directly from eq. (18) for the case $E << E_o$, and similar to eq. (20):

$$\sigma^{c}_{a,b} = \frac{\lambda^2}{2\pi} \, q \, \frac{\Gamma_e \Gamma_1 E^2}{E_o^4} \qquad (24)$$

taking Γ_1 as the decay width of state (c) to state (b). The treatment of far, off-resonant, anti-Stokes Raman scattering will be explored in future work, here we consider larger photon energies.

For larger photon energies, the resonant fluorescent limit is reached when $E = E_o$. In this case, the distinction between a concerted two-photon process and a sequential absorption and decay is an artifact, dependent only upon the lifetime of state (c). In this instance, when Γ_1 is so small that $\Gamma_t = \Gamma_e$ and the decay to state (b) is ignored:

$$\sigma_{a,c} = \frac{\lambda^2}{2\pi} \, \frac{\Gamma_e}{\Gamma_t}, \qquad (25)$$

the usual absorption cross section. We will use the complete expression, eq. (24), for $E = E_o$.

3. NUCLEAR LIFETIMES

The rates of electric multipole transitions are obtained in the classical approximation using Fermi's Golden Rule. Rates for transitions between energy states are expressed as the inverse lifetime, τ^{-1}:

$$\frac{1}{\tau_{fi}} = \; \cdot \; (kR)^{2f} \qquad (26)$$

where f is the multipolarity, ω is the nominal photon frequency, k is the wave vector, and R is assumed to be the nuclear radius.

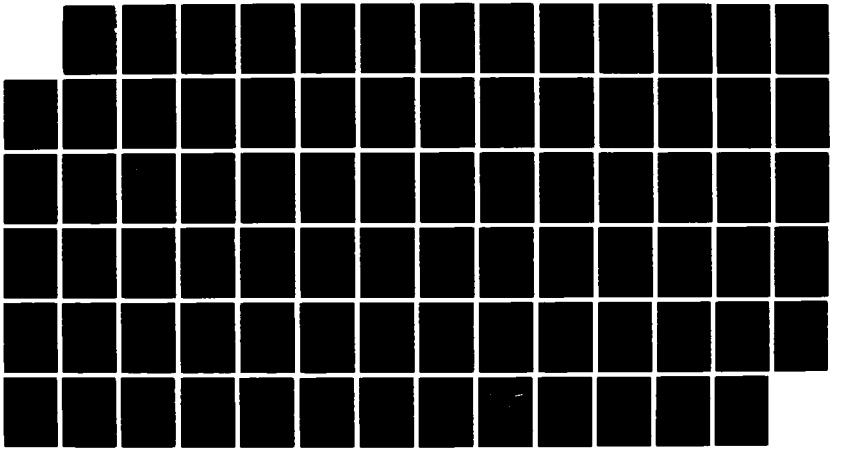

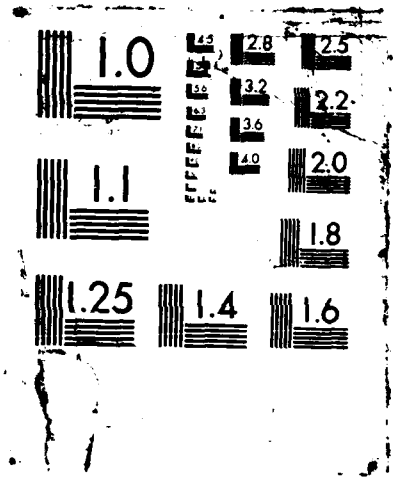
1.0
2.8
2.5
3.2
2.2
3.6
4.0
2.0
1.1
1.8
1.25
1.4
1.6

Convenient units are $e^2 = 1.44$ MeV - fm and $\hbar c = 197$ MeV - fm, where the fine structure constant $\alpha = e^2/\hbar c$.

It is useful to introduce the nuclear radius R for a "liquid drop" nucleus (Ref. 35) of uniform nucleon density: $R = r_o A^{1/3}$. Here, A is the nuclear atomic mass and r_o is taken to be 1.2 fm. Noting, in nuclear units, $e^2 = r_o^2$ and substituting the nuclear radius for R in the expression for the electromagnetic decay rate, the empirical expression is:

$$1/\tau_{E\ell} = \frac{(\alpha^{2\ell+1})\ (E^{2\ell+1})\ A^{2\ell/3}}{h4^{\ell}\pi^{\ 2\ell}\ e^{2\ell}} \quad , \tag{27}$$

or numerically:

$$\Gamma_{E\ell} = \frac{(1.28 \times 10\text{-}4)^{\ell}}{137} E^{2\ell+1}\ A^{2\ell/3} \quad , \tag{28}$$

which is the simplest approach taken in single-particle models. Specific expressions for a select number of electric and magnetic transitions are listed in Ref. (16). We will use eq. (28) for the specific electromagnetic transitions we discuss. Magnetic transitions of polarity ℓ are generally as rapid as electric transitions of polarity $\ell + 1$ (see Ref. (16) for details) and they are predominant for parity change opposite that for electromagnetic transitions. The single-particle estimate is only a first approximation.

Many nuclei undergo collective transitions. These transitions are, for example, collective quadrupole transitions, rotational transitions, and vibrational transitions. For deformed odd or odd-odd nuclei, discussed later, transitions of particles in deformed wells are treated.

In order to account for deviations from single-particle rates, we include, crudely, a transition matrix element factor $|M_\ell|^2$ of multipolarity ℓ in the expressions for the nuclear decay widths (Γ), in the manner of Ref. 33:

$$\Gamma = \Gamma_{\text{single-particle}} |M|^2 \tag{29}$$

then, in summary:

$$\sigma^{c}_{a,b}(E) = \frac{\lambda^2}{2\pi}\left(\frac{g}{4}\right)\frac{(1.28 \times 10^{-4})^{\ell_e+\ell'} A^{2\ell_e/3} A^{2\ell'/3}}{(137)^2} |M_{\ell}|^2 |M_{\ell'}|^2$$

$$\times \frac{(E_o)^{2\ell_e+1} (E + E_a)^{2\ell'+1}}{(E - E_o)^2 + 1/4\ \Gamma_t^2}\ , \tag{30}$$

where ℓ_e is the multipolarity of the excitation transition, ℓ' is the multipolarity reflective of the (c) to (b) decay rate, and $\Gamma = \Gamma_e + \Gamma_f$.
Here,

$$\Gamma_e = \frac{(1.28 \times 10^{-4})^{\ell_e}}{(137)} E_o^{2\ell_e+1} A^{2\ell_e/3} |M_{\ell e}|^2\ , \tag{31}$$

and

$$\Gamma_f = \frac{(1.28 \times 10^{-4})^{\ell'}}{(137)} (E_c - E_b)^{2\ell'+1} A^{2\ell'/3} |M_{\ell'}|^2\ . \tag{32}$$

The number density N_γ of γ-emitting states is given in terms of the initial number density N as:

$$N_\gamma = N\sigma^{c}_{a,b}\ \tau_L \tag{33}$$

where τ_L is the pumping pulse duration, ϕ is the photon flux, and $\sigma_{a,b}$ is the pumping cross section.

With this model we examine the basic interrelationships among multipolarities and energy spacings in subsection D.

General conclusions are drawn concerning tenets worth considering when searching for appropriate systems in real nuclei. Subsection E, we examine applications to actual or realistic, nuclear levels. General conclusions are drawn concerning features to consider when searching for suitable systems in real nuclei.

D. INTERRELATIONSHIPS AMONG MULTIPOLARITIES AND ENERGY SPACINGS IN THE SINGLE-PARTICLE APPROXIMATION

This section is devoted exclusively to the identification and understanding of basic assumptions used on this memorandum. The emphasis here is on simple, analytical approaches and order of magnitude calculations to illustrate basic facets of the interrelationships of three level nuclear systems with on- or near-resonant photon frequencies. The treatment of far-from-resonant (low-energy) laser frequencies has been initially reported in Ref. 33 and will be treated in a separate report. Of concern in this latter problem is the behavior of anti-Stokes Raman scattering in situations not expected to be well described by approaches based on the form of eq. (23) in the previous subsection. Of additional importance are the atomic, molecular, and crystal inelastic cross sections involving interactions of such particularly low-energy photons.

The cross section for resonant $E = E_o$ or near-resonant $E \approx E_o$ photon absorption is determined from eq. (19) as described there. The term of the form $6\pi\lambda_0^2$ in the classical photon cross section is interpreted in the quantum-mechanical case $4\pi\lambda_0^2(\frac{1}{2})(\frac{2J_e+1}{2J_a+1})$, as applying to a dipole transition, where $J_e = 1$ and $J_a = 0$. This approach is suggestive of inclusion of spin multiplicities which are evidently absent in the completely classical approach. On the other hand, nuclear electromagnetic transition rates are computed in the quantum mechanical model by averaging over the initial states and summing over the final states. This approach thus includes the

total angular momenta in the transition rates. We will assume this latter approach and retain the general form of eq. (20) as describing the general (dipole) photon absorption cross section. This is at the outset identical with the approach of Ref. 33. The justification for this will be clear shortly.

The decay rates (Γ) derived in a simple manner in the previous subsection are simple in two respects: First, they do not include explicit wavefunction overlaps nor do they include spin multiplicity factors--even from the viewpoint of single-particle transitions. Such assumptions lead to more complex expressions derived in Ref. 35 with the numerical form noted in Ref. 16. With the exception of a single multiplicative factor, the analytical form of the expressions (as far as functional dependence on A or E goes) is identical. The numerical factor does not significantly differ, for our purposes, from the simple form of eq. (28). This is because spin multiplets do not play a major role as far as order-of-magnitude calculations are concerned.

Second, transitions are usually not "single-particle" in real nuclei. Nuclear transitions are generally quite complicated, often collective, and model-dependent. This is very evident in the collective quadrupole transitions of deformed rare earth nuclei in between closed shells. As one example, transitions involving outwardly similar and closely spaced 0^+ bandhead members have drastically different E2 transition rates due to geometric shape effects (Ref. 37). Here, such collective effects are included in the "parameter" $|M|^2$, which includes the matrix element and statistical effects. These effects can only be adequately treated for the specific nuclear transitions of interest, as will be seen in the example in the next subsection. Here we consider implications of energy spacing and of multipolarities evident in eq. (28), in the general theoretical approach. Such important considerations need to be highlighted with respect to searches for γ-ray laser candidates.

State (a) is intended to be a long-lived isomeric level. Since we prefer (a) to have a hindered decay to state (c) by a multipolarity we label Eℓ", the electric multipolarity of state (a) to state (b) should be large. This in turn both hinders decay of (a) to (b) if (b) is lower in energy than (a), or (b) to (a) if (b) is higher in energy than (a). We thus conclude that larger $\Delta\ell$ values are preferred in (a) to (c) to (b) transitions so that (a) to (b) transitions have the largest multipolarity differences; similarly, low-energy spacings between (a) and (b) are desirable. These are general, broad statements probably not applicable to any one specific, real nuclear system, but appropriate to the overall picture.

Collective or model-dependent effects are discussed in Subsection E. A self-consistent matching of energies and transition rates (such as multipolarity sequences) is an important initial consideration in identifying an optimum system. In the next section we study the example based on a real nucleus of reported interest.

E. RESONANT X-RAY PHOTON ABSORPTION IN ^{186}Re--AN EXAMPLE

The nucleus ^{186}Re has one of the longest lived isomeric levels known--a tentative 8^+ level at ~ 150 keV. The level scheme for ^{186}Re is shown in Fig. 35. The rotational bands of ^{186}Re are believed to arise from intrinsic states constructed from an odd-neutron and odd-proton whose K-projections are found in accordance with the Nilsson model (Ref. 37). The high level density predicted with this model arises primarily due to the large density of orbits available for the odd-neutron. One description of all low-lying rotational band intrinsic states is discussed in Ref. 38, which additionally addresses predicted, approximate energy levels. More quantitative approaches to the energy levels in ^{186}Re can be pursued. The state assignments for bands in ^{186}Re are very important for estimates of electromagnetic transition rates.

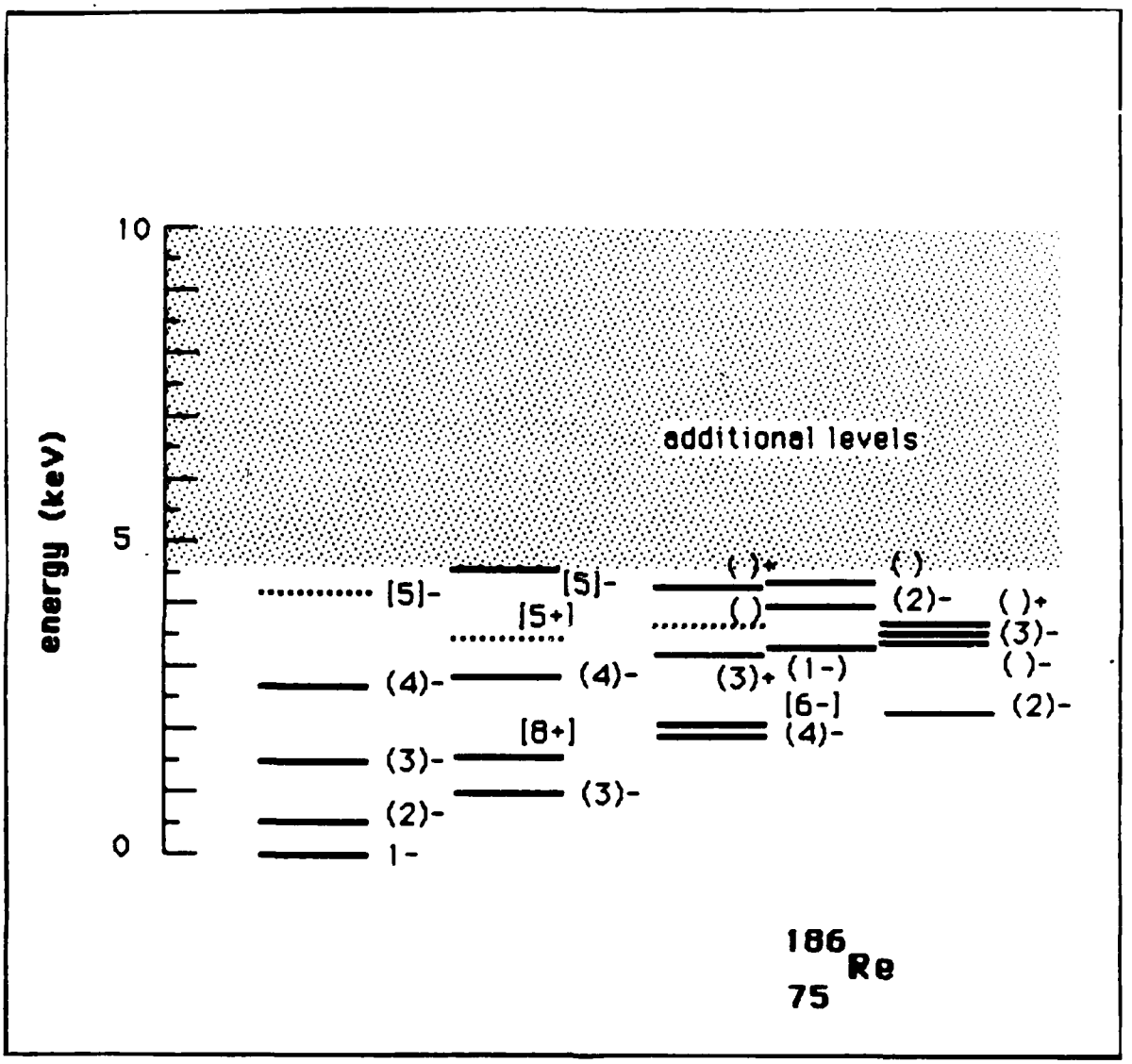

FIGURE 35. Nuclear levels in ^{186}Re. The low-lying levels in ^{186}Re are depicted in the vicinity of the isomeric [8+] level. These levels are expected to be related to the coupling of a single odd proton and a single odd neutron in the Nilsson scheme.

We consider on-resonant pumping. In this case the photon energy matches an energy spacing between the 8^+ isomeric level and some excited state energy level. Preferably a 9- or 7- level would exist which could be pumped because this would constitute an E1 transition which could have a large cross section, as suggested in Ref. 39. Collective effects also play a role and are included here.

A suitable energy level diagram for ^{186}Re is depicted in Fig. 36, taken from Ref. 39. This is expected to provide a good illustrative example for x-ray pumping a nuclear transition. The only reason we refer to x-ray energies as opposed to any other photon energies is the particular energy sequences for the nucleus depicted here. The excited 7- state is preferred (Ref. 39) over a 9- state since the states of ^{186}Re lower than the 8+ isomer all have angular momentum less than 8. The mean lifetime of the 7- excited level can first be assumed to be 5 ps (Ref. 39). The single-particle E1 transition rate, for a 36 keV transition width is found to be $\Gamma_{E1} = 1.4 \times 10^{-3}$ eV, using the Weisskopf-like, single-particle estimate of eq. (28). This corresponds to a 0.5 ps mean transition lifetime. The postulated width Γ_f is assumed to be 10^{-4}eV. In the absence of any collective effects, we would conclude that the 7- state predominantly decays back to the 8+ isomeric level. This would not be too surprising, given the lack of E1 transitions to lower lying levels.

Hindrance factors must be considered. These are included as described in eq. (29). The coupled proton and neutron configurations listed in Ref. 38 are summarized in Table 6. The Nilsson (Ref. 37), quantum number Ω is the projection of angular momentum on the nuclear symmetry axis, N is the total number of harmonic oscillator boson excitations, n_3 is the number of axial boson excitations, Λ is the quantum number representative of the cylindrical SU(2) symmetry, K is the intrinsic projection of angular momentum for an individual nucleon and Σ is a spin projection quantum number.

TABLE 6. NILSSON BANDHEAD STATES

185Re Proton States		185W Neutron States		186Re Coupled States	
State	keV	State	keV	State $\{\Omega_p, \Omega_n\}$	keV
5/2+[402]	0	3/2-[512]	0	1-{5/2,3/2}	0
		1/2-[510]	23.6	3-{5/2,1/2}	99.3
9/2-[514]	368.2	7/2-[503]	243.5	8+{5/2,11/2}	150
		11/2+[615]	197.4	4-{5/2,3/2}	174
		9/2+[624]	720	6-{5/2,7/2}	186
		9/2-[505]	790	2-{5/2,1/2}	210
		5/2-[512]	890	3+{5/2,11/2}	314
		1/2-[521]	1007	1-{5/2,7/2}	316
		7/2-[514]	1058	(5+){9/2,1/2}	(330)
				(3+){9/2,3/2}	351.2

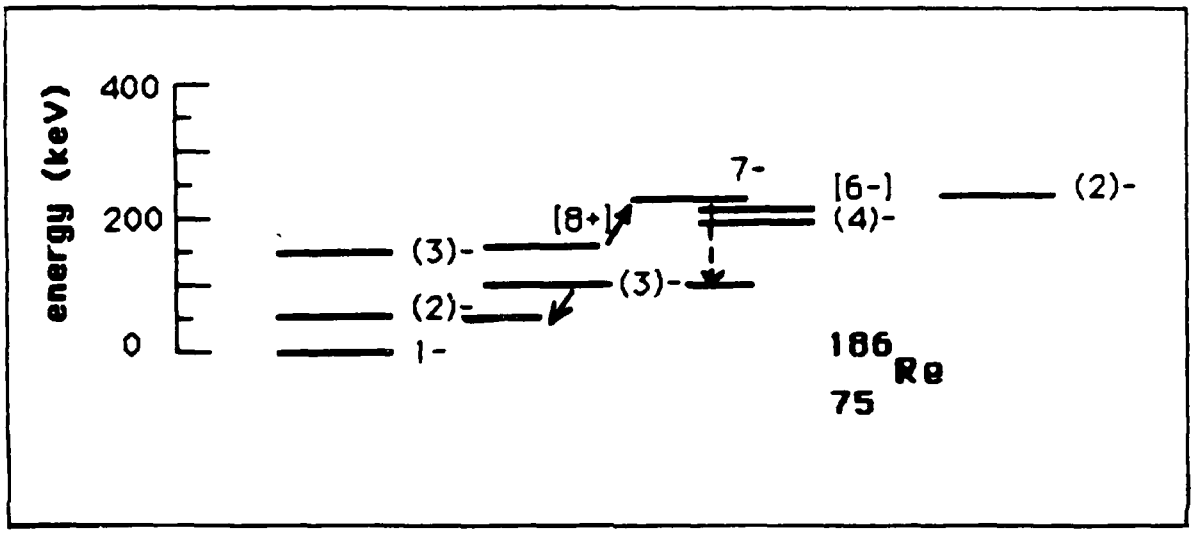

FIGURE 36. Pumping scheme in the Re-like system. The [8+] 7- transition is the pumping transition. The (3)- to (2)- transition is the lasing transition.

The transition matrix element for the 8+ to 7- electromagnetic transition is estimated as follows. The 8+ bandhead intrinsic state is taken as the coupled configuration of an Ω = 5/2+ proton and an Ω = 11/2+ neutron. The proton configuration is taken to be 5/2+ [402] and the neutron configuration is 11/2+ [615]. The 7- state has the same proton configuration 5/2+ [402] but the neutron configuration is expected to arise from the Nilsson 9/2- [505] orbit. The 8+ to 7- transition is then seen to involve a neutron transition from 11/2+ [615] with Σ = + 1/2 to the predominant configuration 9/2- [505] with Σ = - 1/2. This transition then has the quantum number changes $\Delta N = 1$, $\Delta\Lambda = 1$ and $\Delta\Omega = 0$. The selection rules are summarized in Table 7. For the case here, the Δn_3 and $\Delta\Sigma$ selection rules are violated, and the E1 transition is hindered. Hindered E1 transitions are discussed, for example, in Ref. (37). For qualitative estimates, one expects a reduction by approximately 10^4 in the matrix element and factors of 10 each due to pair correlation effects and Coriolis coupling (Ref. 37). We assume for further illustration, a hindrance factor of 10^6. These numbers are crude; for example, a 10^5 hindrance can be computed using wavefunctions for a hindered E1 transition in ^{159}Tb (Ref. 37) and the additional 10^2 hinrances are expected, in general, as described here.

With the assumed collective deviations in the transition matrix element, the resonant absorption cross section is then computed. Note first that the mean lifetime is now found to be 1.1×10^{-7} seconds for the E1 transition or $\Gamma_e \sim 1 \times 10^{-9}$ eV. Hence, $\Gamma_f >> \Gamma_e$, recalling $\Gamma_f = 3 \times 10^{-5}$ eV. Thus, decay of the 7^- state to some intermediate state other than the 8^+ state is taken to be preferred.

The photon resonant absorption cross section (σ_R) is calculated using eq. (25), where the degeneracy factor g = (15/17), and the wavelength is 0.34 Å. We find $\sigma_R \approx 50$ barns. Note that this cross section is directly dependent on the square of the transition matrix element.

TABLE 7. SELECTION RULES FOR E1 AND M1 TRANSITIONS (Ref. 37)

Multipole	$\Delta\Omega$	$\lvert\Delta N\rvert$	$\lvert\Delta n_3\rvert$	$\Delta\Lambda$	$\Delta\Sigma$
E1	± 1	1	0	± 1	0
	0	1	1	0	0
M1	± 1	0,2	1	± 1	0
	± 1	0	0	0	± 1
	0	0	0	0	0

We next consider a potential lasing transition involving the 3- and 2- states of ^{186}Re depicted in Fig. 36. This transition crosses between two rotational bands. (Rotational bands are typically indicated by aligning the states vertically in a figure.) The 3- state has a lifetime of 30 ns. The 2- state decays to the 1- ground state in an interband transition. Its lifetime is assumed to be 1 ns, as estimated from a similar transition in ^{186}W.

The cross section for photo-nuclear absorption competes with photon-electron interactions in the atom. These interactions, for x-ray energies, are primarily Compton scattering and photo-electron scattering.

The Compton scattering cross section (σ_{CS}) is estimated, assuming the bulk material is rhenium, with proton number Z = 75. This cross section is empirically given by:

$$\sigma_{CS} = (0.658)\ Z \exp\ [-2.95 \times 10^{-3}\ E] \qquad (34)$$

for E in MeV and σ in barns (Ref. 3). Thus, σ_{CS} = 44 barns.

The photo-electric scattering cross section σ_{PE} (Ref. 3) is empirically given by:

$$\sigma_{PE} = KZ^{4.5}\ E^{-3}\ , \qquad (35)$$

where E is in MeV, σ in barns and K is a coefficient, depending upon the electron binding energy. In rhenium, the 36 keV photon energy lies between the L and K shell-binding energies, thus K = 0.70. The photo-electron cross section is found to be $\sigma_{PE} \approx 4100$ barns, clearly the dominant cross section.

The computation of laser gain coefficients is discussed in Ref. 3, summarized in Ref. 11, and studied for a wide class of nuclides in Ref. 40.

In a manner detailed in Ref. 40, we determine the physical quantities listed in Table 8. Assuming a 100 percent

TABLE 8. PHYSICAL PROPERTIES OF ^{186}Re 3- - 2- TRANSITIONS

Excited state energy	99 keV
Excited state half-life	2.2×10^{-8} s
Excited state spin	3
Lower state energy	59 keV
Lower state half-life*	6.93×10^{-10} s
Lower state spin	2
Branching ratio*	0.5
Internal conversion coefficient**	3 (e^-/γ)
Isomer recoil energy	0.0046 eV
Recoilless fraction at 10 K**	0.77
Linear extinction coefficient**	36.4 cm^{-1}
Effective Debye temperature	275 K
Gamma energy	40 keV, 0.31 Å
Resonant absorption cross-section**	4100 barns
Maximum critical number density**	6.8×10^{22} nuclei/cm^3
Maximum gain†	28 cm^{-1}
Laser gain coefficient†	-8.7 cm^{-1}

*estimated
**computed
†sensitive to inhomogeneous line-broadening effects, assumed to be a = 10.

population inversion (certainly an extreme case), corresponding to a critical density of $\Delta n^* = 6.8 \times 10^{22}$ excited nuclei/cm^3, the positive gain terms ($\Delta n^* \sigma_R$) are computed as a function of the inhomogeneous line-broadening parameter a. Note that we estimate the internal conversion coefficient from tables in Ref. 41, and assume a uniform material temperature in the calculation of the recoilless fraction. We also ignore hindrance factors in the 3- to 2- transition matrix element. All of these assumptions serve to improve the gain terms and are overly optimistic. The positive gain term ($\sigma_R \Delta n^*$) as a function of inhomogenous broadening is shown in Fig. 37, for temperatures of 10 K and 100 K. The bold horizontal line indicates the magnitude of the loss terms or linear extinction coefficient (μ) due to photo-absorption in the rhenium material. (If a Borrmann effect is assumed, the loss terms diminish, and the corresponding bold horizontal line moves in the direction indicated.) The region of the plot where the positive gain terms exceed the loss terms is the region of (initial) net laser gain. A net positive laser gain coefficient is a necessary but insufficient criterion for a γ-ray lasing transition. For this case, inhomogenous line-broadening parameters approximately less than a = 10 are required to achieve a net positive laser gain. Since the transition matrix element is expected to be less than 1 by factors of 10, gain looks quite difficult with this particular choice of parameters.

Nonetheless, we can assume no inhomogenous broadening and a Borrmann reduction of the linear extinction coefficient by a factor 1/100 to find a minimum $\Delta n^* \approx 6 \times 10^{20}$ to achieve a positive gain. We also assume we have on the order of 30 ns to achieve this population inversion in the 3- upper state of the lasing transition. We do this by also assuming that the population transfer from the 7- level to the 3- level occurs instantaneously. Using eq. (16), with an initial 8+ density of $N_a = 6 \times 10^{22} \frac{\text{nuclei}}{\text{cm}^3}$, τ = 30 ns, $N_e = 6 \times 10^{20}$ and σ_R = 50 barns,

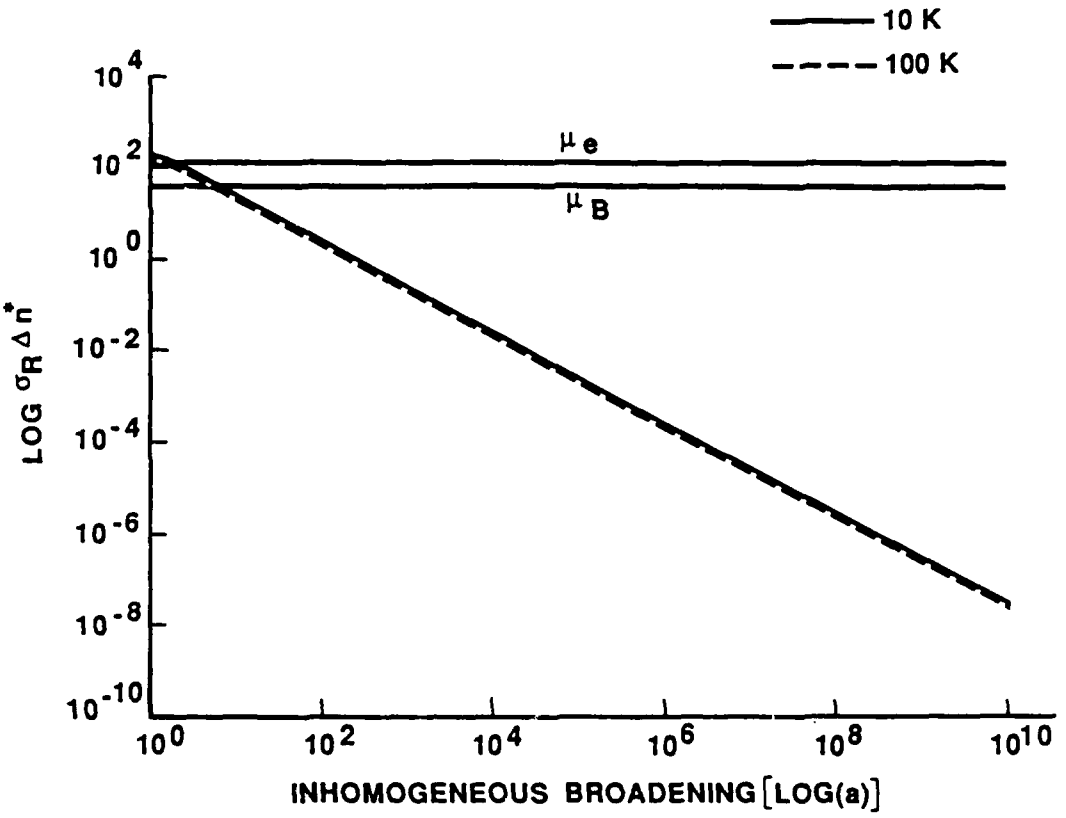

FIGURE 37. Gain curve for the ^{186}Re system. The log of the positive gain terms is shown as a function of the log of the inhomogeneous line-broadening parameter a. The linear extinction coefficient for pure rhenium metal is shown as the horizontal bold line. With a Borrmann effect, the line moves lower as indicated.

and assuming ~ 99 percent (4150/4200) of all photons scatter from the spectral beamwidth, we find $\phi \approx 10^{30}$ photons/cm^2-s. This is a very high photon flux and well beyond the capabilities of any existing source. The energy content over 30 ns for monoenergetic photons of 36 keV is ~ 1.7 x 10^8 J/cm^2, corresponding to 6 x 10^{15} W/cm^2. The output photon energy is 40 keV. A laser pulse from 6 x 10^{20} excited nuclei/cm^3 releases approximately 4 x 10^6 J/cm^3, on the order of 10^{14} W/cm^3 material. Although this is a net energy loss, the output is coherent and directed. The results here may see some improvement with better systems, as further discussed in the conclusion, but this specific system is not good.

We now compute, for illustration, photon pumping fluxes required to achieve positive laser gain coefficients for the 3- to 2- transition in the ^{186}Re-like system. The previous calculations fail to address the kinetics of pumping.

We assume the dynamic picture illustrated in Fig. 38. A sample of material is assumed to be pure ^{186}Re in the isomeric level at 8+. The 8+ level is pumped at rate $\phi\sigma$ where ϕ is the photon flux at 36 keV and σ is the computed pumping cross-section per nucleus. Photon scattering and internal heating of the crystal are ignored. These serve to further aggravate the lasing requirements. The 7- level is assumed to instantly decay to the 3-, upper lasing level. The mean lifetime of this 3- level is 30 ns; and as noted earlier, the lower 2- level is assumed to have a lifetime of 1 ns. We additionally assume an inhomogenous line-broadening parameter a = 10, a uniform rod temperature of 10 K, and a Borrmann effect of 1/10, all of which are still critical to seeing a significant positive laser gain coefficient, even with the large isomeric population density initially assumed.

The results of the pumping calculations are depicted in Fig. 39. Here we see that typical minimum fluxes on the order of 10^{30} photons/cm^2-sec (i.e., about 10^{15} W/cm^2 of 36 keV

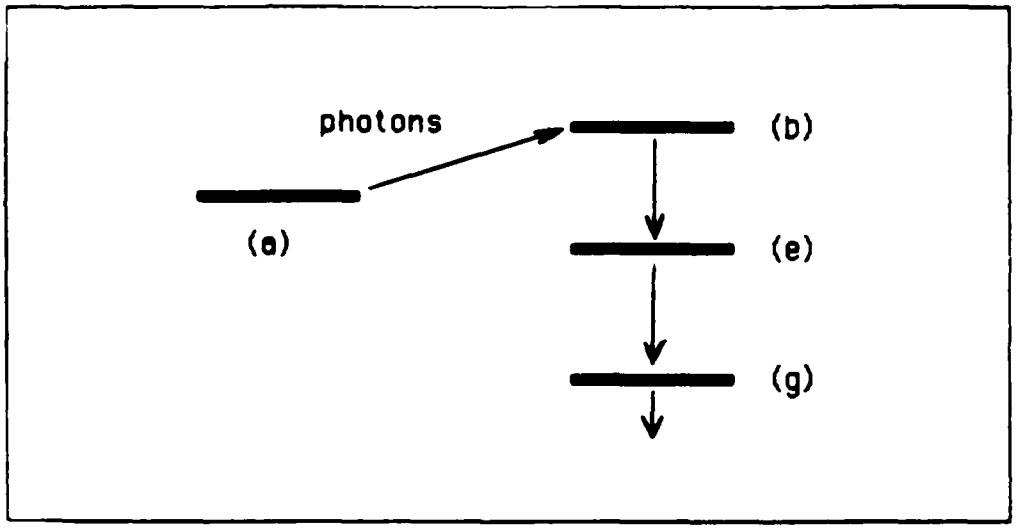

FIGURE 38. Kinematics for photon pumping are calculated using an overall rate of (a) to (b) transitions and instantaneous transfer t level (e). Transition (e) to (g) is the lasing transition. Stage (g) can also decay.

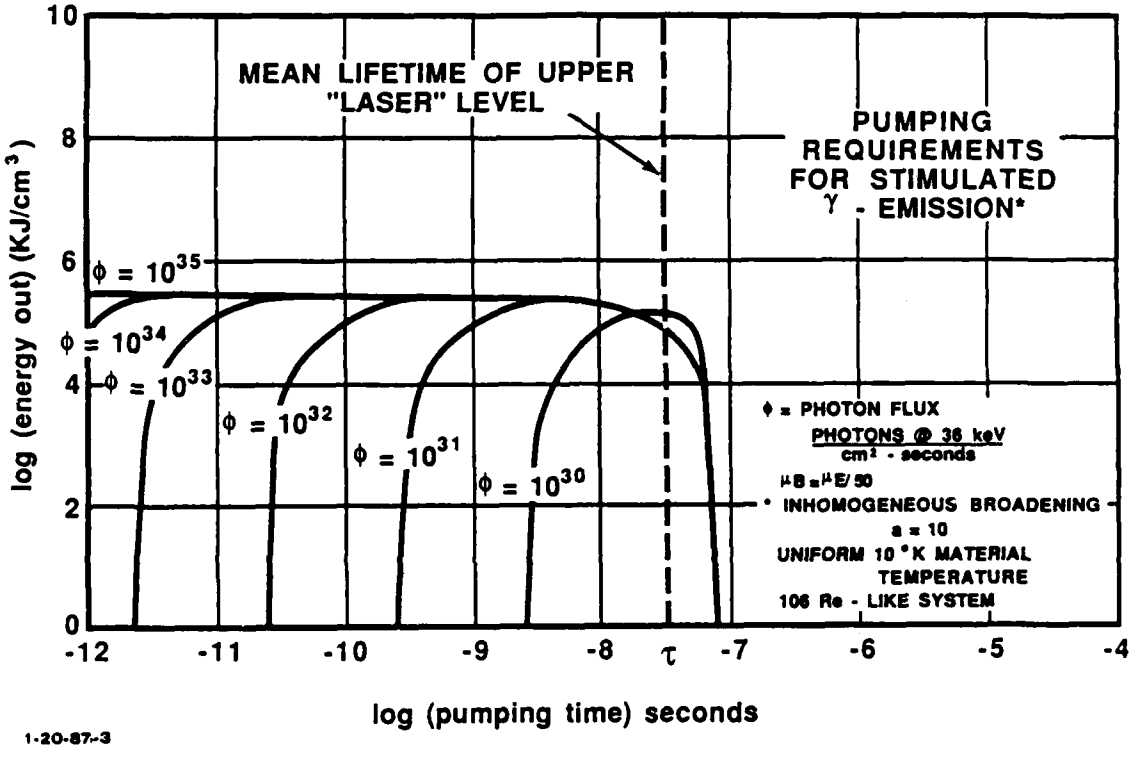

FIGURE 39. Energy out as a function of pumping time for various x-ray photon fluxes in the Re-like system and the assumed parameters in the gain equation.

photons) are required to obtain a positive gain coefficient and directed energy out of the system.* The temperature dependence of the system is not as critical as the effects of line broadening, as noted previously. The achievement of such very large population inversions is a crucial source of positive gain when computing lasing thresholds in this particular system -- thus this specific system must be ruled out.

F. SUMMARY AND CONCLUSIONS

In summary, we report on the scope of photon fluxes required to achieve a positive laser gain coefficient in a given example. A number of conservative assumptions is made. Note that lasing is an extreme case. Smaller photon fluxes will still induce γ-emission at an accelerated rate. The process discussed in the example happens to be an x-ray process. Cases where the photon energy is very small relative to the pumping transition energy (E_o) are under investigation.

We emphasize that systems and transitions other than the specific case of interest here can be expected to show improved characteristics, although lasing is a far more difficult objective. With the basic considerations highlighted in this report in mind, we are actively attempting to establish parameters for an optimized system. One may then search for the ideal nuclear candidate for this scheme with the goal of identifying a suitable experimental test of the concept -- inducing γ-emission from a nuclear isomer.

*Note: This is an unrealistically high flux. Its existence might obviate the need for a gamma-ray laser.

VI. NUCLEAR STRUCTURE ASPECTS OF ^{186}Re PERTINENT TO THE PUMPED ISOMERIC STATE γ-RAY LASER CONCEPT

A. NUCLEAR STRUCTURE ASPECTS OF THE PUMPED-ISOMER LASING SCHEME

A number of concepts (Ref. 3, 23, 39, 42, and 43) involving the stimulated emission of low-energy gamma photons from the decay of excited nuclear levels incorporate isomeric states into their schemes. One such concept (Ref. 39) calls for pumping an isomeric state by an initial, rapid, electromagnetic transition which ultimately leads to a second, short-lived, excited nuclear level. This second excited level subsequently decays by gamma emission to a third state, as depicted in Fig. 40. The short lifetime of the second excited level is expected to lead to an enhancement in the photon cross-section for stimulated emission but cannot be so short as to pose difficulty in pumping the level. In this scheme, then, the isomeric state provides for long-term energy storage. The release of this energy is accomplished and controlled by relatively lower energy electromagnetic radiations. The specific details of nuclear spin and parity assignments, collective modes, and transition rates depend on the choice of an actual nucleus.

One nucleus of possible interest to research (Ref. 39) leading to a γ-ray laser of this type is ^{186}Re. Excited levels of this nucleus are typical of the high-level density generally found in odd-odd nuclei. Such nuclei are likely systems in which to search for unusual energy level sequences required in the pumped-isomer concepts.

A quick assessment of the ^{186}Re structure and a brief description of the Nilsson model are described in this chapter. Comparison to an Interacting Boson Approximation (IBA)-based super-symmetry scheme, as well as detailed Nilsson-based

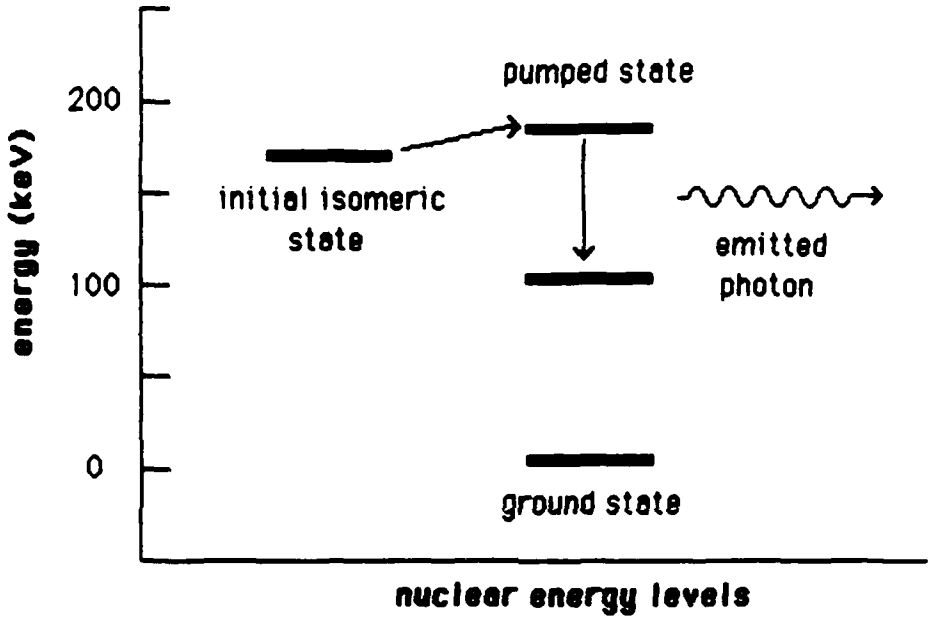

FIGURE 40. Energy level scheme for the pumped γ-ray laser concept. In this concept, stimulated emission occurs between a pumped state and a state which is lower in energy by approximately 100 keV. The pumped state is reached from the initial isomeric level by the absorption of energy through some suitable mechanism, such as optical, electronic, or collisional excitation.

calculations would suggest directions to take for more technical calculations.

The ^{186}Re nucleus has one identified isomeric state (Ref. 7) lying approximately 150 keV in energy above the ground state. This rapidly spinning isomer is believed to have eight units (I = 8) of angular momentum--much higher than the angular momentum ($I \leq 3$) of the nuclear states lying lower in energy. The large angular momentum difference between the isomer and lower-energy rotational band members contributes to the long half-life for an electromagnetic isomeric transition of 2×10^5 years.

In contrast to the long lifetime of the [8+] excited state, the 1- ground state of ^{186}Re is very short-lived. This ground state decays by β^- emission (92.2 percent) to the long-lived isotope ^{186}Os or by orbital electron capture (7.8 percent) to the stable isotope ^{186}W. The composite half-life of 90.6 hours is observed for the decay of the ^{186}Re ground state. These features of the ^{186}Re decay are depicted in Fig. 41. Effectively, a few days after an initial production, the only ^{186}Re nuclei remaining are the isomeric nuclei--nuclei which are trapped for over 200,000 years in a rapidly spinning stored energy level.

It is suggested (Ref. 39) that the unique combination of nuclear states required in the pumped isomeric laser concept could possibly exist in the excited state spectrum of ^{186}Re. This odd-odd rotational nucleus has a fair nuclear level density. As will be seen, it lies in a region of nuclear deformation involving numerous Nilsson neutron levels. Of particular interest is the possible existence of new states with angular momentum near I = 8 and lying close in energy to that of the isomeric state. Such an intermediate level could potentially be pumped using relatively low photon energies. In addition, it has been noted in Ref. 39 that such states could have thus far escaped experimental detection. Consequently, this chapter provides for an introductory examination of the low-energy nuclear structure of ^{186}Re.

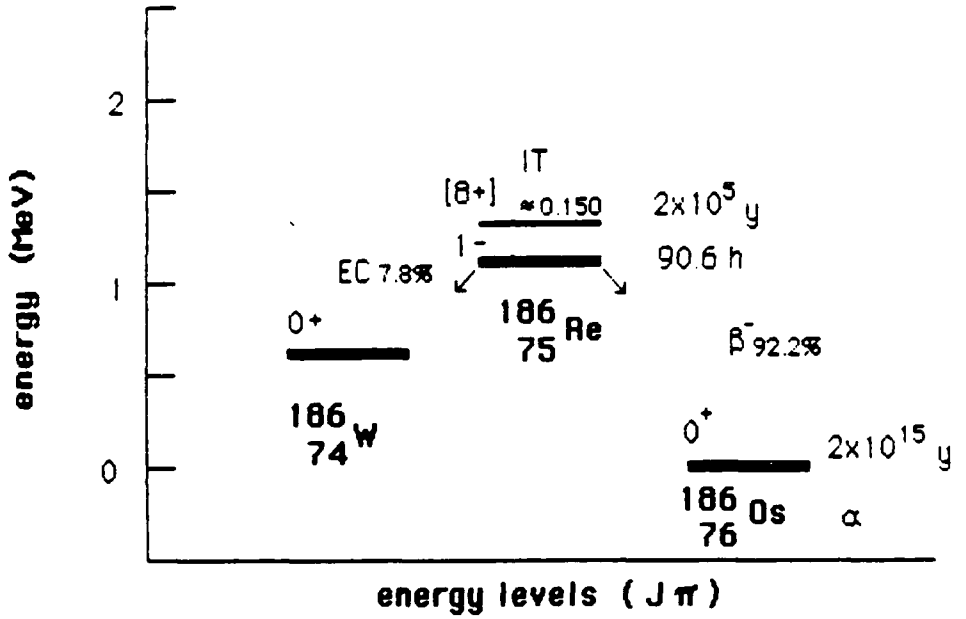

FIGURE 41. The decay scheme for ^{186}Re. The odd-odd nucleus ^{186}Re decays by β- emission or electron capture to two even-even nuclei with a relatively short half. The long-lived [8+] isomeric state in ^{186}Re is of interest to γ-ray laser concepts if it can be successfully pumped to possible nearby excited levels of the Re nucleus.

Although current models of nuclear structure are incapable of precise quantitative predictions of all nuclear energy levels, they are quite successful in providing an understanding of the lower-lying features of most nuclei (Ref. 37). The basics of the Nilsson model are outlined in Subsection B. Conclusions are drawn concerning the possibility of a 7- state lying close in energy to the isomeric [8+] state, as discussed in Subsection C. More generally, the usefulness of even the simplest aspects of nuclear structure theory are noted in Subsection D.

B. THE NILSSON MODEL DESCRIPTION OF DEFORMED NUCLEI

The ^{186}Re nucleus is composed of an odd number of protons (75) and an odd number of neutrons (111). All of these nucleons are bound in a small region of space by the strong interaction. The mean or average strong attractive field generated by the nucleons is, to a first approximation, closely described by a spherical isotropic harmonic oscillator potential well with a significant nucleonic spin-orbit interaction. The nucleons are then assumed to occupy the characteristic orbitals of the nuclear shell model (Ref. 15).

In the case of ^{186}Re, 25 protons and 29 neutrons comprise valence nucleons outside of the major closed shells at Z = 50 and N = 82, respectively. In this instance, and for situations involving many-valence nucleons in general, configurations of neutrons and protons consistent with a deformed nucleonic well are observed to lie low in the energy spectrum. Such configurations are identified with axially-deformed, spheroidal, nuclear intrinsic states. Sequences of higher energy levels arise from successively faster rotations of these intrinsic nuclear states.

The single-particle nucleonic orbitals in the deformed picture are related to orbitals in the spherical limit as described by Nilsson (Ref. 44 and in Ref. 37). In the spherical limit, the good quantum numbers consistent with the overall spatial symmetry (Ref. 45) [SU(3)] of the spinless isotropic

harmonic oscillator well are in general: $(\lambda\mu)$, the major shell principal quantum numbers; L (or ℓ), the orbital angular momentum; M_L, an orbital angular momentum component; and K, the projection of orbital angular momentum on the nuclear symmetry axis. In the special case of single-particle states $\mu = 0$ and $\lambda = N$, where N is the usual principal quantum number associated with the single-particle states of the isotropic harmonic oscillator. Additionally, in this special case, the quantum numbers K and M_L are indistinguishable. The parity $\pi = (-)^L$ reflects the inversion symmetry of the nuclear wavefunction.

Single-particle nuclear states may be labelled by their symmetry quantum numbers. Spherical states are labelled with the quantum numbers N, L, M_L, and π. If the effects of spin-orbit (L·S) coupling are then included, the states are additionally labelled by the quantum number J (or I) which is the total nuclear angular momentum. The value of J can be determined in the usual manner from the vector coupling of $\vec{L}$ and $\vec{S}$, where $\vec{S}$ is the single nucleon spin. With the effects of spin-orbit coupling included, the single nucleon states are completely labelled by the quantum numbers N, L, J, M_J, and π. These quantities are shown for the levels of the nuclear shell model in Fig. 42. Also depicted in the figure are the occupancies of the ^{186}Re valence nucleons.

In the Nilsson model, the spherical symmetry is first broken to the U(1) x SU(2) symmetry typical of the axially deformed harmonic oscillator well. (It is generally convenient to use the cylindrical or asymptotic basis in treating the Nilsson states of the rotational, heavy nuclei.) In this picture, the single-particle levels in the deformed well can be found by picturing the distribution of the N oscillator L = 1 excitations, associated with the principal quantum number N, amongst the new axial oscillator [U(1)] and the planar oscillators [SU(2)]. One may then have n_3 axial excitations and n_p planar excitations where $n_p + n_3 = N$. The planar excitations

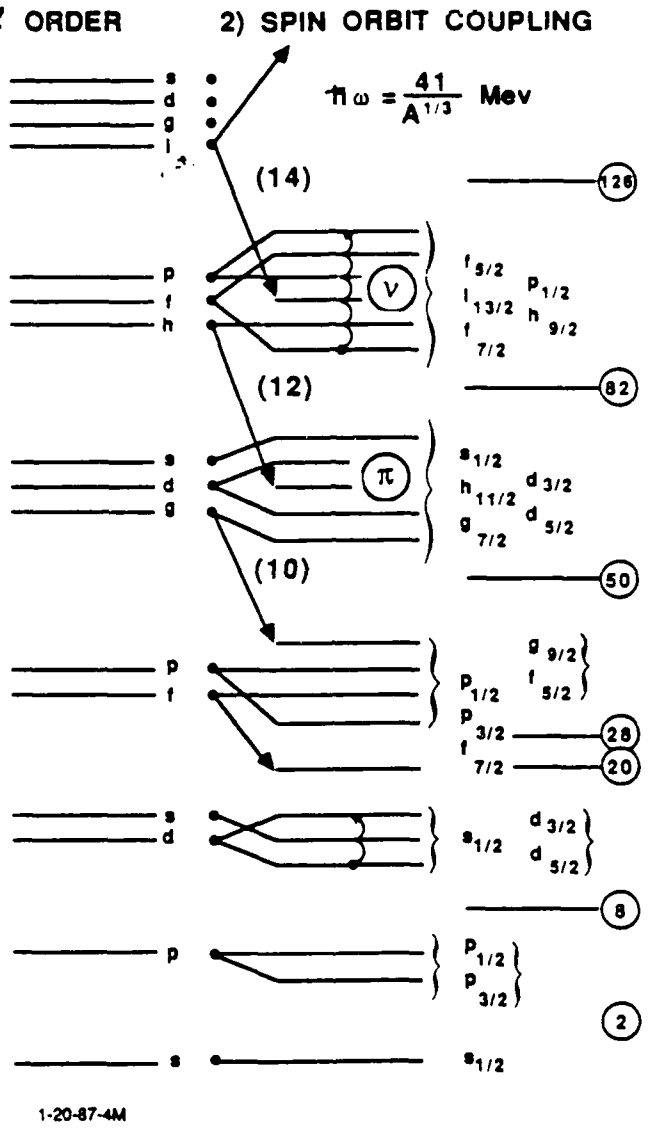

FIGURE 42. Nuclear shell model levels occupied by neutrons and protons in ^{186}Re. The sequence in part 1) depicts energy levels for a single-particle which is bound in an isotropic harmonic oscillator potential well. These levels levels are then successively filled with nucleons. The effects of spin-orbit coupling are depicted in part 2). Here the states are labelled by their l and j spherical quantum numbers and the location of the last valence proton (π) and neutron (ν) are indicated prior to the inclusion of the Nilsson level splittings. These further splittings arise due to the presence of cylindrical symmetry in the rotational intrinsic states.

lead to planar wavefunctions which can be characterized by the quasi-spin quantum numbers $\bar{\Lambda}$ and $\bar{K} = \bar{\Lambda}, \bar{\Lambda}-2,\ldots,-\bar{\Lambda}$. In the Nilsson scheme, however, the quasi-spin quantum number $\bar{\Lambda}$ is restricted to the single value n_p. When the SU(2) oscillator symmetry is further broken to the simpler O(2) symmetry; the components $\pm\bar{K}$ are grouped in pairs labelled by the new Nilsson quantum number $\Lambda = |\bar{K}|$, with components $\pm\Lambda$.

The nucleon spin components Σ are coupled to the orbital angular components Λ to give the total spin projection quantum number $\Omega = \Lambda + \Sigma$. The final Nilsson states are usually labelled by $|Nn_3\Lambda\Omega\rangle$. The relationships between the spherical shell model states and the deformed Nilsson states (Ref. 37) are shown as a function of the nuclear deformation parameter δ in Figs. 43 and 44. These figures depict the splitting of the proton and neutron shells in the regions of $Z > 50$ and $N > 82$. Here, $\delta = 3(\omega_p-\omega_3)/(2\omega_p+\omega_3)$ where ω_p and ω_3 are planar and axial oscillator frequencies. The Nilsson single-particle Hamiltonian is given by:

$$H = \frac{p^2}{2m} + \frac{1}{2}m\left[\omega_3^2 x_3^2 + \omega_p^2 (x_1^2 + x_2^2)\right] + v_{\ell\ell}(h/2\pi)\omega_o\,(\vec{\ell}^2-\langle\vec{\ell}^2\rangle_N) + v_{\ell s}(h/2\pi)\omega_o(\vec{\ell}\cdot\vec{s}) \quad , \qquad (36)$$

where $\vec{p}$ is the nucleon momentum, m is the nucleon mass, $\omega_o = 1/3\ (2\omega_p+\omega_3)$, $\langle\vec{\ell}^2\rangle_N = N(N+3)$ and the parameters $v_{\ell\ell}$ and $v_{\ell s}$ introduce the angular momentum rotational effects. This Hamiltonian is then diagonalized in the cylindrical basis. Physically, states of higher ℓ and of higher J lie lower in energy than states with lower values of ℓ or J.

The many-particle states of the Nilsson model are found by filling the single-particle levels with nucleons in conformance with the Fermi exclusion principle. In the Nilsson model, the ground state of a given nucleus has all doubly

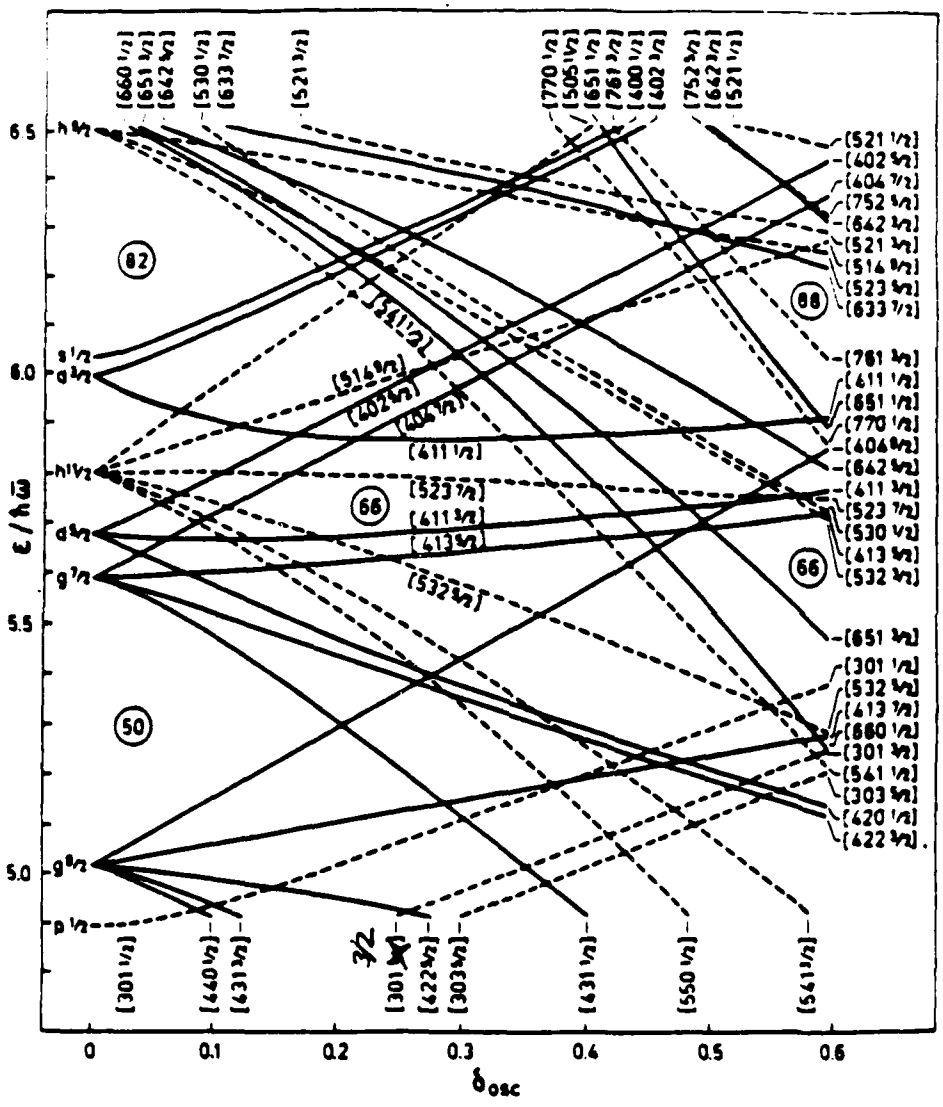

FIGURE 43. Nilsson levels for protons in the region of $50<Z<82$. The cylindrical Nilsson orbitals (reproduced from Ref. 37) are shown as a function of the energy parameter $\varepsilon/\hbar\omega$ and the deformation parameter δ for the region of the valence protons in ^{186}Re. This nucleus has 75 protons and the deformation parameter is approximately $\delta \approx 0.22$. The ground state proton configuration is most likely 5/2+ [4 0 2], arising primarily from the d 5/2 level in the spherical limit (at 5.7 $\varepsilon/\hbar\omega$).

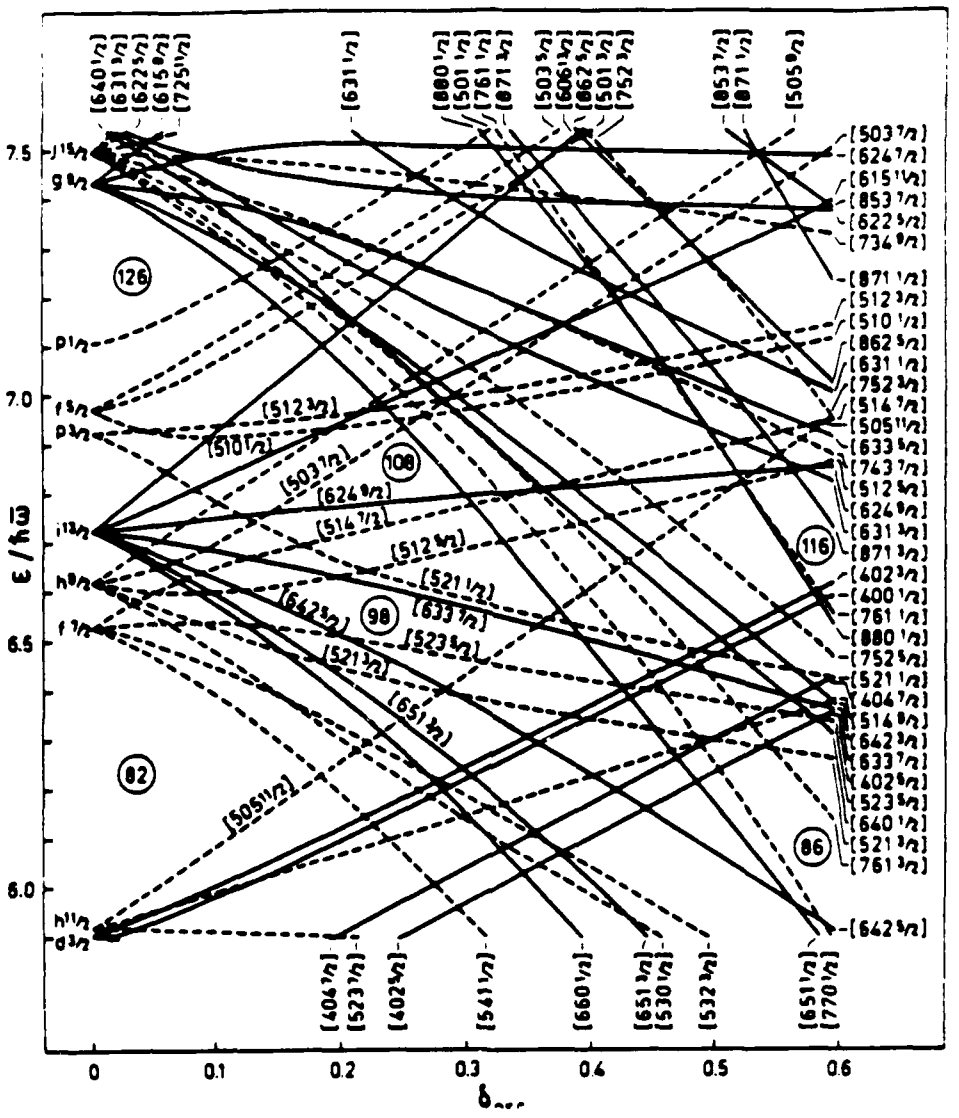

FIGURE 44. Nilsson levels for neutrons in the region of $82 \leq N \leq 126$. The cylindrical Nilsson orbitals (reproduced from Ref. 37) are shown as a function of the energy parameter $\varepsilon/\hbar\omega$ and the deformation parameter δ for the region of the valence neutrons in ^{186}Re. This nucleus has 111 neutrons and the deformation parameter is approximately $\delta \approx 0.22$. The neutron level density in this region is seen to be quite high. The ground state neutron configuration is most likely 3/2- [5 1 2] arising primarily from the p 3/2 level in the spherical limit (at 6.9 $\varepsilon/\hbar\omega$).

degenerate levels for neutrons and protons separately filled with pairs of nucleons, up to the Fermi level. The final complete wavefunction describes a state with the projection of total angular momentum on the nuclear symmetry axis, K, given by the sum of the projections Ω_i for each nucleon (i). In the ground state, $K = |\sum_i \Omega_i| = ||\Omega_p| \pm |\Omega_n||$ where Ω_p and Ω_n are the quantum numbers of the odd proton and odd neutron, where applicable. The power and success of the Nilsson model lies not only in its ability to describe wavefunctions of a particular nucleus but also to describe relationships amongst nuclei in deformed regions throughout the periodic table. These systematic trends permit a qualitative understanding of nuclear energy levels.

In Figs. 43 and 44, the single-particle spherical shell model states are listed by their ℓ and J quantum numbers. The states of good orbital angular momentum ℓ are superpositions of states of good cylindrical symmetry. When the spherical symmetry is broken, the associated energy levels split into doubly-degenerate energy levels associated with the cylindrical states. These states are labelled in Fig. 43 and 44 by the asymptotic Nilsson quantum numbers [N n_3 Λ Ω].

C. ANALYSIS: SYSTEMATIC TRENDS IN THE LOW-LYING ENERGY LEVELS OF ^{186}Re AND NEARBY NUCLEI

The Nilsson level scheme is expected to provide a good description of nuclear rotational levels. As noted in the discussion of ^{166}Ho (Ref. 37), one can attempt a description of the low-lying energy levels of the spectrum of an odd-odd nucleus in terms of the coupled configurations of the last odd proton and the last odd neutron in Nilsson levels near the Fermi surface. In such an approach, the two-valence nucleon states determine the intrinsic states of rotational bandheads. This bandhead is the first member of a rotational band. Excited members of the rotational bands comprise successively

higher rotational states of the same intrinsic state. It is with this picture that we analyze the low-lying nuclear structure in ^{186}Re.

In proceeding to account for the low-lying levels of ^{186}Re, the configurations of the last odd proton and the last odd neutron must be determined. These configurations will be used to directly obtain the intrinsic state configurations. This is easily done by considering two items: (1) the applicable Nilsson diagram and (2) the states of the uncoupled odd-neutron and odd-proton.

The applicable Nilsson splitting diagrams are shown in Figs. 43 and 44. The energy unit ($\hbar\omega_o/2\pi$) $\approx 47A^{-1/3}$ MeV is approximately 7.2 MeV, where A is the atomic mass number. For ^{186}Re, the nuclear deformation parameter (δ) is expected to be $\delta \approx 0.22$, based on systematics of nuclear quadrupole deformations of nearby nuclear ground states (Ref. 37). With the Nilsson diagrams as a guide, we next find the states of the uncoupled nucleons. If, for example, we were to remove the single odd neutron from ^{186}Re, we would obtain ^{185}Re (Fig. 45). The intrinsic states of ^{185}Re would then involve configurations of the single odd proton. Likewise, the removal of a proton from ^{186}Re reveals the odd neutron states in the spectrum of ^{185}W. This is not the only information available from nuclear systematic trends. We can add, rather than remove, single nucleons to ^{186}Re to reveal states of the other remaining nucleon. Finally, the addition or removal of nucleon pairs to odd nuclei provides additional information as described below.

1. Odd Proton Levels

It is convenient to first consider the nuclear structure of ^{185}Re. This nucleus has one less neutron than in ^{186}Re. The net projection of angular momentum on the nuclear symmetry axis is then given solely by the uncoupled valence proton since all of the neutrons are paired. From the Nilsson level splitting

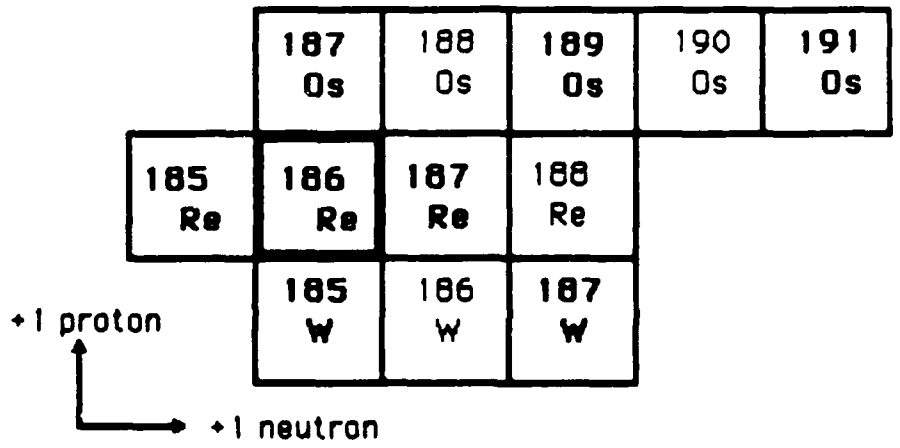

FIGURE 45. Nuclides in the vicinity of ^{186}Re

diagram, using values of the deformation parameter $\delta \approx 0.22$, it is seen that the π 5/2+ [402] and π 9/2- [514] proton orbitals are expected to be major contributors to the states in the lower energy region of the spectrum. In this notation, the symbols π or ν refer to proton or neutron orbits, respectively. The remaining numbers are the Nilsson quantum numbers now expressed in the form $K^{\pi}[Nn_3\Lambda]$. For the bandhead member (lowest energy state) of a rotational band having no rotational energy, the K quantum number is equal to the total nuclear spin. (In the case of K = 0 bands, the additional rotational quantum number $r = \pm 1$ is required to distinguish states of equal K but of differing symmetry under a rotation of π radians around an axis perpendicular to the intrinsic symmetry axis.)

Experimentally, it is found that the ground state of ^{185}Re is associated with the Nilsson state π 5/2+ [402] and that the next bandhead state at 368.2 keV is associated with the Nilsson state π 9/2- [514]. Using $(\hbar\omega_o/2\pi) \approx 7.2$ MeV, the 368 keV energy spacing is approximately 0.05 $(\hbar\omega_o/2\pi)$, quite consistent with the order of magnitude of the Nilsson spacing associated with the deformation parameter $\delta \approx 0.22$. It is noted that the next higher orbitals, the π 1/2- [541] and π 5/2+ [402] lie much higher in energy than these latter two orbitals. (The level scheme for ^{185}Re is reproduced in Fig. 46.)

The addition of one neutron to ^{186}Re leads to the nucleus ^{187}Re. Here the same 5/2+ [402] ground state and 9/2- [514] excited bandhead state are experimentally observed. Other additional bandhead states are also observed above 500 keV. With these identifications, the lower lying configurations of ^{186}Re are expected to involve the 5/2+ [402] and 9/2- [514] proton orbitals, as listed in Table 9.

2. Odd-Neutron Levels

In contrast to the smaller number of Nilsson proton orbitals, the number of valence Nilsson neutron levels is higher.

This increased density of Nilsson levels was seen in the neutron-level splitting diagram of Fig. 44 in the deformation region of $\delta \approx 0.22$ and for a neutron number (N) of N = 111. Considering the complexity of the level-splitting, it appears very important to study levels of actual nuclei to understand the appropriate single-particle Nilsson level sequences. This approach differs from that taken in Ref. 39. Nilsson configurations which actually occur can arise from local deviations of the overall Nilsson parameters from their average values.

The structural aspects of the nucleus ^{185}W are considered first. This nucleus has one less proton than ^{186}Re. Hence, all remaining protons are paired. The low-lying states of ^{185}W are expected to arise from rotational bands built upon a Nilsson configuration associated with a single odd neutron. In the region of 111 neutrons, in the deformation range of 0.2 to 0.3, it is seen from the general Nilsson splitting diagram that a good number of Nilsson orbitals are present. Of these, nine states have been identified in ^{185}W and are listed, along with their associated energies, in Table 9. (The level scheme for ^{185}W is reproduced in Fig. 47.)

Most of the neutron states in this region have odd parity, which is consistent with the odd parity of the 3p-2f-1h isotropic harmonic oscillator shell. The only positive parity subshell (i 13/2) arises from the 1i harmonic oscillator level. This level lies low in the single-particle spectrum for it is substantially stabilized by strong spin-orbit effects. This state, as will be seen shortly, can lead to an isomeric state in ^{186}Re.

It is noted that the nucleus ^{183}Hf is obtained from ^{185}W by the removal of a pair of protons. The ground state of ^{185}W is observed to have $J^{\pi} = 3/2-$, consistent with the 3/2- [512] Nilsson model assignment. Likewise, the states of ^{187}Os reveal the 1/2- [501], 3/2- [512], 7/2- [503] and 11/2+ [615] low-lying bandhead states. This particular nucleus has one more proton

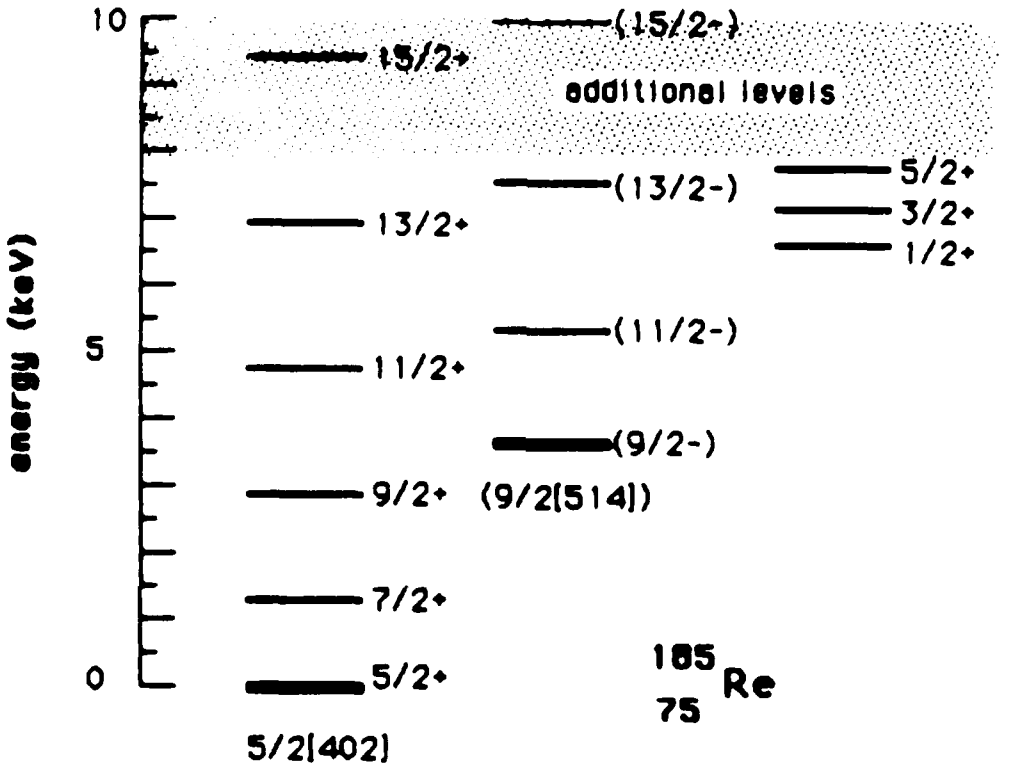

FIGURE 46. Nuclear Levels in ^{185}Re. The nuclear spectrum depicted here is characterized by two low-lying rotational bands built upon Nilsson orbitals for a single odd proton. The single odd proton states are expected to be similar to the contributing proton states in ^{186}Re.

TABLE 9. NILSSON BANDHEAD STATES

^{185}Re Proton States		^{185} Neutron States		^{186} Coupled States	
State	keV	State	keV	State$\{\Omega_p.\Omega_n\}$	keV
5/2+[402]	0	3/2-[512]	0	1-{5/2,3/2}	0
		1/2-[510]	23.6	3-{5/2,1/2}	99.3
9/2-[514]	368.2	7/2-[503]	243.5	8+{5/2,11/2}	150
		11/2+[615]	197.4	4-{5/2,3/2}	174
		9/2+[624]	720	6-{5/2,7/2}	186
		9/2-[505]	790	2-{5/2,1/2}	210
		5/2-[512]	890	3+{5/2,11/2}	314
		1/2-[521]	1007	1-{5/2,7/2}	316
		7/2-[514]	1058	(5+){9/2,1/2}	(330)
				(3+){9/2,3/2}	351.2

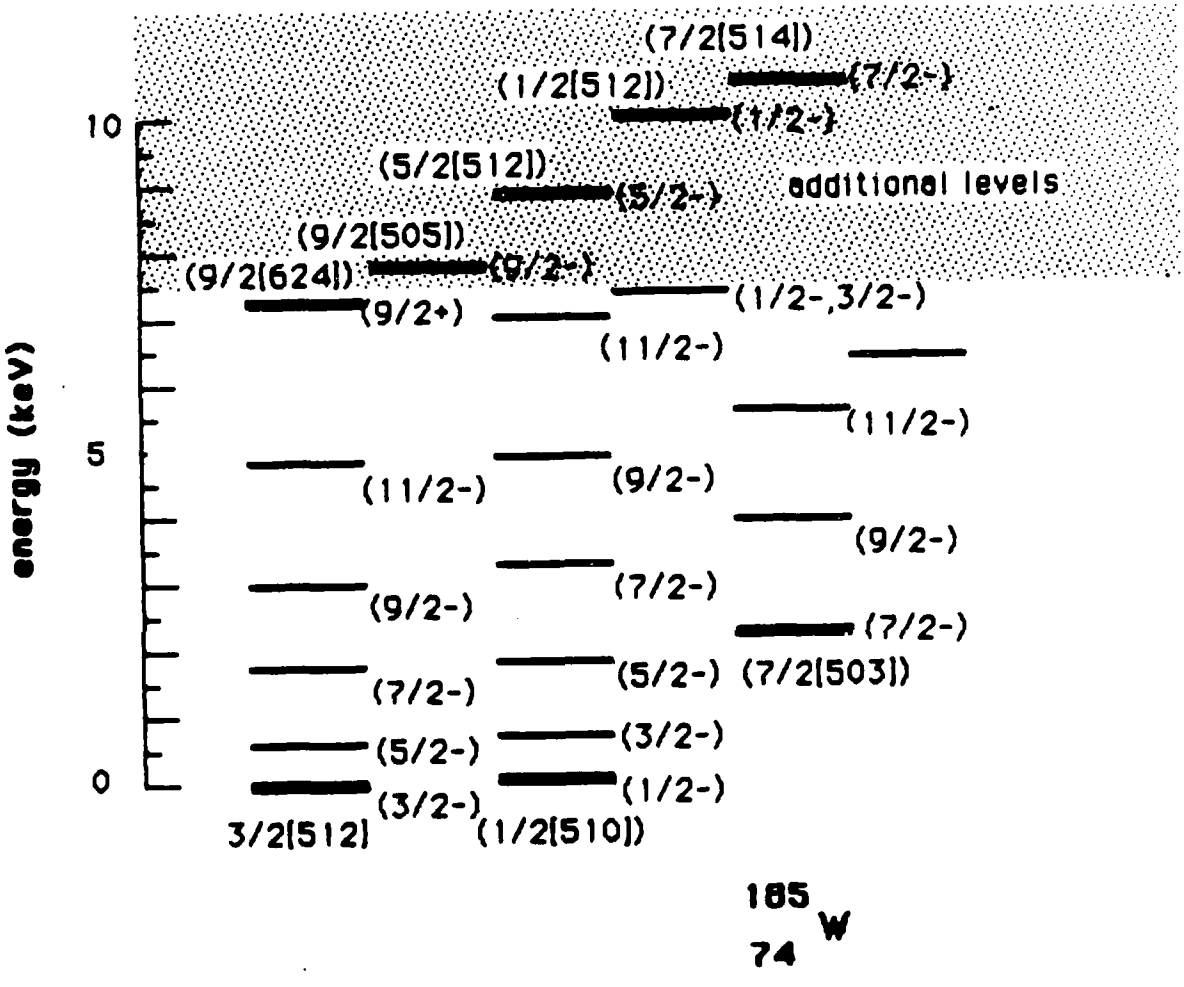

FIGURE 47. Nuclear Levels in ^{185}W. The nuclear spectrum depicted here is characterized by four low-lying rotational bands built upon Nilsson orbitals for a single odd neutron. The single odd neutron states are expected to be similar to the contributing neutron states in ^{186}Re.

than ^{186}Re; consequently, only states which involve a single odd-neutron are observed. (The level scheme for ^{187}Os is reproduced in Fig. 48.)

3. States in ^{186}Re

One may consider the lowest states in ^{186}Re as arising from the coupling of the π 5/2+ [402] and π 9/2- [514] proton states with the lower-lying valence neutron states. The states of good K are now given by $|K_i| \pm |K_j|$, $K_j \leq K_i$, where i and j are neutron and proton single-particle labels. Using the ordering of neutron levels of ^{185}W or ^{187}Os and the proton levels of ^{185}Re or ^{187}Re, the bandheads listed in Table 9 are obtained. (The level scheme for ^{186}Re is reproduced in the Fig. 49.) It is important to note that this approach leads to a description of the 1- ^{186}Re ground state in terms of the π 5/2+ [402] x ν 3/2- [512] coupling as opposed to the ν 7/2- [503] coupling discussed in Ref. 39. The former assignment is also consistent with the experimentally known magnetic moment of the ground state as discussed by Ernst, Hagn, and Zech (Ref 46).

The bandhead states associated with the single π 5/2+ state coupled to the four lowest neutron states and their associated rotational band members comprise all assigned levels in the low-lying spectrum of ^{186}Re. The tentative [8+] isomeric states probably arise primarily from the π 5/2+ [402] and ν 11/2+ [615] nucleon couplings. (Note that the π 9/2- [514] and ν 7/2- [503] states also couple to yield a K = 8+ state, but this state is expected at higher energy.)

The bandhead state energies are, in a rigid-rotor approximation, given as the sum of the intrinsic state energy; and an energy spacing proportional to I(I + 1). Thus, for the bandhead states identified here, many of the rotational band spacings are also observed. With this simplest approach it is initially concluded that there are no additional states expected to lie in the vicinity of the [8+] isomeric state. Nonetheless, there

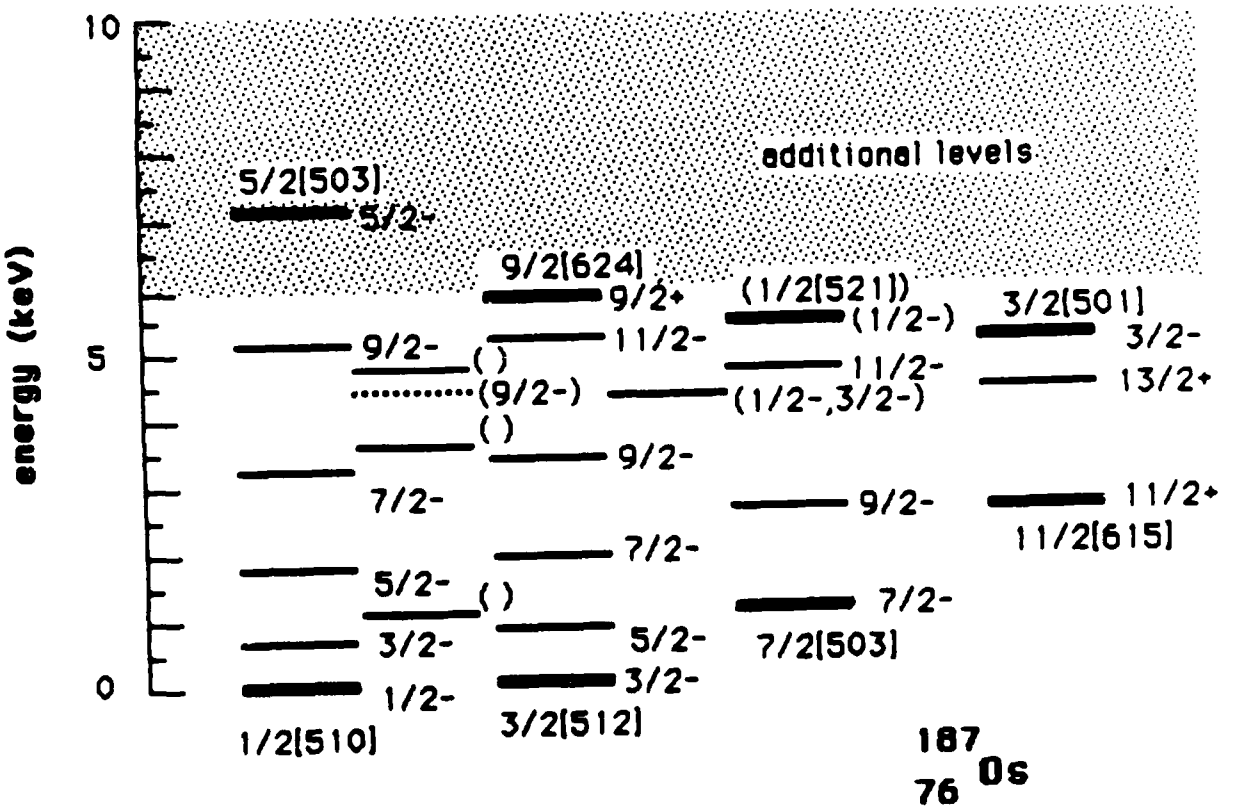

FIGURE 48. Nuclear Levels in ^{187}Os. The nuclear spectrum depicted here is characterized by four low-lying rotational bands built upon Nilsson orbitals for a single odd neutron. The single odd neutron states are expected to be similar to the contributing neutron states in ^{186}Re. Note that four possible levels shown here are not assigned to rotational bands.

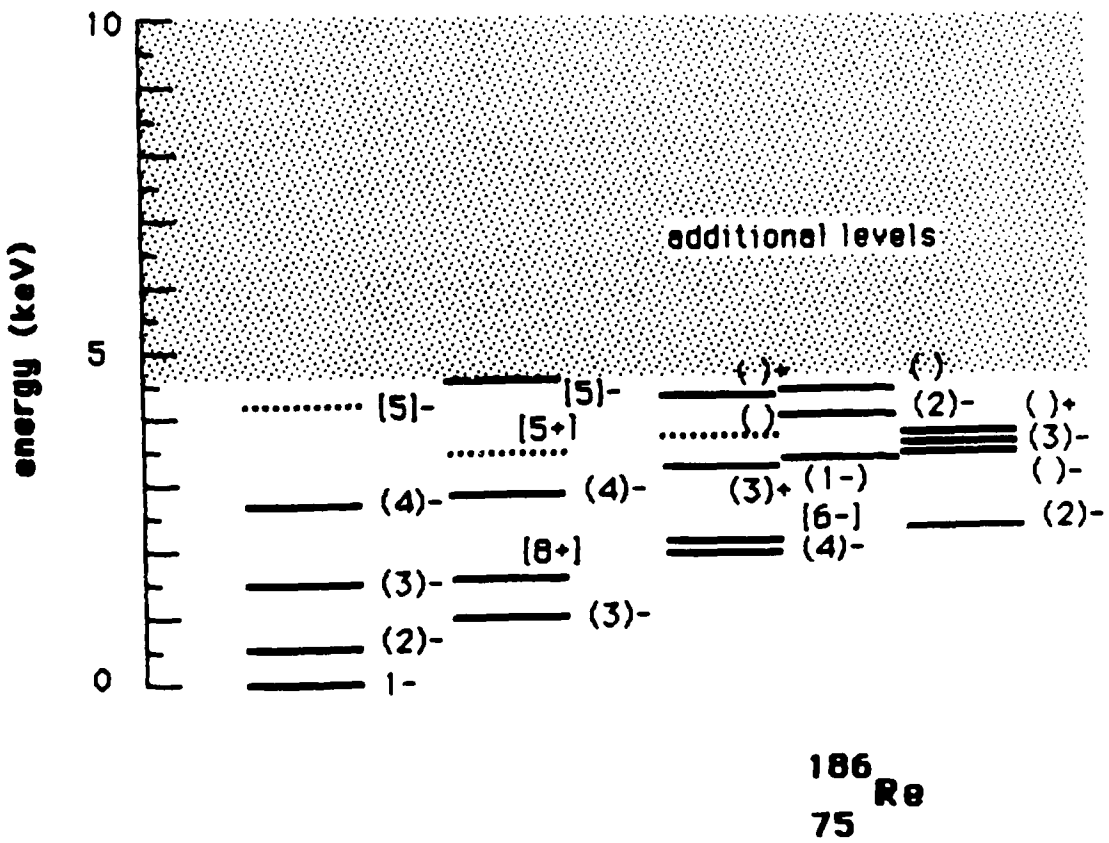

FIGURE 49. Nuclear levels in ^{186}Re. The low-lying levels in ^{186}Re are depicted in the vicinity of the isomeric [8+] level. These levels are expected to be related to the coupling of a single odd proton and a single odd neutron in the Nilsson scheme.

are other factors to consider and simple approaches are not expected to be all-conclusive.

4. $J\pi = 7-$ States of Interest in ^{186}Re

Since a state with angular momentum and parity 7- would be useful from the viewpoint of an E1 photon pumping scheme which uses the [8+] isomeric state as an initial state, that prospect now is considered. Such a state could presumably arise from ν 9/2[505] x π 5/2+ [402] or as the excited rotational member of the tentative 6- rotational band. Using the fairly consistent rotational band energy spacings of approximateiy 15 I(I + 1) keV, this latter rotational band member is predicted to lie around 400 keV. This is found using the calculated energy spacing between I = 6 and I = 7 and adding it to the bandhead energy. (Smaller energy deviations are expected to arise from particle rotational couplings.)

Another 7- level can arise from a 9/2- [505] neutron level coupled to a 5/2+ [402] proton level. States of ^{186}Re which involve the 9/2- [505] neutron level are expected to lie high in the low-lying energy level spectrum, above the [8+] isomeric state, if one considers the neutron levels in ^{185}W or ^{187}Os. To understand such systematics it is convenient to consider the addition or subtraction of one proton to ^{186}Re and then the successive addition of neutron pairs. When this is done, the neutron orbitals are systematically filled. Such a filling places an odd neutron in higher energy orbits, thus altering the ground state spin as well as decreasing the energy required to excite the odd neutron to the 9/2- [505] level. It is important to note that uncertainties in Nilsson parameters taken from systematics will arise.

With the removal of one proton and the addition of two neutrons (-1π, $+ 2\nu$) to ^{186}Re (^{187}W) the lowest neutron orbitals are found to be: 3/2- [512], 1/2- [510], 7/2- [303], 11/2+ [615] and then 9/2- [505]. The 9/2- [505] state is indeed

lowered in energy. The nucleus obtained from (-1π, $+4\nu$) is not well studied. The addition of one proton and two neutrons ($+1\pi$, $+2\nu$) to ^{186}Re leads to ^{189}Os. This nucleus has the low-lying bandhead states 3/2- [512] and 9/2+ [624]. In ^{191}Os ($+1\pi$, $+4\nu$) the first instance of the 9/2- [505] level as a ground state configuration is found. The next excited bandhead states of this nucleus are 3/2- [512] and 1/2- [510]. Noting that the 9/2- [505] states thus consistently rise in energy upon removal of neutrons from ^{191}Os, a tentative 7- state associated with the 9/2- [505] neutron is best expected to lie greater than approximately 500 keV in energy above the ^{186}Re ground state. This is estimated using the average of energy spacings between the 11/2+ [615] and 9/2- [505] levels in ^{185}W (approximately 600 keV) and the 11/2+ [615] and lowest unassigned 9/2 level in ^{187}Os (approximately 200 keV). It is also assumed that no substantial relative energy shifts occur between the 8+ and 7- states thus generated when coupled to the same proton. This can happen, but such further detailed calculations are beyond the scope of this assessment. On the basis of the odd-neutron and odd-proton coupling scheme it is not immediately surprising that no 7- state (or any additional states in general) are thus far detected below 300 keV in ^{186}Re. Nonetheless, semi-quantitative or even qualitative analysis in nuclear structure theory provide for a useful first screening in the understanding of nuclear energy levels.

D. CONCLUSION: POSSIBILITIES FOR IDENTIFYING ENERGY LEVELS IN NUCLEI

The interaction between nucleons includes the strong interaction associated with the complex interactions of constituent quarks, and to lesser extents, the weak and electromagnetic forces. This aspect, the complicating features of the many-body quantum mechanical problem, are indicative of the complex nature of nuclei. Nonetheless, to the extent that nuclei exhibit a shell structure, the complex nucleonic wave functions can be

replaced by simpler wave functions involving valence nucleons--the approach taken in shell model codes. In these models, large Hamiltonian matrices are diagonalized. For the cases where large deformations are evident, many configurations of shell model states are superimposed to give collective shapes. These more sophisticated models must take into account numerous one- and two- nucleon interactions. The development of such codes (Ref. 47 and 48), and in particular, models for odd-even and odd-odd nuclei, are of interest to the γ-ray laser program. As F.S. Dietrich has indicated, nuclei such as ^{186}Re are statistically most probable to have the desired level schemes.

The transition rates between states are important in γ-ray laser schemes. Given the proper state assignment in a simple model, or improved wave functions from more detailed calculations, transition rates can be calculated and compared with experimental rates. (State assignments here will be used for further rate estimates in this report.) Transition rates using collective state wave functions will differ markedly (orders of magnitude) from the single-particle estimates. Realistic transition rates must be quoted in proposals.

From a different perspective, group-theoretical collective models emphasize the geometrical aspects of nuclei by describing nuclear levels in terms of boson or phonon entities. One forefront approach, the Interacting Boson Model (IBM)(Ref. 49) attempts to describe the low-lying level structure of heavy nuclei by emphasizing the s and d boson nature of many-valence nucleonic wave functions. Recent advances in the cylindrical boson description of axially deformed even-even nuclei and super-symmetric models are also of interest in identifying nuclear energy levels.

In this chapter, the energy levels of ^{186}Re were examined with the objective of using the simplest approach to address the possibility of unidentified energy levels in the low-lying region of the excited state spectrum. It was determined on

the basis of theoretical arguments and nuclear systematics that no 7- level is probably closer than 250 keV to the isomeric [8+] level. More quantitative approaches can be used to refine this estimate; and sophisticated models, further developed in the form of advanced computer codes. Furthermore, transition rates between states can be much more important than energy levels alone. Single-particle estimates can be misleading. In addition, the (IBA) collective models may also provide alternative approaches to the understanding of lower lying nuclear energy levels.

VII. A PROPOSED EXPERIMENT TO VERIFY A CONCEPT CRITICAL TO THE DEVELOPMENT OF γ-RAY LASERS

Recently, a new concept has been proposed for the development of a γ-ray laser using dressed states of long-lived nuclear isomers (by C.B. Collins during a briefing at IDA, February 20, 1985). Figure 50 is a schematic which illustrates the procedure. The concept is based on:

1. Preparation of a long-lived isomeric state $|1\rangle$ of energy E_e (first inversion step),
2. Preparation of a dressed state $|1'\rangle$ of energy Ee' close to the original state $|1\rangle$ of energy E_e by the application of RF fields, and
3. Stimulated emission from the dressed state resulting in γ-ray lasing.

The exciting feature of this concept is that it may provide a means of using long-lived isotopes for γ-ray laser development by obviating the inhomogeneous broadening problem (Ref. 3). The transformation to a dressed state provides a short-lived level, whose resonance is not destroyed by inhomogeneous broadening and thus can be used for stimulated emission. This procedure avoids the problem of inhomogeneous broadening, which not only prevents the use of long-lived isomeric transition for γ-ray laser development, but also inhibits the resonance overlap required for the observation of the Mössbauer effect in these systems.

One critical issue is the existence of isotopes with closely spaced nuclear levels (≈ 1 keV or less), with one of them corresponding to a long-lived isomeric state. In the highly deformed region of the nucleus, coupling schemes lead to

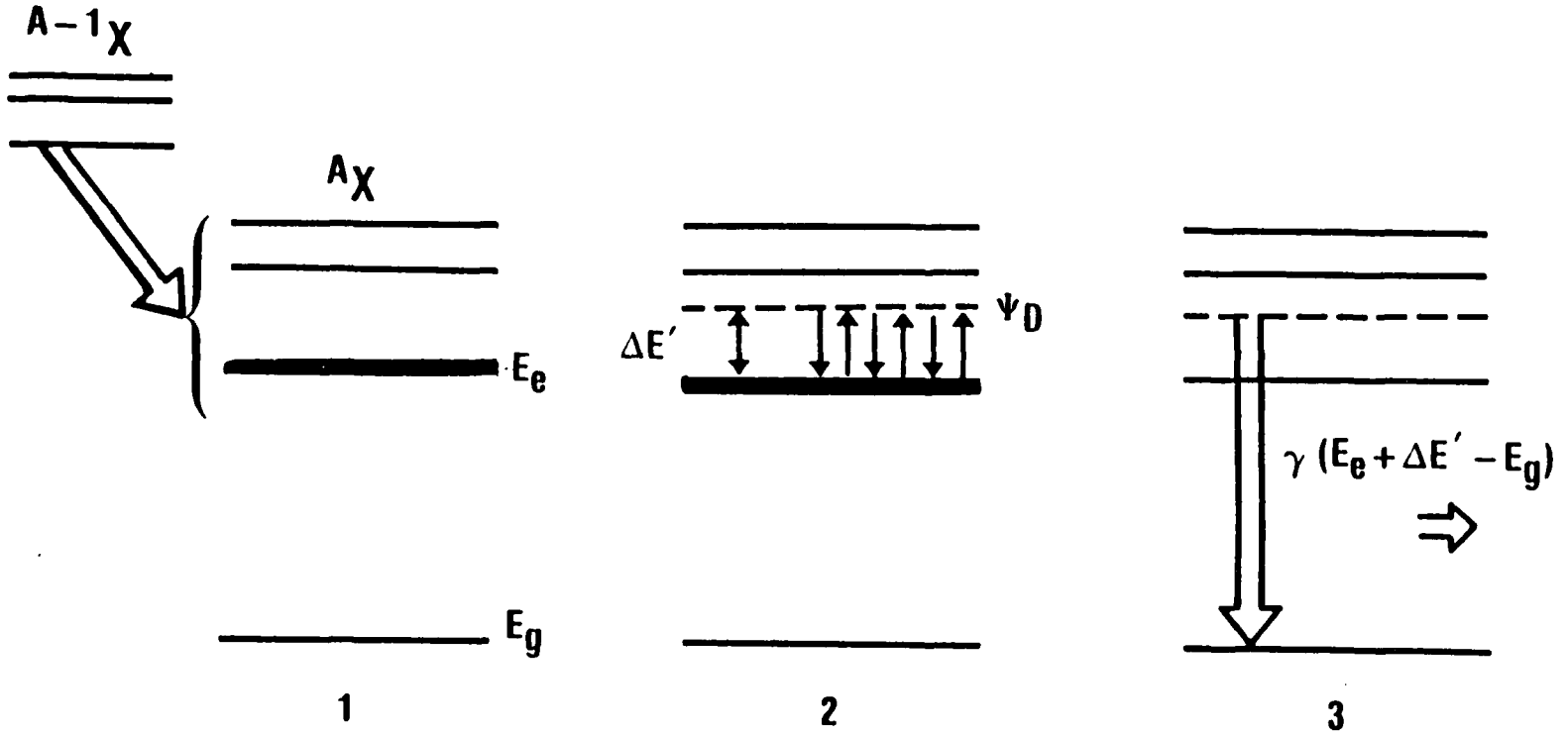

FIGURE 50. "Dressed State" γ-ray laser concept.

levels, not all of which may be identified. Such "missing" levels, close to isomeric states, may play the desired role.* An experimental search for them is ongoing (personal communications with G.C. Baldwin and C.B. Collins).

The other critical issue is the ability of available RF radiation to prepare a dressed nuclear state. Mössbauer transmission experiments with RF fields irradiating iron foils have been reported which show distinct sidebands, as shown in Fig. 51. One group of researchers claims that these are due to acoustic coupling of the magnetic field with the metallic foil (Ref. 50 and 51). Another explanation is given in terms of a dressed state picture (Ref. 4) and the results of the experiments are used as evidence for the preparation of a "dressed state".

Since the dressed state concept is important to the γ-ray laser development program, the author proposes a more discriminating technique, Selective Excitation Double Mössbauer (SEDM) (as described in Ref. 52) to investigate this phenomenon. A short discussion of SEDM is presented in the Appendix. Briefly, SEDM is a Mössbauer flourescence experiment. The setup is shown in Fig. 52. A source of Mössbauer radiation (^{57}Co) is tuned to coincide with one of the resonances of a sample (^{57}Fe foil) and the energy of the scattered radiation is measured with a single-line Mössbauer absorber. Such experiments have been used successfully to obtain new information about paramagnetic relaxation (Ref. 53) and can be used here to study dressed states by applying an RF field to the absorber, as shown in Fig. 52. If this field produces "dressed states" of the nucleus, the emitted radiation should contain different energy components from the unperturbed case and the SEDM spectrum should show resonance

*An examination of levels in ^{186}Re indicates that coupling of the valence p and n leads to a set of 10 levels, 9 of which can be identified with known excited states, with the exception of the J = 7- state. That expected J = 7- state is labeled a "missing state"; if it exists where expected, it would enable a scheme to pump to that level from an isomeric J+ = 8+ state using 36 keV x-rays.

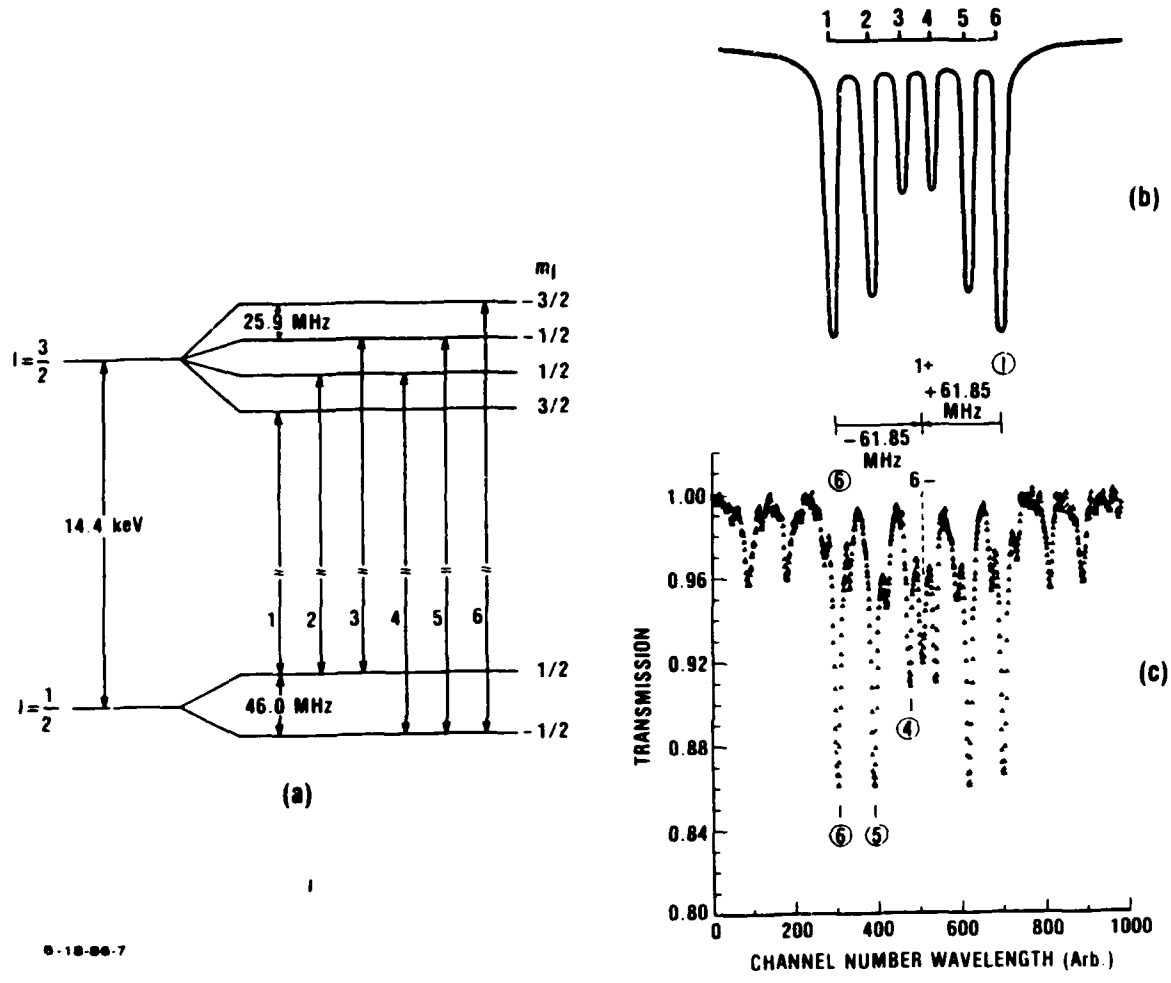

FIGURE 51. Generation of sidebands in Mössbauer spectra of ^{57}Fe. (a) Energy level diagram for ^{57}Fe showing the allowed transitions. (b) Transmission spectrum without an RF field irradiating the sample. (c) With a 61.58 MHz RF field (from Ref. 1).

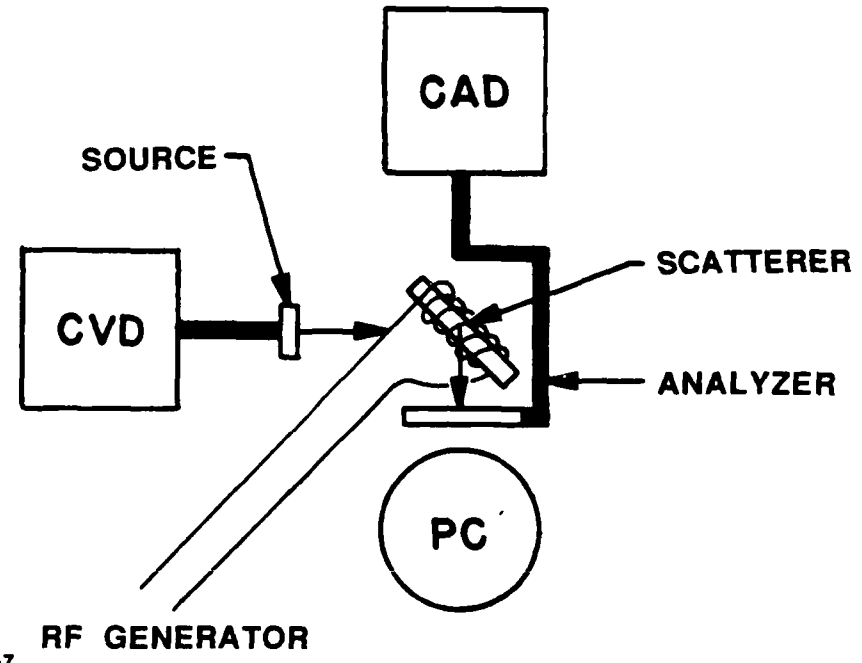

FIGURE 52. The SEDM NMR experimental setup. A ^{57}Co source is attached to the constant velocity drive (CVD). The source velocity shifts the energy of the radiation emitted to correspond with one of the resonances in the sample. A constant acceleration drive (CAD) is used to scan the resonances and measure the energy of the scattered radiation. The modified SEDM NMR experiment uses the RF coil to generate sidebands in the Mössbauer spectrum.

lines corresponding to these transitions. The expected results are shown in Fig. 53.

In Fig. 53(a), the transmission result of Fig. 50 is reproduced. It contains all the resonances of the system in the "dressed state" picture, as well as the resonances possible with the acoustic coupling picture. Figure 53(b) shows the expected SEDM spectra, due to excitation at the energy indicated by the vertical arrow in Fig. 53(a), if the acoustic coupling is responsible for the sidebands in Fig. 53(a). Figure 53(c) shows the expected spectrum if dressed states have been produced and are responsible for the sidebands. The second dip appears because a dressed state would be a linear combination of the nuclear states (Ref. 54) and thus would permit a transition to both ground states (Ref. 52). Variations on this experiment, such as excitation of different resonances [different positions of the vertical arrow in Fig. 53(a)] could, of course, produce further detailed information about the process or processes in question.

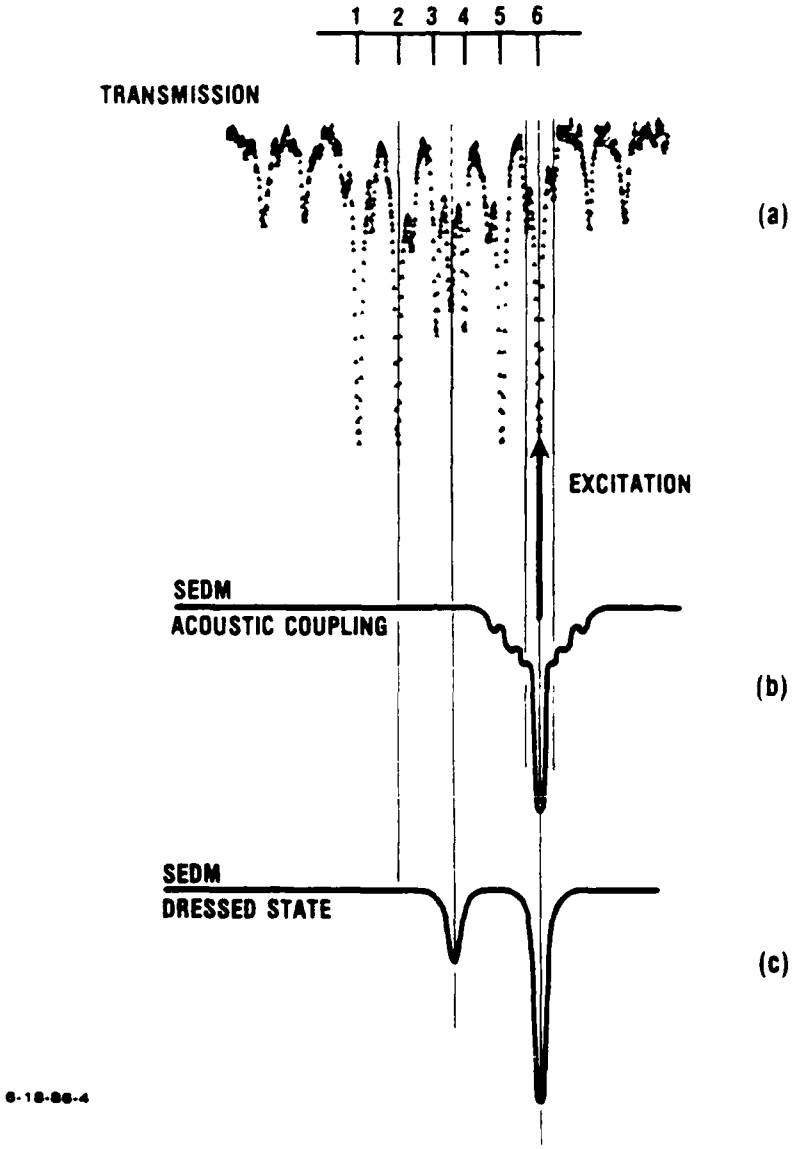

FIGURE 53. SEDM discrimination between two possible sideband generators. (a) Transmission spectrum of ^{57}Fe foil showing sidebands. SEDM spectrum from excitation of the sixth line as shown by vertical arrow in (a) if the acoustic coupling model is operating (b), and if the dressed state model is operating (c). The line in (c) at position of resonance 2 comes from an admixture of $|-1/2>$ to the $|-3/2>$ by the RF field as required by dressed state theory. The acoustic coupling cannot mix states in this way.

VIII. PROPOSED SCREENING EXPERIMENT FOR CANDIDATE NUCLEI FOR A THREE-LEVEL, TWO-PUMP, γ-RAY LASER

As previously described in this report, one of the more promising concepts for the development of a γ-ray laser involves optical pumping of a pre-prepared, long-lived Mössbauer isotope to a higher, nearby level of short lifetime. The advantage of this technique over direct production of a short-lived state from the ground state via neutron bombardment is that much larger quantum fluxes (>> $10^{17}/cm^2\ sec^{-1}$) would be available for the (secondary) pumping process.

Clearly, the critical issue for this technique is whether there is a Mössbauer isotope with the requisite nearby level. Such levels are expected theoretically; however, consistent with the low-frequency resolution typical of nuclear experiments, such levels have yet to be observed.

An experiment to test this critical issue is currently being planned by workers elsewhere. Their design calls for the broadband irradiation of long-lived isotopes, in the hope that if there is an appropriate nearby level, there will be sufficient power near resonance to make an observable difference in the decay rate to ground state.

We propose here an alternative simpler experiment, designed to rapidly screen for candidate nuclei. The basic idea is to heat known long-lived Mössbauer isotopes to high temperatures. If there exists a nearby (1 to 10 eV) short-lived level, then thermal excitation to that level should occur, with an accompanying increase in the rate of decay to ground state.

As an estimate of what one might expect, consider the three-level system depicted in Fig. 54; τ_0 and τ_1 are the lifetimes, respectively, of the long-lived Mössbauer isotope and

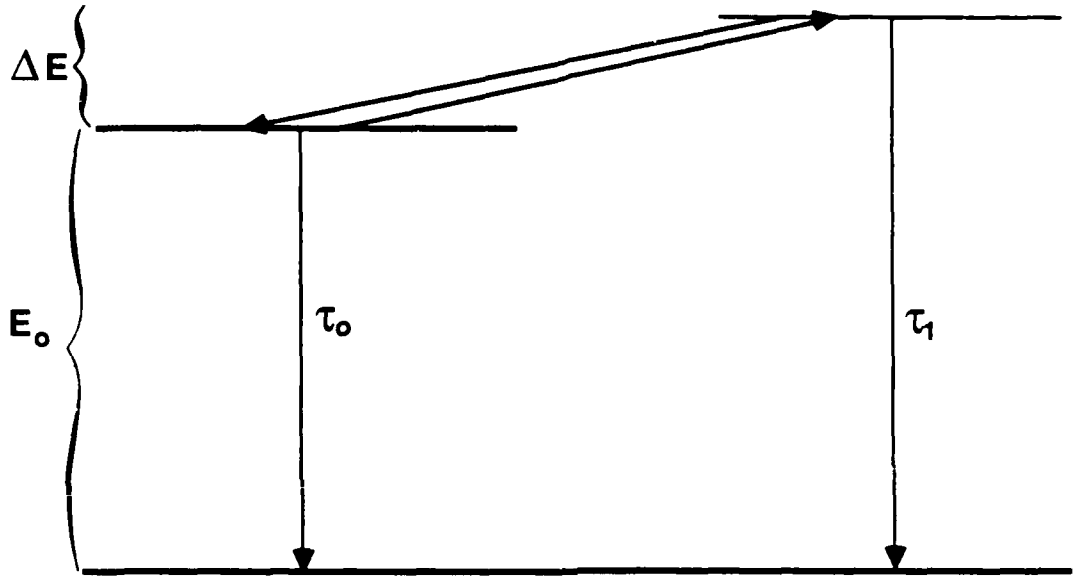

FIGURE 54. Schematic diagram of three-level system. τ_0 and τ_1 ($\tau_0 >> \tau_1$) are the lifetimes of the long-lived short-lived states and ΔE is their energy separation. Rapid thermal equilibration between these two levels is represented by the arrows pointing between them. E_0 is the energy of the long-lived state, and it is assumed that $E_0 >> \Delta E$.

the short-lived nearby level; ΔE is their energy separation. Assuming rapid thermal equilibration between the two excited states, the nuclear transition rate R to the ground state is given by:

$$R = 1/\tau_o + (1/\tau_1)e^{-\Delta E/kT} ,$$

where k is Boltzmann's constant and T is the absolute temperature. The relative increase in rate r in changing from a low temperature T_L to a high temperature T_H is therefore:

$$r = \frac{1 + (\tau_o/\tau_1)e^{-\Delta E/kT_H}}{1 + (\tau_o/\tau_1)e^{-\Delta E/kT_L}} - 1 . \qquad (37)$$

As a canonical example, we take $\tau_o = 10^7$ s, $\tau_1 = 10^{-9}$ s, and $T_L = 300$ K. Values of r corresponding to different values of ΔE and T_H are shown in the table:

TABLE 10. RELATIVE INCREASE IN DECAY RATE WITH TEMPERATURE T_H FOR ISOTOPES WITH VARIOUS ENERGY SEPARATIONS ΔE

ΔE(eV)	T_H(K)				
	500	1,000	5,000	10,000	50,000
1	10^6	10^{11}	10^{15}	10^{15}	10^{16}
5	10^{-34}	10^{-9}	10^{11}	10^{13}	10^{15}
10	10^{-85}	10^{-34}	10^6	10^{11}	10^{15}
50	10^{-487}	10^{-236}	10^{-34}	10^{-9}	10^{11}

For the range of ΔE considered in the table, the decay rate at 300 K is of the order of $1/\tau_o$. Pairs of values of ΔE and T_H

which correspond to observable decay rate enhancement (i.e., $r \gtrsim 1$) are those appearing above the dashed line. For instance, if the Mössbauer isotope has a nearby level with $\Delta E \leq 10$ eV, a temperature increase of 5000 K is sufficient to insure a marked increase in the rate of decay to ground state.

By monitoring the decay rate, while slowly increasing the temperature from 300 K, an estimate for ΔE can be obtained by finding the minimum temperature at which a marked increase in decay rate takes place. This information could be used as an aid in the selection of pumping frequencies to be used in more sophisticated, follow-on experiments on candidate nuclei.

A null result in the above experiments does not necessarily insure the absence of a nearby level. The assumption of rapid thermal equilibration of the two excited states may not hold and, if this is the case, the decay rates at elevated temperatures will be lower than those predicted by the model considered here. However, if a nearby level does exist but is not discovered through simple heating, it is likely that it will not have the characteristics required for γ-ray lasing, for optical pumping to the nearby level will then also be difficult.

IX. DISTINCTIONS IN SUPERRADIANT THEORIES -- COHERENT PARTICLE EMISSION

A. SYMMETRY ASPECTS OF ENHANCED SPONTANEOUS DECAY

The coherent (stimulated) emission of a directed beam of particles from transitions involving excited nuclear internal degrees of freedom (Ref. 55), is of immediate interest to our understanding of superradiant emission in a theoretical gamma-ray laser (Ref. 56, 57). In this report we make distinctions between superradiance in the original theory of Dicke (Ref. 58), an effect which can be thought of as a quantum enhanced spontaneous decay, and the macroscopic superradiance (or superfluorescence associated with the evolution of an intense, transient, laser pulse (Ref. 59). One could concisely suggest that tentative evidence for a nuclear quark super-radiator has already preceded the appearance of a gamma-ray "laser" (Ref. 60).

The intent here is to identify the subtleties of Dicke superradiance in two-level systems, extensions of three and n-level systems (Ref. 61), and the relevance of quark transitions to superradiant theory.

Coherence in spontaneous radiation processes was first predicted by Dicke in Ref 58. The essence of the effect (first cast in the context of molecular transitions) is that all emitters interacting with a common radiation field cannot be treated as independent quantum mechanical systems. The entities in the system are assumed to have two levels, denoted as $|\alpha\rangle$ and $|\beta\rangle$, which can be thought of as basis states of a system described by a dynamic SU(2) symmetry (Ref. 62 and 63). The many-body wave function is then written as $\psi_{gm} = U_g\ (r_1 \ldots r_n)\ [+ + - + \ldots]$

where the factor Ug denotes center-of-mass position coordinates and the second factor lists the signs of internal energies. Here, m is a quantum number, to be discussed, and g refers to other quantum numbers not of interest. One associates the difference in occupation number of excited states, n_+, and lower states, n_-, with the only diagonal SU(2) generator $\sum_{j=1}^{n} R_{j3} = R_3$. The Hamiltonian is $H = H_c + E\sum_{j=1}^{n} R_{j3}$. Thus, the energy of the n particle system is $E_{gm} = E_g + mE$ where $m = 1/2\ (n_+ - n_-)$. The complete multiplets of states are labelled by the quantum number r, where r(r+1) is the eigenvalue of $R_1^2 + R_2^2 + R_3^2$, and the quantum number m, the eigenvalue of R_3. Here R_1, R_2, and R^3 are the known SU(2) generators.

In a weight diagram (Ref. 62) one plots state coordinates m on a line (Ref. 61). This is depicted in Fig. 55. Transitions will now appear as lattice shifts, and lattice shifts are only generated by R_1 or R_2. The association of the electromagnetic interaction $\vec{p}\cdot\vec{A}$ with off-diagonal group generators $-\vec{A}(\vec{r}_j)\ .\ (\hat{e}_1 R_{j1} + \hat{e}_2 R_{j2})$ is sufficient to identify:

$$\psi_{gmr} = [(R^2 - R_3^2 - R_3)^{-1/2}(R_1 - iR_2)]^{r-m}\ \psi_{grr}\ , \quad (38)$$

where $\vec{A}$ is the electromagnetic vector potential, and $\hat{e}_1$ and $\hat{e}_2$ are polarization vectors. The intensity is then expressed in the usual manner (using the well known angular momentum theory described in Ref. 64):

$$I = I_o\ (r + m)(r - m + 1)\ , \quad (39)$$

where I_o is the intensity of the usual spontaneous decay. If r is large (the limit of maximum symmetric permutation symmetry) and |m| is small, then $r \approx n/2$, $m \approx 0$ and $I = I_o\ (n/2)(n/2 + 1)$.

The superradiant state occurs at zero population inversion and with a high cooperation number r. The intensity of its

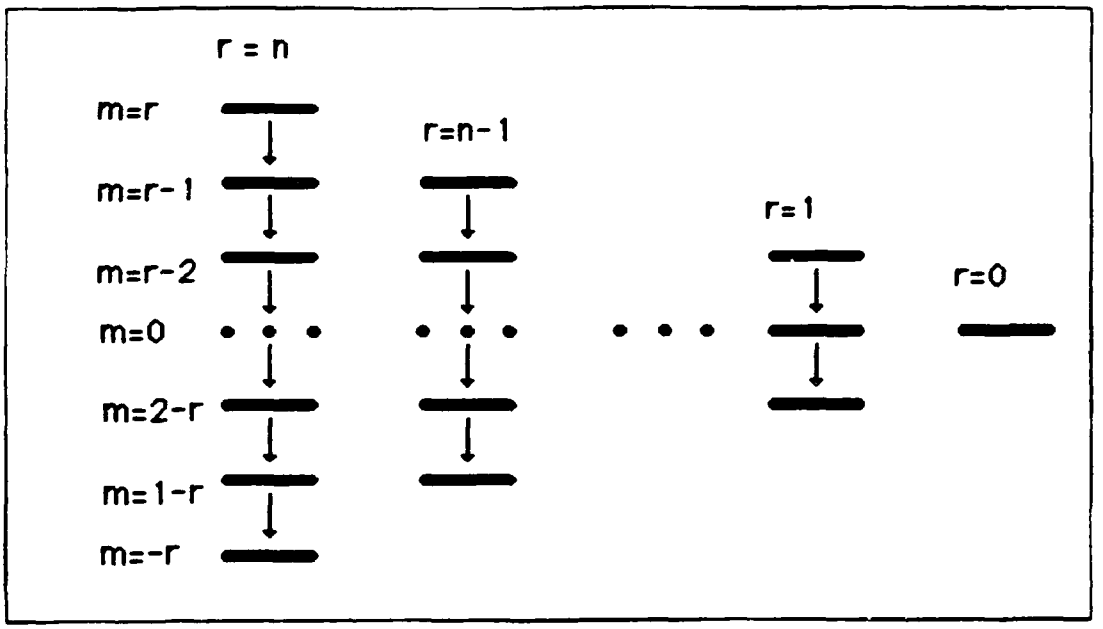

FIGURE 55. Multiplets in the Dicke superradiant model.

decay is proportional to n^2. It is important to note the prediction that low r multiplets have diminished rates. One way to test the appearance of low r multiplets is to exploit the temperature dependence they will introduce. This temperature dependence is determined by a statistical distribution of states of the entire system among all multiplets. Then the superradiant intensity

$$I = (1/4)I_o n(n-1)\tanh^2(E/kT) + nI_o/2 \qquad (40)$$

should follow (Ref. 58). This differs from the case involving only the symmetrically coupled maximum r multiplet. Here, k is Boltzmann's constant and T is the temperature.

The treatment of situations involving (a) particle systems with dimensions larger than the radiation wavelength and (b) regions small with respect to the reciprocal of the natural linewidth require the specification of direction $\vec{k}$:

$$I(\vec{k}) = I_o(\vec{k})\,[(r+m)(r-m+1)] \quad . \qquad (41)$$

The important results are that the radiation is assumed to be a plane wave with propagation vector $(\vec{k})$, coherent in the $\vec{k}$ direction, and has coherence destroyed to the extent that emission in other directions causes transitions to lower r multiplets.

The explicit features of non-symmetric multiplets and smaller r multiplets is lost in the Feynman, Vernon, and Hellwarth (Ref. 65) representation of superradiance. This arises from the inability of this approach to treat the permutation number symmetry.

In this latter, well-known approach, the vector $\vec{r}$ (whose 3-axis component in an internally rotating coordinate frame is indicative of the population inversion) rotates according to $\frac{d\vec{r}}{dt} = \vec{\omega}(t) \times \vec{r}$ where ω_1 and ω_2 are transition rates and $\omega_3 = \omega$. Superradiant emission occurs when all emitters at some time, t_o,

contribute coherently to a single giant dipole moment. Such an approach is devoid of the other r multiplets; and features such as N different states having $n_+ = n_-$ are not distinguished. Still, a fully inverted system is brought to superradiance after a $\pi/2$ pulse at time $t_o = \omega/(2|\omega_I|)$, where $\omega_I = -2\mu E/\hbar$ and μ is the transition dipole moment. The radiated power is proportional to n^2. Details of the conditions for creating such a superradiant state are given in Ref. 65.

In connecting the quantum and semi-classical approaches to superradiant emission (Ref. 66), the maximum cooperation number and cooperation times are addressed. For a rod geometry:

$$I(\vec{k}') = I_o(K')(n/4)(1 + n\,|\langle e^{i(\vec{k}-\vec{k}')\cdot\vec{x}}\rangle|^2) \ , \qquad (42)$$

where $\vec{k}'$ is chosen along the rod axis (Ref. 58). For emission confined to a cone of aperture $\Delta\Omega \simeq 4\pi\lambda^2 A$, the enhancement in emission rate is $\gamma_D = \gamma\lambda^2 n/4A$, where γ is the spontaneous emission rate. Clearly, decay rates for large n systems can be very short. Non-independent decay is postulated to occur in samples whose length $l \lesssim c/2\gamma$ -- all emitters are in the same radiation field before the decay process is completed.

In assessing this picture of superradiance, we note that the theory of superradiance proposed by Dicke is heavily embedded in the assumption of an underlying symmetry, from the viewpoint of the field, of the collective emitter wave functions.

Two possibilities interest us:

- The theoretical extension of superradiant processes to other than SU(2) pictures. That is, it would be interesting to investigate coherent emissions in SU(N) systems where competing (and non-commuting) SU(2) subgroups enter, as this addresses multilevel effects, and closely related;
- Coherent spontaneous interactions with other than the photon field.

Both of these facets enter into unusual systems, such as multilevel electromagnetic systems (i.e., effects in parametric oscillators) multi-dimensional systems; and emissions into boson fields -- such as the case of the pi-meson.

B. COHERENT PION EMISSION

This proposed effect is of sufficient interest in justifying a broader interpretation of superradiant emission that it is briefly summarized here in terms appropriate to the level of the discussion.

In the three-quark baryon multiplets (Ref. 62 and 63) depicted in Fig. 56 as SU(3)-subgroup weight diagrams (neglecting other than up ψ_1 down ψ_2 or strange ψ_3 quarks) we highlight the appearance of nucleons (proton and neutron) and deltas (Δ^{++}, Δ^{+}, Δ^{0} and Δ^{-}). These are solely dependent on up and down quarks as given by their highly simplified isospin-hypercharge wave functions:

$$\Delta^{++} = \psi_1\psi_1\psi_1$$
$$\Delta^{+} = 1/\sqrt{3}\ (\psi_1\psi_1\psi_2+\psi_1\psi_2\psi_1+_2\psi_1\psi_1)$$
$$\Delta^{0} = 1/\sqrt{3}\ (\psi_1\psi_2\psi_2+\psi_2\psi_1\psi_2+_2\psi_2\psi_1)$$
$$\Delta^{-} = \psi_2\psi_2\psi_2$$
$$p = 1/\sqrt{3}\ (\psi_1\psi_1\psi_2-\psi_2\psi_1\psi_1),\ 1/\sqrt{2}\ (\psi_2\psi_1\psi_1-\psi_1\psi_2\psi_1)$$
$$n = 1/\sqrt{2}\ (\psi_1\psi_2\psi_2-\psi_2\psi_2\psi_1),\ 1/\sqrt{2}\ (\psi_1\psi_2\psi_2-\psi_2\psi_1\psi_1)$$

Here, two sets of proton and neutron wavefunctions must be coupled to spin and color degrees of freedom for an overall anti-symmetric wavefunction. Other additional flavors introduce higher dimensional groups. We take the hypercharge Y and the three-component of isospin I_3 as good quantum numbers to form the two-dimensional planar weight diagram which is sufficient for our purposes.

Now note that the pi-meson appropriate to this particular system encompasses quark anti-quark pairs solely involving up and down quarks. The usual meson-baryon interaction (Ref. 55) is written as $H_{int} = g\phi_\pi\ ^{\dagger}J^{-}$ + H.C., where g is a coupling

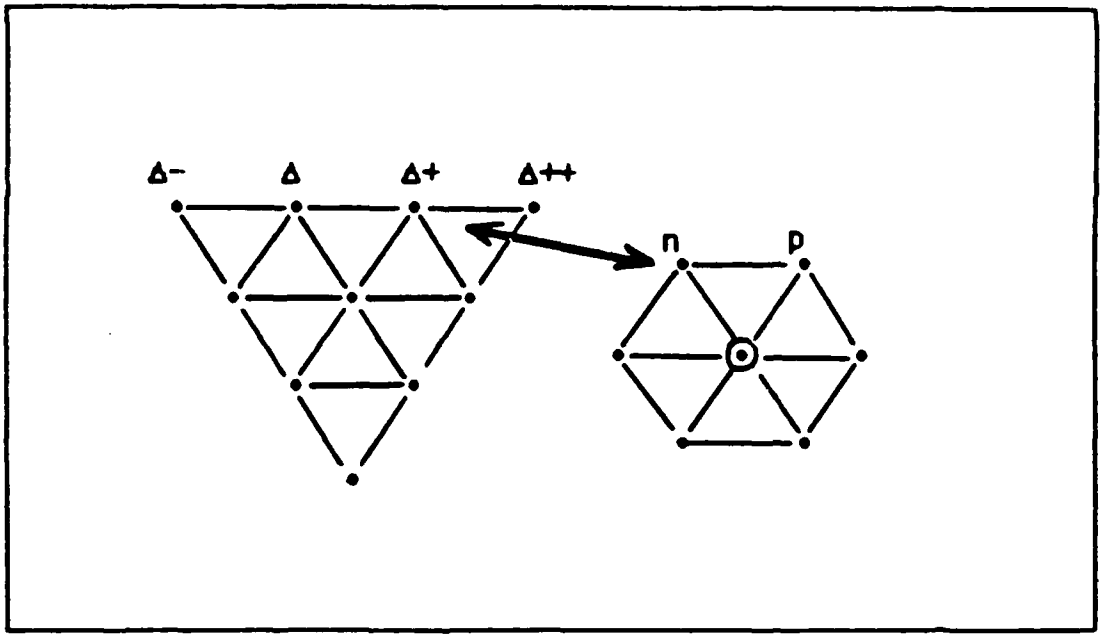

FIGURE 56. Delta and Nucleonic Transitions.

constant; ϕ_π is the pi-meson field, and J^- the Δ - N lowering operator. Clearly, the assumption of the two-level system now follows the form of Dicke [in the SU(2) picture] and transitions indicated in Fig. 56 can occur.

Consequently, the emission of coherent pions includes the matrix element of the form $\langle JM\ 1\ J-\ 1J\ M+1\rangle \approx n/2$ for maximum J and minimum M. The striking observation of coherent pion emission in heavy-ion collisons which populate the Δ-nuclear states is a promising test of Dicke's theory. The important point is that the quantum aspects of superradiant emission are the result of collective behavior of particles with respect to a common field.

C. CONCLUSIONS

The following conclusions are drawn:

1. Dicke superradiance may allow for coherent emission in the meson field, that is -- directed particle emission;
2. The temperature-dependent effects in the Dicke superradiant theory are expected to differ from the semiclassical theory;
3. The distinction and understanding of the Dicke-superradiant mode is a critical item in our assessment of the feasibility of a gamma-ray laser; and the heavy ion collision results tend to reinforce distinctions from usual laser (stimulated) processes.

The following are being investigated by the authors:

1. The study of the superradiator effect in n-level systems with possible results in multilevel electromagnetic systems.
2. The less-relevant directed pi-meson beam and associated decay products, which are also of interest.

In summary, recent results in heavy-ion reactions prompt the reinvestigation of superradiant effects which we have been

exploring. Superradiance is currently expected to play some role in a successful gamma-ray laser concept.

X. THE MÖSSBAUER EFFECT AND RECOIL IN GAMMA-RAY LASERS

In reviews of gamma-ray lasers (Ref. 2 and 3), there is a great deal of discussion of the need for a Mössbauer effect in the host crystal to enable a nucleus to emit its gamma ray with the full transition energy. The energy of the recoilless component is sharply defined, having a radiation width comparable to the natural Lorentz width. In discussing the stimulation of emission of nuclear radiation, it is assumed that stimulation will occur only under the same resonance condition as for absorption, i.e., with the stimulating radiation originating from a recoilless emission; also, only then will the natural radiation width be approximated. This idea was disputed at the IST/IDA Gamma-Ray Laser Workshop (see Ref. 2). It was shown that if all the atoms in a sample of gas--atoms containing excited nuclei of interest--could be brought to rest, stimulated emission could occur at an energy equal to the transition energy reduced by the Doppler recoil. There was the additional benefit that absorption would not occur because the recoil energy is generally greater than the natural width of the transition. It became clear that the Mössbauer effect is important for the gamma-ray laser, not because zero recoil is essential for stimulation, but because the effect makes each emitting nucleus appear to be at rest and to undergo the very same recoil, which in this case happens to be zero. Furthermore, it reduces the Doppler width to a value close to the natural width.

If lasing can be achieved under the condition that all the atoms are at rest, it can also be achieved under the condition that all atoms have identical velocities of arbitrary value.

To verify this, merely transform from the laboratory frame to one in which the atoms are at rest. Stimulation can then occur in that frame and, therefore, also in the laboratory frame. Whether there might be a more preferred velocity at which the narrowest possible velocity distribution can be achieved is of interest. One immediately thinks of the opposite end of the velocity spectrum, the speed of light, c. In the case of accelerating beams of relativistic particles, as more energy is delivered to the particles, the velocity distribution is squeezed more tightly against the upper limit c. Assume that a highly relativistic beam of heavy nuclei is achieved with an energy E and an energy spread ΔE; E is given by γMc^2 and ΔE by $(\Delta\gamma)Mc^2$, where $\gamma = (1 - \beta^2)^{-1/2}$ and $\beta = v/c$. Assume also that the transition of interest has an energy of about 50 keV and a lifetime of about 10^{-8} sec, i.e., a radiation width Γ of about 6×10^{-8} eV. To estimate a value for an acceptable velocity spread, i.e., one which will enable us to achieve lasing, simply equate the Doppler broadening to the natural width. Thus,

$$\Delta_D \approx E_o \cdot \Delta\beta' \approx \Gamma \ , \tag{43}$$

where $\Delta\beta'$ is the velocity spread (divided by c) in a reference frame moving with the beam of particles. Then

$$\Delta\beta' \approx \frac{6 \times 10^{-8}}{5 \times 10^{4}} \approx 10^{-12} \ . \tag{44}$$

This corresponds to a velocity spread of about 0.03 cm/sec.

In the laboratory, $\beta = (1 - \frac{1}{\gamma^2})^{1/2}$. From this relationship,

we easily obtain the result

$$\Delta\beta = \frac{1}{\beta}\,\frac{\Delta\gamma}{\gamma^3} \approx \frac{\Delta\gamma}{\gamma^3} \quad , \tag{45}$$

since by our assumption of a relativistic beam, $\beta \approx 1$. To get a relationship between $\Delta\beta'$ and $\Delta\beta$, consider two nuclei in the beam. In the laboratory frame, they are moving with velocities v_1 and v_2. In a frame attached to particle 1, the laboratory is moving wth a speed $-v_1$, and particle 2 is moving with a speed

$$v_2' = \frac{v_2 + (-v_1)}{1 + \dfrac{v_2 \times (-v_1)}{c_2}} \approx \gamma^2 \cdot (v_2 - v_1) \tag{46}$$

$$\Delta v' = v_2' - v_1' = v_2' \approx \gamma^2 \cdot \Delta v$$

(since $v_1' = 0$ in the moving frame), or

$$\Delta\beta' \approx \gamma^2 \Delta\beta$$

$$\approx \gamma^2 \cdot \frac{\Delta\gamma}{\gamma^3} \quad ,$$

or

$$\Delta\beta' \approx \frac{\Delta\gamma}{\gamma} \quad . \tag{47}$$

In the example above, $\Delta\beta' \approx 10^{-12}$. Therefore, the energy spread in the beam must be one part in 10^{12} to achieve stimulation in a hypothetical device.

What energies and resolutions are actually available? For light nuclei, Van de Graaff accelerators can yield, at best,

resolutions of the order of $\frac{\Delta\gamma}{\gamma} = 10^{-5}$ with energies per nucleon of about 5 MeV; these are distinctly non-relativisitic beams. At Michigan State University, proton beams of about 15 MeV have been produced with resolutions of about 10^{-3}; at Los Alamos Meson Physics Facility (LAMPF) 800 MeV protons, at an energy resolution of about 10^{-4}. For heavy nuclei ranging from iron to uranium, the Bevalac at Lawrence Berkeley Laboratory (LBL) has produced beams ranging from less than 1 GeV/nucleon to about 2 GeV/nucleon. The upper limit is 2.1 GeV/nucleon. The energy resolutions are of the order of 1/2 percent to 1 percent.* In none of these cases do we approach the highly relativistic beams that we were seeking.

We see that the accelerator, just as atomic cooling (discussed in Ref. 2), has not reached the level of technology that can provide beams of excited nuclei with narrow velocity distributions adequate for the needs of gamma-ray lasers. We therefore appear to be tied to using Mössbauer crystals to achieve our goals, at least for the foreseeable future.

---

*Private conversations with R. Bassel, J. Kidd, N. Seeman of the Naval Research Laboratory and Sam Penner of the National Bureau of Standards.

REFERENCES

1. "Report on the IST/IDA Gamma-Ray Laser Workshop," Editors Bohdan Balko, Leslie Cohen, and Francis X. Hartmann, IDA Memorandum Report M-122, January 1986.

2. Proceedings of the IST/IDA Gamma-Ray Laser Workshop, Editors Bohdan Balko, Leslie Cohen, and Francis X. Hartmann, IDA Memorandum Report M-162, January 1986.

3. G.C. Baldwin, J.C. Solem, and V.I. Gol'danskii, Rev. Mod. Phys., 53 (4), pp. 687-744, 1981.

4. C.B. Collins and B.D. DePaola, J. Opt. Soc. Am. (accepted for publication).

5. "Nuclear Wallet Cards," edited by J.K. Tuli, National Nuclear Data Center, Brookhaven National Laboratory, Upton, NY, January 1985.

6. "Nuclear Data Sheets," edited by Nuclear Data Project, Vol. 8 (44), Academic Press, Inc., New York, NY 1972-1985.

7. Table of Isotopes, Seventh Edition, edited by C.M. Lederer and V.S. Shirley, Lawrence Berkeley Laboratory, UCLA, John Wiley and Sons, Inc., New York, NY 1978.

8. "Chart of the Nuclides, Thirteenth Edition," General Electric Co., San Jose, CA 1984.

9. "Internal Conversion Tables. Part I: K-, L-, M-Shell Conversion Coefficients for Z = 30 to Z = 103," R.S. Hager, E.C. Seltzer, Nuclear Data A4, 1, 1968.

10. I.M. Band, M.B. Trzhaskovskaya, M.A. Listengarten, "Internal Conversion Coefficients for Atomic Numbers Z <30," Atomic Data and Nuclear Data Tables, 18, p. 433, 1976.

11. Bohdan Balko and Wasyl Wasylkiwskyj, "The Gamma-Ray Laser Concept Using Long-lived Nuclear Isomers: Critical Issues and Their Resolution," Proceedings of the IST/IDA Gamma-Ray Laser Workshop, Editors Bohdan Balko, Leslie Cohen, Francis X. Hartmann, IDA Memorandum Report M-162, January 1986.

12. Leslie Cohen, Memorandum Report No. 2947, U.S. Naval Research Laboratory, Washington, DC, 1974.

13. V.I. Gol'danskii and Yu Kagan, Sov. Phys., JETP, 37, 49, 1973.

14. George C. Baldwin, Phys. Rep., 87, 1, 1982.

15. M.G. Mayer and J.H.D. Jensen, Elementary Theory of Nuclear Shell Structure, Wiley, N.Y., 1955.

16. W.C. McHarris, Acc. Chem. Res., 7, 401, 1974.

17. G.T. Trammell and J.P. Hannon, Opt. Commun., 15, 330, 1975.

18. Donald A. McQuarrie, Statistical Mechanics, Harper and Row, N.Y., 1976.

19. Kathleen Lonsdale, ed., International Tables for X-Ray Crystallography, Kynoch Press, Birmingham, England, 1962.

20. Periodic Table of the Elements, Sargent-Welch Scientific Company, 7300 Linder Avenue, Skokie, Illinois, 60076, 1968.

21. J.S. Waugh, L.M. Huber, and V. Haeberlen, Phys. Rev. Lett., 20, 180, 1968.

22. Y.A. Illinskii' and R.V. Khokhlov, Sov. Phys., JETP, 38, 809, 1974.

23. G.C. Baldwin, "Graser Concepts," Proceedings of the IST/IDA Gamma-Ray Laser Workshop, Editors Bohdan Balko, Leslie Cohen, and Francis X. Hartmann, IDA Memorandum Report M-162, January 1986.

24. C.B. Collins, F.W. Lee, D.M. Shemwell, B.D. DePaola, S. Olariu, and I. Iovitzer Popescu, J. Appl. Phys., 53, 7, 4645, 1982.

25. P.P. Wintersteiner, Investigation of Time-Dependent Effects in Solids Using Time-Delayed Coincidence Mössbauer Spectroscopy, Ph.D. Thesis, Boston University, 1976.

26. G.E. Bizina, A.G. Beder, N.A. Burgor, and A.V. Darydov, Sov. Phys., JETP 18, 973, 1964.

27. See Ref. 11.

28. P. Boolchand, "Experimentally Realized Linewidths of Narrow ($<10^{-10}$eV) Nuclear Gamma Resonances," Proceedings of the IST/IDA Gamma-Ray Laser Workshop, Editors Bohdan Balko, Leslie Cohen, Frank X. Hartmann, IDA Memorandum Report M-162, January 1986.

29. W. Wildner and U. Gonzer, J. de Physique Coll., 2 Supl. au No. 3, 40, 2-47, 1979.

30. M. Blume, in Hyperfine Structure and Nuclear Radiations, edited by E. Mathias and D.A. Shirley, North Holland Publication Co., Amsterdam, pg. 911, 1968.

31. J.C. McGilvery and M.S. Feld, Appl. Phys. Lett., 31, 74, 1977.

32. M.I. Skolnik, Radar Handbook, McGraw-Hill Book Co., N.Y., pg. 4-6, 4-7, 1970. Also see article by W. Wasylkiwskyj, in IDA Midcourse Discrimination Report (1985) Interactive Techniques (U), IDA Paper P-1963, edited by B. Balko and L. Cohen (SECRET).

33. B. Arad, S. Eliezer, and Y. Paiss, Phys. Lett., 74A, 395, 1979.

34. J.D. Jackson, Classical Electrodynamics, John Wiley & Sons, New York, 1975.

35. J.M. Blatt and V.F. Weisskopf, Theoretical Nuclear Physics, John Wiley & Sons, New York, 1960.

36. M.G. Bowler, Nuclear Physics, Pergamon Press, New York, 1973.

37. A. Bohr and B.R. Mottelson, Nuclear Structure, Vol. II, W.A. Benjamin, Reading, MA, 1975.

38. F.X. Hartmann, "Nuclear Structure Aspects of Re^{186} Pertinent to the Pumped Isomeric State Gamma-Ray Concept," page 103, this report.

39. C.B. Collins, "Coherent and Incoherent Upconversion Techniques for the Pumping of a Gamma-Ray Laser," Proceedings of the IST/IDA Gamma-Ray Laser Workshop, Editors Bohdan Balko, Leslie Cohen, Frank X. Hartmann, IDA Memorandum Report M-162, January 1986.

40. F.X. Hartmann, C. Hayes, B. Balko, A.A. Cohen, L. Cohen, "Study of the Photon Gain Condition for Long-Lived Nuclear Isomeric Transitions," page 25, this report.

41. See Ref. 7.

42. See Ref. 11.

43. L. Cohen, "Proposal for a Gamma-Ray Laser with Recoil," Proceedings of the IST/IDA Gamma-Ray Laser Workshop, Editors Bohdan Balko, Leslie Cohen, Frank X. Hartmann, IDA Memorandum Report M-162, January 1986.

44. S.G. Nilsson, Mat. Fys. Medd. Dan. Vid. Selsk. 29, No. 16, 1955.

45. J.P. Elliot and M.K. Dawber, Symmetry in Physics, MacMillan, London, 1979.

46. H. Ernst, E. Hagn, and E. Zech, Phys. Rev. C, 23, 1739, 1981.

47. D. Strottman, E.D. Arthur, and D.G. Madland, "A Search for Candidate Levels," Proceedings of the IST/IDA Gamma-Ray Laser Workshop, Editors Bohdan Balko, Leslie Cohen, Frank X. Hartmann, IDA Memorandum Report M-162, January 1986.

48. F.S. Dietrich, "Comments on Nuclear Physics for Gamma-Ray Lasers," Proceedings of the IST/IDA Gamma-Ray Laser Workshop, Editors Bohdan Balko, Leslie Cohen, Frank X. Hartmann, IDA Memorandum Report M-162, January 1986.

49. A. Arima and F. Iachello, Ann. Phys., N.Y. 111, 201, 1978.

50. L. Pfeiffer, N.D. Heiman, and J.C. Walker, Phys. Rev., B6, 74, 1972.

51. C.L. Chein and J.C. Walker, Phys. Rev., B13, 1876, 1976.

52. B. Balko, G.R. Hoy, Phys. Rev., B10, 36, 1974.

53. B. Balko, G.R. Hoy, J. de Phys. Coll., Paris, C2, supl. au No. 3, 40 C2-17, 1979.

54. Y.R. Shen, The Principles of Nonlinear Optics, John Wiley & Sons, New York, 1984. (See page 422, equation 22.10.)

55. G.N. Fowler and R.M. Weiner, Phys. Rev. Lett., 55, 1373, 1985.

56. G.T. Trammell, J.T. Hutton, and J.P. Hannon, "Perfect Crystal Grasers," Proceedings of the IST/IDA Gamma-Ray Laser Workshop, Editors Bohdan Balko, Leslie Cohen, and Francis X. Hartmann, IDA Memorandum Report M-162, January 1986.

57. G.C. Baldwin and M.S. Feld, "Kinetics of Superradiance," American Institute of Physics Conference Proceedings No. 146, November 18-22, 1985, edited by William C. Stwaley and Marshall Lapp, American Institute of Physics, New York, NY, 1986.

58. R. Dicke, Phys. Rev., 93, 99, 1954.

59. N. Skribanowitz, I.P. Herman, J.C. MacGillivray, and M.S. Feld, Phys. Rev. Lett., 30, 309, 1973.

60. G.C. Baldwin and J.C. Solem, Laser Focus Magazine, June 1982, 6.

61. M.S. Feld, Frontiers in Laser Spectroscopy, Session XXVII, 1975, edited by Balian et al., North Holland Publications Co., Amsterdam, 1977.

62. Particle Data Group, Rev. Mod. Phys., 56, S33, 1984.

63. I.V. Schensted, A Course on the Application of Group Theory to Quantum Mechanics, NEO Press, Peaks Island, Maine, 1976.

64. D.M. Brink and G.R. Satchler, Angular Momentum, Clarendon Press, Oxford, 1968.

65. A. Yariv, Quantum Electronics, John Wiley & Sons, New York, 1975.

66. F.T. Arecchi and E. Courtens, Phys. Rev. A, 2, 1730, 1970.

APPENDIX

SELECTIVE EXCITATION DOUBLE-MÖSSBAUER SPECTROSCOPY

APPENDIX

SELECTIVE EXCITATION DOUBLE-MÖSSBAUER SPECTROSCOPY

Mössbauer effect (ME) spectroscopy (Ref. A-1) is uniquely suited to the investigation of the dynamics of the interaction between nuclei, electrons, and external fields because of the sensitivity of the spectra to the details of the hyperfine interactions. Consequently, ME spectroscopy is used to study diverse dynamic phenomena. Most ME experiments are performed in the popular transmission geometry shown in Fig. A-1. This technique, although relatively simple experimentally, produces spectra that are often difficult to interpret, as for example the results shown in Fig. A-2. Clearly, most of the lines expected theoretically, as indicated in the bar diagram at the top of the figure, are not revealed in the experimental spectra. The situation is even more complicated when one considers that the relaxation effects which are assumed to be present in the sample tend to modify the line shape.

To investigate such complex dynamic phenomena, a more selective and discriminating technique is required. For the problem of interest we propose a new technique called Selective Excitation Double Mössbauer (SEDM), described in Ref. A-2. SEDM allows a direct measurement of energy transfer in the solid, obviating the major problems with the transmission technique and reveals more details of the process under investigation.

The procedure for obtaining an SEDM spectrum is discussed in Ref. A-2. The physical arrangement is shown in Fig. A-3(a). The characteristic feature of SEDM is that the differential scattering cross section of the Mössbauer isotope is measured instead of the absorption cross section, as in transmission experiments. Consequently, in the SEDM technique, two Doppler

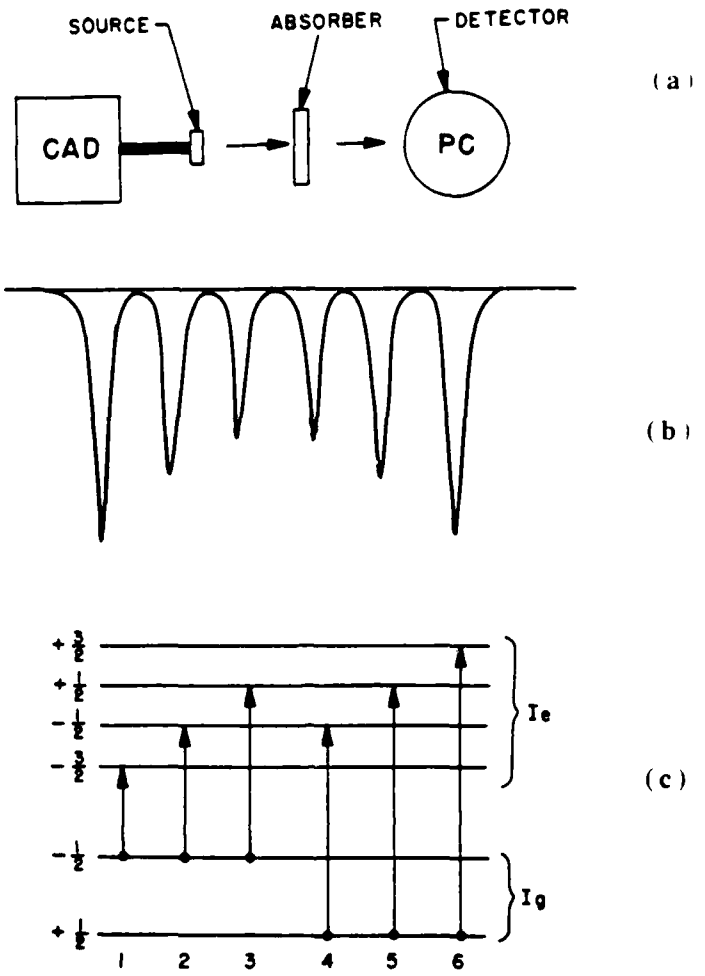

FIGURE A-1. Transmission Geometry. A typical setup for Mössbauer transmission experiments is shown in view a. The energy spectrum of the ion-containing sample is obtained by moving the source at different velocities (Doppler effect) and counting the transmitted photons at each velocity. An example of a Mössbauer transmission spectrum is shown in view b. This is a spectrum of α-Fe_2O_3 at 300 K. From the number and position of the dips we determine the internal magnetic field, the electric field gradient, and the isomer (or chemical) shift. From these measurements we obtain information about the valence state of the iron ion, the symmetry of its environment, the electronic charge density, and the presence of different iron sites in the material. From the relative intensities and widths of the lines, information is obtained about inhomogeneous fields and the dynamic behavior of the iron environment, such as electronic relaxation. View c shows the transitions giving rise to the spectral lines in view b.

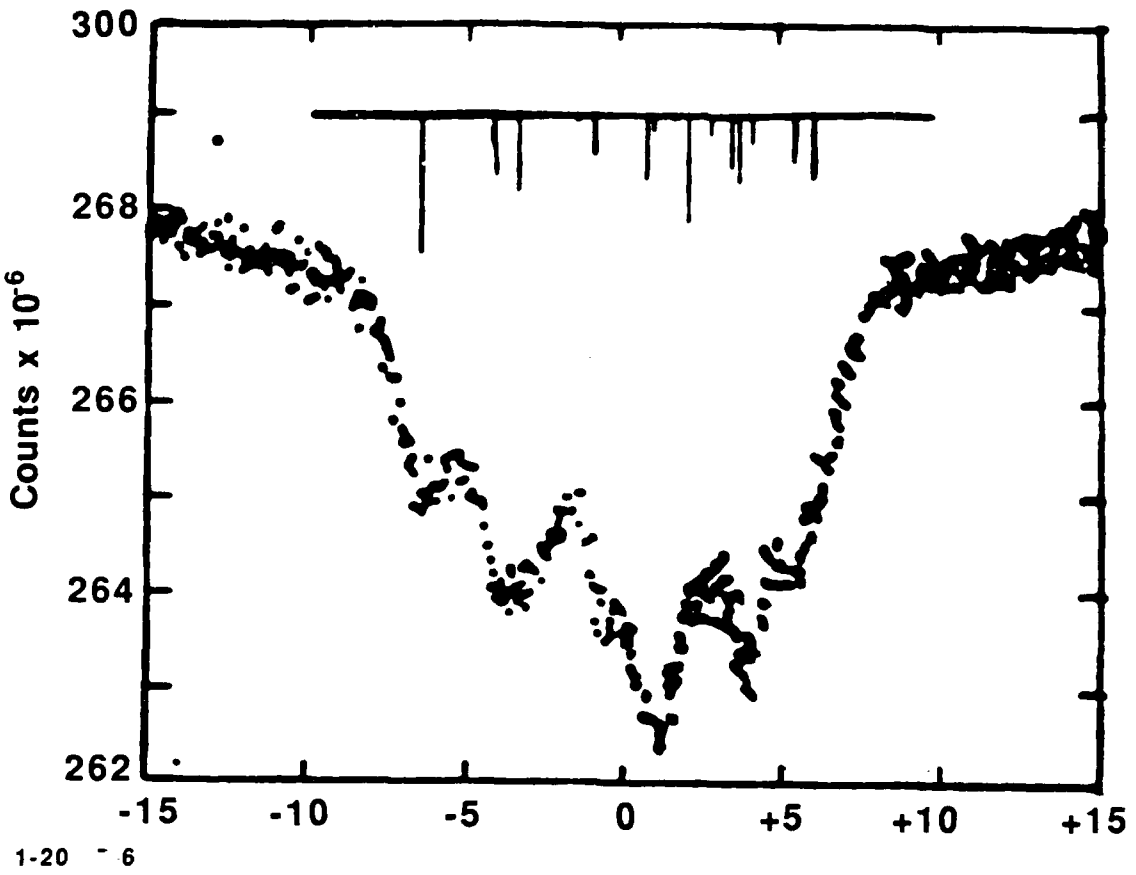

FIGURE A-2. Comparison of predicted absorption lines and the 1.2 K hemoglobin azide data. The breadth of the observed absorption line is attributed to spin relaxation. Adapted from Ref. A-3.

modulators are used to record the four recoilless events: (1) emission of photon γ_1, by the ^{57}Co source; (2) absorption of the photon γ_1, by the ^{57}Fe nucleus in the material under investigation; (3) subsequent reemission of another photon γ_2 and; (4) its absorption by a ^{57}Fe nucleus in the single-line analyzer. These processes are depicted in the energy level diagram in view C of Fig. A-3 and the resulting SEDM spectra for two excitation energies are shown in view b of Fig. A-3.

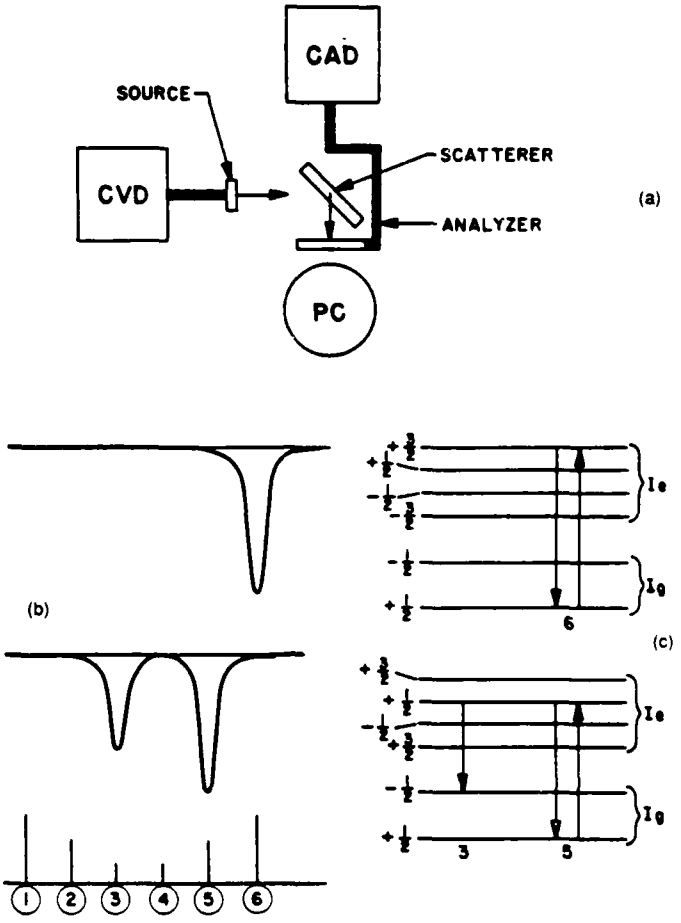

FIGURE A-3. SEDM Geometry. The SEDM experimental setup is shown in view a. A ^{57}Co source is attached to the constant velocity drive (CVD). The source velocity shifts the energy of the radiation emitted to correspond with one of the resonances in the sample. A constant acceleration drive (CAD) is used to scan the resonances and measure the energy of the scattered radiation. View b shows SEDM spectra obtained with ^{57}Fe as the scatterer by exciting line number 6 (top) and line 5 (bottom). The first excitation produces only one line in the SEDM spectrum, but from the second excitation we obtain the two lines, one at the excitation energy, line 5, and the other at line 3, as allowed by the selection rule for M1 radiation as shown in the energy diagram of view c. The SEDM spectra, in general, are simpler than transmission spectra since only lines that are coupled to the excited line by a selection rule or relaxation appear in the spectrum.

A comparison of the spectra shown in Fig. A-1 and A-3 clearly indicates that the transmission spectrum is more complex because it exhibits all the resonances of the system while the SEDM spectrum shows only lines coupled to the specific resonance excited by the radiation from the source. This reveals precisely the advantage inherent in the SEDM technique which stems from the possibility of separating and identifying weak components of a resonance system. Such components could be concealed by stronger lines in a transmission spectrum. Thus, SEDM may be used effectively to search for small admixtures of nuclear states, such as that due to an electric quadrupole interaction, to look for possible E2 transitions in the nuclear radiation spectrum, or to unravel complex spectra consisting of several hyperfine patterns originating from inequivalent sites.

Figure A-4 shows how this technique could be applied to relaxation studies in a sample where two completely different modes of relaxation may be present (view a, Mode A consists of NMR transitions in the excited state and the other, Mode B is a nuclear energy modulation due to electronic spin flip. From the transmission spectra shown in Fig. A-4(a) it is not only difficult to separate out these processes but even to determine the presence of relaxation. On the other hand, the SEDM spectra shown in Fig. A-4(b) clearly show a distinction between the two modes. Thus, the presence of two modes of relaxation can be identified and differentiated in the SEDM spectra.

The SEDM lineshape has been investigated theoretically and the technique has been applied to the study of various dynamic phenomena (Ref. A-4). Most recently, it has been used to determine electron spin dynamics in two classical paramagnets (Ref. A-5 and A-6). These studies forced a reinterpretation of the relaxation processes in the two systems because of the new information obtained by the more selective and discriminating SEDM technique.

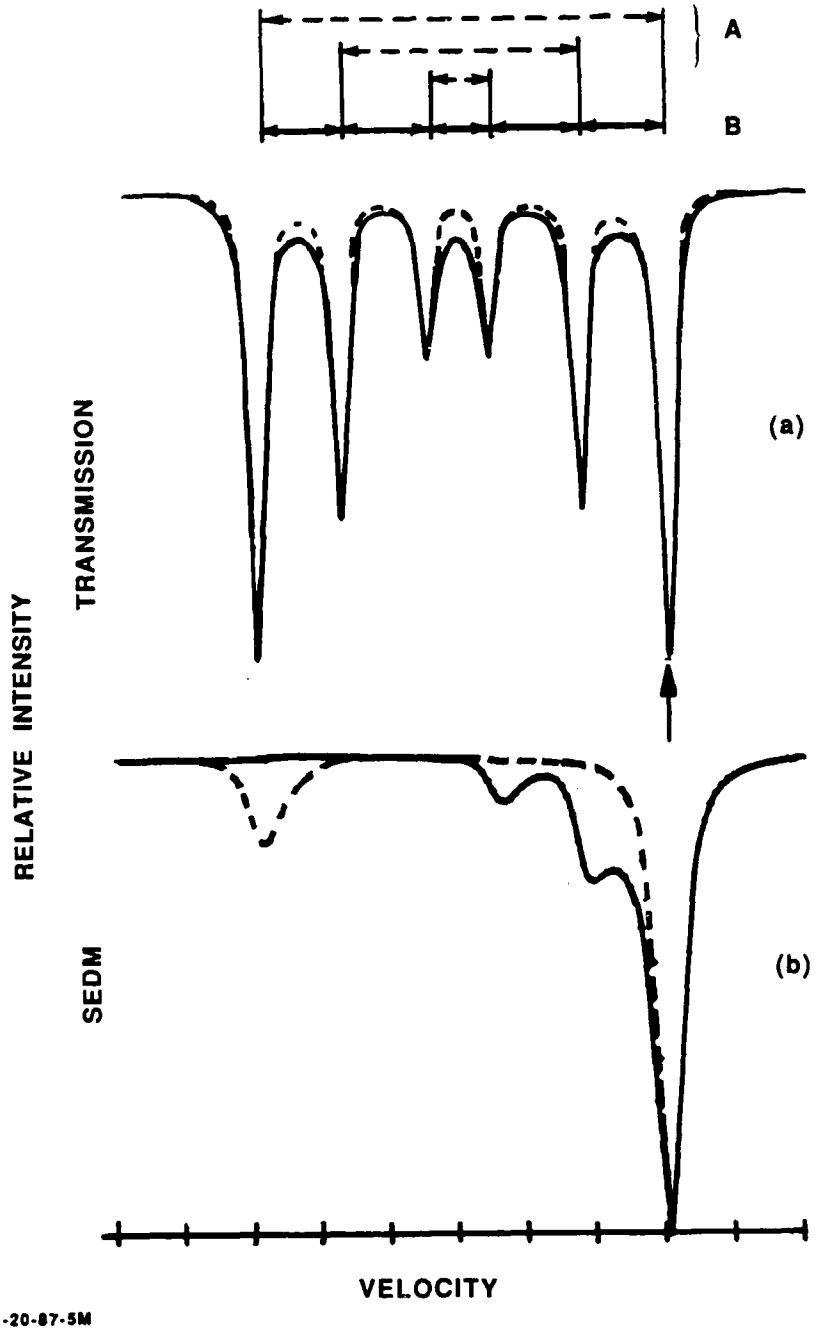

FIGURE A-4. Comparison of transmission, view a, and SEDM, view b, spectra for different relaxation modes A and B. The relaxation kinetics for the two modes are identified in the stick diagram at the top.

END

DATE

FILMED

5-88

DTIC